Depolarization of orthogonal states of polarization in fiber optic high-speed transmission

Pål Roe Sundsøy

Department of Physics - NTNU July 29, 2004

Acknowledgements

This master thesis was carried out at the department of Physics at the Norwegian University of Science and Technology under the guidance of professor Dag Roar Hjelme from the Department of Physical Electronics.
I must acknowledge, foremost, professor Hjelme for his assistance, patience and source of knowledge on the subject.
I would also like to acknowledge Dr. Steinar Bjørnstad at Telenor Research & Development for academic support and for giving me the chance to write this report.

Pål Roe Sundsøy
NTNU, Trondheim
July 2004

Abstract

The purpose of this project is to investigate physical issues related to the optical transport layer in next-generation fiber optic networks which exploit polarization-properties of light. Especially physical limitations of two new concepts are examined.
A new promising technique called polarization division multiplexing (PDM) which uses independent data sets of two orthogonal polarizations on the same frequency to double the total data throughput is investigated.
The other concept, known for reducing non-linear interactions, is known as polarization interleaving where adjacent wavelength channels employ orthogonal polarizations.
From literature it is known that nonlinear effects such as cross-phase modulation (XPM) and linear effects such as polarization mode dispersion (PMD) depolarize the signals, degrading the orthogonality between the polarizations, which make it hard to separate the signals at the fiber end. The purpose of this report is to quantify this depolarization.
In the report pulses of light are treated using classical electrodynamics, and we investigate how two initial orthogonal polarizations behave when propagating in conventional single-mode fibers with random birefringence.
Focusing on polarization, a review of linear and non-linear effects is first presented. Especially we emphasize how PMD affect the states of polarization, both in PDM and polarization interleaving.
By using the Stokes formalism we have found an analytical expression for the degree of polarization versus frequency after one fiber element which is investigated by numerical methods.
We have also suggested a numerical method for quantifying the relative depolarization, and by using parametric bit sequences the polarization separation angle are related to the degree of polarization both in polarization interleaving and PDM.
For polarization interleaving the results showed that, depending on the fiber PMD coefficient, D_p, and channel frequency separation, the orthogonality is quickly lost as the optical waves propagate along the fiber. The larger D_p and channel spacing, the larger the range over which the polarization angles were distributed at any point of the fiber. With $D_p = 1$ ps/km$^{\frac{1}{2}}$ and 0.8 nm spacing, the distribution covered the entire range from orthogonal to parallel after 40 km fiber propagation, while a coefficient of 0.1 ps/km$^{\frac{1}{2}}$ and a 0.2 nm spacing did not affect the initial orthogonality considerably. Nearly analogous conclusions can be drawn for the PDM case, but it seems like the polarization angle deviates more compared to polarization interleaving in low PMD fibers. At the same time it seems like PDM is more tolerant for higher frequency separations.
However, when polarization multiplexed soliton pulses was used the preservation of orthogonality was stable over a wide spectral range. This is due to the so called self-trapping effect which causes group-velocity dispersion to cancel out the effect of PMD. The PSP bandwidth is also verified by simulations.

Contents

1 Introduction **1**
- 1.1 Foreword . . . 1
- 1.2 Objective and outline of the work . . . 3

2 WDM transmission **4**
- 2.1 Why fiber-optic communication? . . . 4
- 2.2 Wavelength-division multiplexing . . . 5
- 2.3 Maximizing spectral efficiency . . . 6

3 General formalism **8**
- 3.1 Classical concept of polarized light . . . 8
  - 3.1.1 Jones formalism . . . 9
  - 3.1.2 Stokes vector and Mueller matrices . . . 10
  - 3.1.3 The Poincaré sphere . . . 11
  - 3.1.4 Degree of polarization and depolarization . . . 12
  - 3.1.5 Comparison of Mueller calculus and Jones calculus . . . 12
- 3.2 Fiber Modes experiencing birefringence . . . 13

4 Linear effects **15**
- 4.1 Chromatic dispersion . . . 15
- 4.2 Polarization mode dispersion . . . 16
  - 4.2.1 Polarization mode coupling . . . 18
  - 4.2.2 Principal States of Polarization . . . 20
  - 4.2.3 The PMD vector . . . 21
  - 4.2.4 Higher order PMD . . . 23
  - 4.2.5 Bandwidth of the Principal states . . . 24
  - 4.2.6 Concatenation of PMD vectors . . . 25
- 4.3 Polarization dependent effects in in-line devices . . . 26
  - 4.3.1 Polarization-dependent loss . . . 26

4.3.2 Polarization-dependent gain . . . 27
4.3.3 Polarization hole burning . . . 27
4.4 The autocorrelation function . . . 28
4.4.1 Autocorrelation function for PMD . . . 28
4.4.2 Autocorrelation function for PMD and PDL . . . 29

5 Nonlinear effects **31**
5.1 Origin of nonlinear birefringence . . . 31
5.2 The coupled Nonlinear Schrödinger equations . . . 33
5.2.1 Cross-phase modulation (XPM) . . . 35
5.2.2 Four wave mixing (FWM) . . . 36

6 Depolarization of orthogonal waves **40**
6.1 Depolarization of orthogonal polarized channels . . . 40
6.2 Relative depolarization . . . 45
6.2.1 Crosstalk between states of polarizations . . . 47

7 Simulations **50**
7.1 WDM Polarization interleaving . . . 51
7.1.1 Verifying the polarization angle dependence on FWM 51
7.1.2 Verifying the bandwidth of the principles states in Polarization interleaving . . . 52
7.1.3 Relative depolarization using alternating bits . . . 54
7.1.4 Simulation results . . . 58
7.1.5 Influence of XPM on orthogonality . . . 65
7.1.6 Polarization interleaved solitons . . . 66
7.2 Polarization-division multiplexing . . . 68
7.2.1 Relative depolarization of one PDM signal . . . 68
7.2.2 Relative depolarization between two PDM signals. . . 69
7.3 Comparison of the polarization separation angles . . . 74

8 Conclusions **75**
8.1 Discussion . . . 75
8.2 Summary . . . 78

A From Maxwell equations to Helmholtz equation **79**
A.1 Fiber modes . . . 81

B Principal States of Polarization **83**

C Autocorrelation functions of PMD and PDL **85**

D From Jones Matrix to Mueller matrix **87**
D.1 Pauli matrices 87
D.2 Calculation of Mueller matrix elements from fiber Jones Matrix 88
D.3 Finding Mueller matrix elements 89
D.4 Stokes vectors at fiber output 91
D.5 Frequency spectrum plot 92
D.6 Stokes components (M_11,M_21 and M_31 multiplied with frequency spectrum (l=fˆ2 above) 94
D.7 Evaluation of degree of polarization (DOP) for Channel A . . 95

E Polarization interleaving setup **96**

Bibliography **98**

List of Figures

2.1 Schematic diagram for key technologies for high-capacity DWDM transmission. Hybrid technologies may be implemented using photonics and/or electronics. CD and PMD denote chromatic and polarization mode dispersion respectively [**?**] 6
2.2 Principle sketches of **(a)** Polarization interleaving **(b)** Polarization-division multiplexing. The vector notations will be clarified in the next chapter. 7

3.1 Parameters of elliptical vibration having components of amplitude $2E_{ox}$ and $2E_{oy}$ along x and y respectively: $\tan\nu = E_{ox}/E_{oy}$; the major and minor axes of the ellipse are $2a$ and $2b$ respectively; the ellipticity $e = \tan\epsilon = b/a$; the azimuth is at an angle θ with respect to the x-axis [**?**]. 9
3.2 The Poincaré sphere showing the representation of an elliptically polarized vibration by a point M. From the spherical triangle OMT the parameters of the vibration can be found. Points on the equator OO' represent linearly polarized light. The sense of rotation of the ellipse is left and right in the upper and lower hemispheres respectively. The poles P_1 and P_2 represent left and right circularly polarized light respectively [**?**]. 11

4.1 Frequency-domain picture of PMD for a launch state on the azimuth near the birefringent S_1-axis. 18
4.2 Schematic of how PMD behaves in the time-domain. A pulse launched with equal power on the two birefringent axes results in two pulses at the output separated by the differential group delay $\Delta\tau$. 18

4.3 A concatenation of fiber elements with varying birefringence axes. 19
4.4 Output PMD vector $\boldsymbol{\tau}(\omega)$ of a fiber with a mean DGD of 35 ps as a function of frequency [**?**]. The figure shows the three vector components of $\boldsymbol{\tau} = [\tau_1\ \tau_2\ \tau_3]^T$. As indicated, the measurement is done over a 130 Ghz spectral range 22
4.5 Schematic diagram of the PMD vector $\boldsymbol{\tau}_{\omega_0}$ and the second-order PMD components showing the change of $\boldsymbol{\tau}_{\omega_0}$ with frequency. Note that $\mathbf{q}_\omega$ is perpendicular to $\mathbf{q}$. The angular rotation rate $d\phi/d\omega$ of the PMD vector $\boldsymbol{\tau}_{\omega_0}$ with ω is described by the depolarization rate $|\mathbf{q}_\omega|$. 24
4.6 Wavelength intervals for measurement of PMD. To avoid inaccuracy from higher order psp, $\Delta\lambda_{psp}$ should be bigger than the wavelength interval. 25
4.7 Concatenation of PMD-vectors divided in m sections.The Mueller matrices M_n, and output PMD vectors $\boldsymbol{\tau}_n$ are known. 26
4.8 Comparison between a normalized ACF of SOP without PDL (crossline) and a normalized ACF with PDL (solid line). . . . 29

5.1 Four-wave mixing efficiency vs transmission distance for two initially orthogonally polarized signals with different channel spacing for increasing transmission distances [**?**]. 39

6.1 (a) Plot of the gaussian frequency spectrum used in the calculation (b) DOP versus frequency for $\hat{\mathbf{s}}_A$. The inner curve is calculated for a lower DGD value $\Delta\tau$. 45
6.2 Arbitrary SOP's represented on the Poincare sphere. $\hat{\boldsymbol{s}}_A$ and $\hat{\boldsymbol{s}}_B$ represent the polarizations before realignment to the azimuth, and $\hat{\boldsymbol{s}}_{A'}$ and $\hat{\boldsymbol{s}}_{B'}$ after the realignment. 46
6.3 Arbitrary SOP's projected on the plane of linear polarizations of the Poincare sphere. 47
6.4 (a) Projection of $\hat{\boldsymbol{s}}_A$ on the axis of PBS for polarization demultiplexing. The amplitude length $\sqrt{s_{0A}}$ can be understood from Fig.(3.1) where the length of the semiminor axis a and the length of the semimajor axis b have the property that $E_{ox}^2 + E_{oy}^2 = a^2 + b^2$ (b) Schematic of the orientations of two multiplexed signals with respect to the PBS. The PBS are assumed aligned to the x-axis. 48

7.1 Principle sketch of the initial stokes vectors. $\hat{\mathbf{s}}_A^y$ and $\hat{\mathbf{s}}_B^x$ are anti-parallel and 180° opposed to each other in Stokes space. 51
7.2 **(a)** Channel performance versus polarization angle between adjacent channels in absence of PMD **(b)** Channel performance versus polarization angle between adjacent channels with PMD present. The angle is taken in Jones space. 52
7.3 **(a)** $\hat{\mathbf{s}}_B$ is inside the half PSP bandwidth of $\hat{\mathbf{s}}_A$. **(b)** $\hat{\mathbf{s}}_B$ is outside the half PSP bandwidth of $\hat{\mathbf{s}}_A$. 53
7.4 DOP versus bandwidth for two initial orthogonal channels $\hat{\mathbf{s}}_A$ and $\hat{\mathbf{s}}_B$. The apparently random behavior of the DOP is the result of the random behavior of PMD, and only one seed value is used for each frequency step. 54
7.5 (a) Before fiber propagation the Stokes vectors are orthogonal, $\hat{\mathbf{s}}_A^y \cdot \hat{\mathbf{s}}_B^x = -1$. (b) After propagating a distance z the Stokes vectors are separated by a polarization angle 2ξ. λ_B is varied relative to $\lambda_A = 1537.4$ nm to check the frequency dependence of $\xi(\omega)$ which is related to $\boldsymbol{\tau}_\omega$. 54
7.6 The topology setup of channel A and B. 55
7.7 The relation between DOP and relative angle (taken in Jones space) for different modulations. 57
7.8 Relative angle ξ versus fiberlength, z, between channels at 50 Ghz apart. Fiber PMD coefficient is 1.0 ps/km$^{\frac{1}{2}}$.There are 50 simulation runs at each km fiber increment. 59
7.9 Probability distributions of relative angles ξ. Channels are spaced 50 Ghz and fiber PMD coefficient is 1.0 ps/km$^{\frac{1}{2}}$. The angles are normal distributed at 1, 10 20 and 40 km. 59
7.10 Average relative angle ξ versus fiberlength, z, between channels at 12.5 Ghz, 25 Ghz and 50 Ghz apart. Fiber PMD coefficient is 1.0 ps/km$^{\frac{1}{2}}$ 60
7.11 Standard deviation versus fiberlength for channels spaced 12.5 Ghz, 25 Ghz and 50 Ghz. Fiber PMD coefficient is 1.0 ps/km$^{\frac{1}{2}}$ 61
7.12 DOP shown on the Poincaré surface in the average PMD case for increasing fiber distances. **(a)** $z = 0$ km, $\Delta\overline{\tau} = 0$ ps, $\xi = 90°(180°)$ **(b)** $z = 20$ km, $\Delta\overline{\tau} = 4.47$ ps, $\xi = 68°(136°)$ **(c)** $z = 40$ km, $\Delta\overline{\tau} = 6.32$ ps, $\xi = 55°(110°)$ **(d)** $z = 80$ km, $\Delta\overline{\tau} = 8.95$ ps, $\xi = 41°(82°)$ **(e)** $z = 200$ km, $\Delta\overline{\tau} = 14.14$ ps, $\xi = 39°(78°)$ **(f)** $z = 500$ km, $\Delta\overline{\tau} = 22.36$ ps, $\xi = 32°(64°)$ The polarization separation angle in Stokes space is emphasized in parenthesis. 61

7.13 Relative angle ξ versus fiberlength, z, between channels at 50 Ghz apart. Fiber PMD coefficient is 0.1 ps/km$^{\frac{1}{2}}$. There are 50 simulation runs at each km fiber increment 62
7.14 Average relative angle ξ versus fiberlength, z, between channels at 12.5 Ghz, 25 Ghz and 50 Ghz apart. Fiber PMD coefficient is 0.1 ps/km$^{\frac{1}{2}}$. 63
7.15 Standard deviation versus fiberlength for channels spaced 12.5 Ghz, 25 Ghz and 50 Ghz. Fiber PMD coefficient is 0.1 ps/km$^{\frac{1}{2}}$ 63
7.16 **(a)**Average relative angle ξ versus fiberlength, z, between channels at 12.5 Ghz, 25 Ghz and 50 Ghz apart. Fiber PMD coefficient is 2.0 ps/km$^{\frac{1}{2}}$.**(b)** Standard deviation of ξ. 64
7.17 High intensity fiber. Relative angle versus fiber length. 50 Ghz channel spacing, 1.0 ps/km$^{\frac{1}{2}}$. 65
7.18 Soliton transmission. **(a)** Relative angle ξ versus fiberlength with 50 Ghz spacing and 50 simulation runs at each km. **(b)** Average angle versus fiberlength. . Fiber PMD coefficient is 1.0 ps/km$^{\frac{1}{2}}$. 66
7.19 Relative angle ξ between intra-channels $|s_A^x\rangle$ and $|s_A^y\rangle$ versus fiber length. $D_p = 1.0$ ps/km$^{\frac{1}{2}}$. 68
7.20 (a) Before fiber propagation the Average Stokes vectors are parallel, $\hat{\mathbf{s}}_A^{ave} \cdot \hat{\mathbf{s}}_B^{ave} = 1$. (b) After propagating a distance x the Stokes vectors are separated by a polarization angle 2ξ. λ_B is varied relative to $\lambda_A = 1537.4$ nm to check the frequency dependence of $\xi(\omega)$ which is related to $\boldsymbol{\tau}_\omega$. 69
7.21 The setup for polarization-division multiplexing of 2 channels. The polarization rotator is only used to find the relationship between the DOP and the average angle ξ between $\hat{\mathbf{s}}_A^{ave}$ and $\hat{\mathbf{s}}_B^{ave}$. 70
7.22 Length of DOP vector versus relative angle ξ. 71
7.23 (a) ξ versus fiberlength for 2 PDM channels spaced 50 Ghz. $D_p = 1.0$ ps/km$^{\frac{1}{2}}$. (b) Probability distributions of relative angles ξ. The angles are normal distributed at 1, 10 20 and 40 km. 72
7.24 (a) Average relative angle ξ versus fiber length. $D_p = 1.0$ ps/km$^{\frac{1}{2}}$. (b) Average relative angle ξ versus fiber length. $D_p = 0.1$ ps/km$^{\frac{1}{2}}$. 73

A.1 LP-modes in step-index fiber. Normalized propagation constant b versus the V-number. 82

E.1 Setup for measuring the Q-value for different input angles . . 97

List of Tables

2.1 Summary of bandwidth and channels 5

7.1 Comparison of polarization angle deviations $\Delta\xi$ for PDM and Polarization interleaving (PI) for increasing fiber lengths. The PMD coefficient, D_p, is given in $\frac{\text{ps}}{\text{km}^{\frac{1}{2}}}$. Angles are given in Jones space. 74

Acronyms used in report

ACF	Autocorrelation function
BER	Bit-error rate
DGD	Differential group delay
DOP	Degree of polarization
FWM	Four-wave mixing
GVD	Group velocity dispersion
PI	Polarization Interleaving
ISOP	Input state of polarization
MMF	Multimode fiber
NLS	Nonlinear Schrödinger equation
NRZ	Non-return to zero
OOK	On/Off keying
PBS	Polarization beamsplitter
PCD	Polarization-dependent chromatic dispersion
PDG	Polarization-dependent gain
PDL	Polarization-dependent loss
PDM	Polarization-division multiplexing
PHB	Polarization-hole burning
PMD	Polarization mode dispersion
PMF	Polarization maintaining fiber
PSP	Principle state of polarization
RZ	Return to zero
SOP	State of polarization
SPM	Self-phase modulation
WDM	Wavelength division multiplexing
XPM	Cross-phase modulation

Chapter 1

Introduction

1.1 Foreword

Civilizations has advanced as people discovered new ways of exploiting various physical resources such as materials, forces and energies.
In the twentieth century information was added to the list when the invention of computers allowed complex information processing to be performed outside human brains.
We are moving towards a society which requires that we have access to information at our finger tips *when we need it, where we need it, and in whatever format we need it.*
The information is provided to us through our global mesh of communication networks, whose current implementations, e.g. today's Internet, do not have the capacity to support the huge bandwidth demands.
Fiber-optic technology can be considered our saviour for meeting our above need because of its potentially limitless capabilities, huge bandwidth (nearly 50 Tb/s), low signal attenuation, low signal distortion, low power requirement, low material usage, small space requirement and low cost [Coc95, Muk97].
With these advantages optical fiber has become the obvious choice as a medium transmission for future networks. Though the fiber has bandwidth capacitites in the order of Tb/s, the electronic end devices can only transmit at peak rates of a few Gb/s. Due to the absence of an optical switching device, the optical data signal was forced to undergo opto-electronic conversions at the intermediate nodes. The speed limit of end devices and the absence of optical switches led to under utilitzation of the fiber bandwidth. But breakthroughs in the optical technology like optical cross-connects and

wavelength division multiplexing (WDM) have led to the emergence of a next generation all-optical WDM network.
Optical pulses propagating in WDM fibers offer several degrees of freedom, including phase, frequency and state of polarization (SOP). The combined coding over these degrees of freedom has seldom been explored as a means to increase the transmission capacity in fibers. A new viable technique for greatly increasing the bandwidth capacity of existing commercial fiber-based networks are now being explored. Using orthogonal polarization states of light, it is possible to add an extra set of channels to those split by wavelength in transmission systems based on WDM.
Another concept for increasing the bandwidth capacity is where adjacent WDM channels employ orthogonal polarizations.
However, due to depolarization caused by temporal and spatial variations in the fiber's birefringence[1] in combination with non-linear effects the orthogonality degrades in a complicated manner, which makes it difficult to separate the signals at the fiber end. This influence leads to crosstalk and a high bit-error rate.
The aim of this report is to investigate how the SOPs are affected as they propagate in conventional single-mode fibers with random birefringence. The first chapters are mainly a review of linear and non-linear effects that leads to depolarization of the optical signals. Polarization-mode dispersion (PMD) , which is the main source for polarization degradation of light fields at different frequencies, is treated in particular detail.
Later we will attempt to quantize, using analytical and numerical calculations, how each polarization depolarizes due to PMD, and show how polarization crosstalk can be quantized.
Using the concepts mentioned above, we will also attempt to find expressions for the relative depolarization and relate it to the evolution of the polarization angle that separates the polarizations at each frequency. The separation angle and its dependence on PMD and channel width will constitute important knowledge for estimating how large bandwidth it is possible to demultiplex at the fiber end.

A more detailed chapter division is emphasized on the next page.

[1] Polarization of electromagnetic fields is a complex subject, particulary when light propagates in a medium with different refractive index in different directions due to birefringence.

1.2 Objective and outline of the work

This report is divided into 8 chapters, subdivided into sections.
In chapter 2 the reader is introduced to WDM communication and ways of maximizing the spectral efficiency in such a system is reviewed.
In chapter 3 the notation and formalism used in the rest of the report is given; Jones - and Stokes space are presented. At the end the reader is introduced to fundamental fiber modes which is important to understand birefringence and lies the basis for chapter 4.
Chapter 4 presents the most important linear effects that leads to system degradation - chromatic dispersion, PMD polarization-dependent loss (PDL), polarization-dependent gain (PDG) and polarization hole burning (PDG) are reviewed. The main focus will be on PMD which is analyzed in detail.
At the end of the chapter it is shown, through autocorrelation functions, that the combination of PMD and PDL affect the orthogonality more drastically compared to the case where only PMD are present.
In chapter 5 non-linear birefringence is presented, and the advantages of using orthogonal SOPs for suppression of cross-phase modulation and four-wave mixing are reviewed with the notation used in this report.
In chapter 6 we start our own calculations based on the PMD theory from chapter 4.2. In 6.1 we have found an analytical expression for the degree of polarization (DOP) as a function of frequency for two polarization multiplexed channels after one fiber element, which relates to the depolarization for each of the polarizations. A numerical method has been used to solve the equations. Chapter 6.2 introduces relative depolarization, and how to quantify crosstalk in a single-mode PDM system based on [RWP04] for multimode fibers. The relative angle between the two polarizations are related to the DOP which is used in the simulations in chapter 9.
In chapter 9 simulations are made by using Optsim, where the aim is to quantify the separation polarization angle in polarization-interleaving and polarization division multiplexing.

Appendix A is related to chapter 3.2 where fiber modes is introduced. The wave-equation is derived and it is shortly explained why only one mode is supported by a single-mode fibers.
In Appendix B the principal states of polarization theory is reviewed which constitute the basis for our PMD-simulations in chapter 7.
The last appendices, C and D are related to the calculations done in our analytical approach in chapter 4.4.2 and chapter 6.1.

Chapter 2

WDM transmission

2.1 Why fiber-optic communication?

The Shannon-Hartley theorem [Sha48] states that, regardless of specific technology, the information-carrying capacity is proportional to channel bandwidth, the range of frequencies within which the signals can be transmitted without substantial attenuation - or mathematically

$$C = W \cdot \log_2(1 + \frac{S}{N}) \tag{2.1}$$

where W is the bandwidth of a signal being transmitted over a noisy communications channel, $\frac{S}{N}$ is the signal to noise ratio and C is the channel capacity, measured in bits per second.
It is the frequency of the signal carrier that limits the channel bandwidth. The higher the carrier's frequency, the greater the channel bandwidth and the higher the information-carrying capacity of the system. A copper wire can carry a 1 MHz signal. A coax can carry a 100 MHz signal. A fiber optic transmission link can carry a 1000 THz signal. Now, if bandwidth is, say 10% of the carrier, the bandwidth increases appreciably from copper to fiber optics.
Consider these transmission media in terms of their capacity to carry, simultaneously, a specific number of one-way voice channels. A single coaxial cable can carry up to 13000 channels, a microwave terrestrial link up to 20000 channels and a satellite link up to 100000 channels [MS01]. However, one ordinary fiber-optic communications link, can carry 300000 two-way voice channels simultaneously, which explain why fiber-optic communications systems form the backbone of modern telecommunications and will

Transmission link	Carrier frequency (Hz)	Bandwidth (Hz)	Channels
Copper wire	10^6	10^5	-
Coax	10^8	10^7	13000
Microwaves	10^{10}	10^9	20000
Fiber optic	10^{15}	10^{14}	300000

Table 2.1: *Summary of bandwidth and channels*

most certainly shape its future. Table 2.1 summarizes the bandwidth relations.

2.2 Wavelength-division multiplexing

WDM combines multiple optical signals so that they can be amplified as a group and transported over a single fiber to increase capacity. Each signal carried can be at a different rate (OC3/12/24, etc.) and in a different format (SONET, ATM, data, etc.) For example, a WDM network with a mix of SONET signals operating at OC48 (2.5 Gb/s) and OC192 (10 Gb/s) over a WDM infrastructure can achieve capacities of over 40 Gb/s. A system with WDM can achieve all this gracefully while maintaining the same degree of system performance, reliability, and robustness as current transport systemsor even surpassing it. Present commercial WDM terminals carry up to 80 wavelengths of OC48, a total of 200 Gb/s, or up to 40 wavelengths of OC192, a total of 400 Gb/s.
In 2001 NEC successfully transmitted 10.9 Tb/s (273 channels spaced 50 Ghz, each with 40 Gb/s bit-rate) of information over 117 km[1], which will allow simultaneous long-distance transmission of more than 1 million high-speed ADSL channels over a single fiber.

To get a whole picture of the WDM concept it is important to understand the physics behind the technology, which can often turn out to be rather complicated. A good introductory book treating most aspects is [Kar03a] by S. Kartalopoulos . A comprehensive treatment of the components in a WDM network can be found in the series of A. Dutta and M. Fujiwara [DDF03b, DDF03a].

[1]This was managed employing polarization interleaving, and by using S-band (allowing light amplification in the 1490 nm region) in addition to the conventional C- and L-bands ($1530 - 1560$ nm and $1560 - 1610$ nm).

2.3 Maximizing spectral efficiency

The overall capacity, C $[\frac{\text{b}}{\text{s}}]$, of a WDM transmission system is governed by the available bandwidth, B [Hz], and by the achievable spectral efficiency, $S = \frac{C}{\Delta f}$ $[\frac{\text{b}}{\text{s}\cdot\text{Hz}}]$, where Δf is the channel spacing. Ultimate limits to the spectral efficiency are determined by the information-theoretic capacity per unit bandwidth from Eq.(2.1). The most important limits to the spectral efficiency are due to

- Limits for various modulation and detection techniques
- Nonlinear impairments which arise from the Kerr effect
- Polarization effects

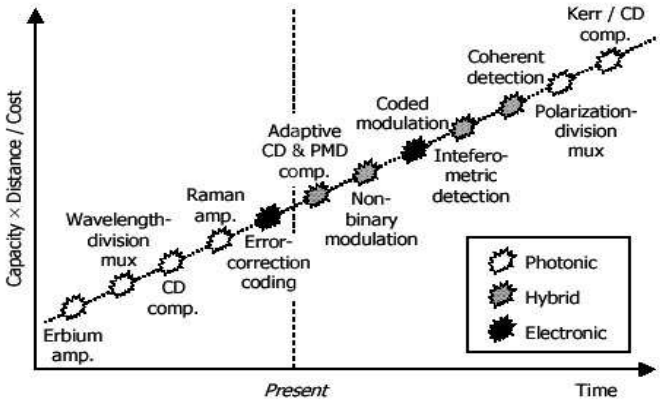

Figure 2.1: *Schematic diagram for key technologies for high-capacity DWDM transmission. Hybrid technologies may be implemented using photonics and/or electronics. CD and PMD denote chromatic and polarization mode dispersion respectively [KH03]*

As shown in Fig.(2.1) a higher spectral efficiency may be obtained with polarization multiplexed WDM-channels as the channel spacing then can be reduced.

We have two different concepts which we would like to study further

Polarization Interleaving where adjacent wavelength channels have orthogonal polarizations. This concept can reduce coherent linear crosstalk

and cross-channel nonlinear effects [Ino91]. A principle sketch of the concept is given in Fig.(6.2.1a).

Polarization-Division multiplexing where two orthogonal polarizations at each wavelength channel is used. This concept can in principle double the spectral efficiency S, launching pairs of signals in orthogonal polarizations, and employing polarization-resolved detection. A principle sketch of this concept is given in Fig.(6.2.1b)

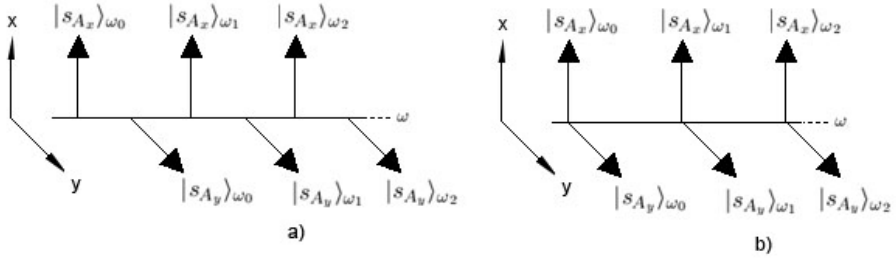

Figure 2.2: *Principle sketches of* **(a)** *Polarization interleaving* **(b)** *Polarization-division multiplexing. The vector notations will be clarified in the next chapter.*

Polarization multiplexed signals are demultiplexed using a combination of a polarization controller (PC) and a polarization beam splitter (PBS). In polarization interleaving the output PBS is usually preceded by an arrayed waveguide router, splitting each waveguide channel to a different output port with its separate PBS (or polarizer).
In PDM systems one can use a shared PBS for both channels, or choose to split the signal path and use a separate PBS for each of the output ports. There exist a lot of experimental work, including simulations that represent these concepts [Hei00, HNW00, CB01, ea92, Hil92], but a unified theory that treats all the problems related to the concepts is still lacking.

Chapter 3

General formalism

In this chapter we will briefly go through the classical theory of polarization of light, which is important background for the study of depolarization in single-mode fibers. The fundamentals of classical light polarization can be found in books such as [Shu62, Hua97]. For a discussion of the quantum theory of light, the reader may consult, for example [Ors00, Lou73, SZ01]. The notation used in the rest of the report will also be emphasized.

3.1 Classical concept of polarized light

Polarization is a property of electromagnetic radiation describing the shape and the orientation of the electric field vector as a function of time, at a given point of the space.

The electromagnetic field vector of an electromagnetic monochromatic plane wave can be expressed in terms of three orthogonal components in a right-handed Cartesian coordinate system.
If light is assumed to progress in the positive z direction, the real instantaneous electric field vector can be written as

$$\mathbf{E}(z,t) = \begin{pmatrix} E_x(z,t) \\ E_y(z,t) \\ E_z(z,t) \end{pmatrix} = \begin{pmatrix} E_{ox}e^{i(\omega t-\beta z+\varphi_x)} \\ E_{oy}e^{i(\omega t-\beta z+\varphi_y)} \\ 0 \end{pmatrix} \tag{3.1}$$

where E_{ox} and E_{oy} are the magnitudes of the components $E_x(z,t)$ and $E_y(z,t)$ respectively and φ_x and φ_x their respective phases.
In the plane $z = 0$ Eq.(3.1) is reduced to

$$\mathbf{E}(t) = \begin{pmatrix} E_x(t) \\ E_y(t) \end{pmatrix} = \begin{pmatrix} E_{ox}e^{i(\omega t+\varphi_x)} \\ E_{oy}e^{i(\omega t+\varphi_y)} \end{pmatrix} \tag{3.2}$$

The equation of the locus of **E** is obtained by eliminating t in Eq.(3.2), hence writing $\varphi = \varphi_x - \varphi_y$

$$(\frac{E_x}{E_{ox}})^2 + (\frac{E_y}{E_{oy}})^2 - 2\frac{E_x E_y}{E_{ox}E_{oy}}\cos\varphi = \sin^2\varphi \tag{3.3}$$

which is the equation of an ellipse circumscribed by a rectangle of sides $2E_{ox}$ and $2E_{oy}$ (see Fig.(3.1)). Corresponding polarization will then be called elliptical, circular or linear.

When $\varphi = \pm n\pi$ $(n = 0, 1, 2, ...)$ the ellipse degenerates into a straight line

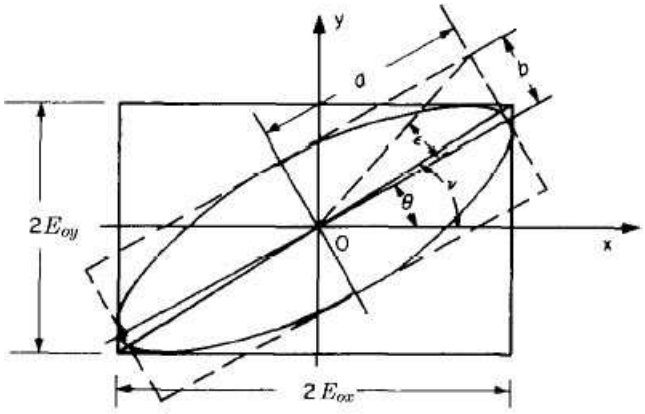

Figure 3.1: *Parameters of elliptical vibration having components of amplitude $2E_{ox}$ and $2E_{oy}$ along x and y respectively: $\tan\nu = E_{ox}/E_{oy}$; the major and minor axes of the ellipse are $2a$ and $2b$ respectively; the ellipticity $e = \tan\epsilon = b/a$; the azimuth is at an angle θ with respect to the x-axis [Jer82].*

with constant orientation but varying amplitude ($E_{ox} \neq E_{oy}$) corresponding to linearly polarized light. When $\varphi = \pm(2n+1)\frac{\pi}{2}$ $(n = 0, 1, 2, ...)$ there is constant amplitude ($E_{ox} = E_{oy}$) but varying orientation giving circularly polarized light. Elliptically polarized light has both varying orientation and amplitude.

3.1.1 Jones formalism

The SOP of a quasi-monochromatic transverse plane wave can also be presented by a 2-D complex ket-vector, called a Jones vector, such as,

$$|s\rangle = \begin{pmatrix} E_{ox}e^{i\varphi_x} \\ E_{oy}e^{i\varphi_y} \end{pmatrix}. \tag{3.4}$$

where we have borrowed the handy Dirac-notation from quantum mechanics [Dir47] to distinguish Jones vectors from Stokes vectors later on. This notation is also used in [GK00] which provides the mathematical basis for treating almost any polarization problem in optical fibers. The bra vector $\langle s|$ indicates the corresponding complex conjugate row vector - i.e. $\langle s| = |s\rangle^\dagger = (E^*_{ox}e^{-i\varphi_x}, E^*_{oy}e^{-i\varphi_y})$. Our Jones vectors are all of unit magnitude, i.e.

$$\langle s|s\rangle = E^*_{ox}E_{ox} + E^*_{oy}E_{oy} = 1 \tag{3.5}$$

If the Jones vector of the incident wave is denoted by $|s_{in}\rangle$, and the Jones matrix of the polarization operator by J, the emergent wave will be denoted

$$|s_{out}\rangle = J|s_{in}\rangle \tag{3.6}$$

3.1.2 Stokes vector and Mueller matrices

In most physical realizable situations, including optical fibers, the wave is not in a pure state. Thus the knowledge of the parameters describing the optical field is incomplete. For practical measurements we must average over an ensemble (or over time) of fields. A useful way to handle this averaging is through the use of Stokes parameters.

The four-dimensional Stokes vector $\hat{\mathbf{s}}$ [Sto52] of unit length corresponds to the Jones vector $|s\rangle$.
The Stokes parameters, generally denoted s_0, s_1, s_2 and s_3, are sufficient to characterize the amplitude, the phase and the polarization of a wave. They are defined as a function of the Cartesian components of the electric field by:

$$\begin{aligned}
s_0 &= |E_x(t)|^2 + |E_y(t)|^2 = E^2_{ox}(t) + E^2_{oy}(t) \\
s_1 &= |E_x(t)|^2 - |E_y(t)|^2 = E^2_{ox}(t) - E^2_{oy}(t) \\
s_2 &= E_x(t)E^*_y(t) + E^*_x(t)E_y(t) = 2E_{ox}(t)E_{oy}(t)\cos\varphi \\
s_3 &= i(-E^*_x(t)E_y(t) + E_x(t)E^*_y(t)) = 2E_{ox}(t)E_{oy}(t)\sin\varphi
\end{aligned}$$

Using the Pauli spin matrices we can express the components, s_i corresponding to $|s\rangle$ in the compact form [Hua97]

$$\hat{\mathbf{s}} = \langle s|\boldsymbol{\sigma}|s\rangle \tag{3.7}$$

where

$$\sigma_0 = \begin{pmatrix} 1 & 0 \\ 0 & 1 \end{pmatrix}, \sigma_1 = \begin{pmatrix} 1 & 0 \\ 0 & -1 \end{pmatrix}, \sigma_2 = \begin{pmatrix} 0 & 1 \\ 1 & 0 \end{pmatrix}, \sigma_3 = \begin{pmatrix} 0 & -i \\ i & 0 \end{pmatrix} \tag{3.8}$$

Every Jones matrix can in general be related to a 4×4 Mueller matrix M defined by its elements M_{ij} $(i, j = 0..3)$ as follows

$$M_{ij} = \frac{1}{2} Tr(J\sigma_j J^{\dagger}\sigma_i) \tag{3.9}$$

where $Tr(X)$ denotes the trace of the matrix X and σ_i is the Pauli matrices in Eq.(3.8).
In future calculations s_0 is normalized to 1 and preserved under transformation which means that s_1, s_2 and s_3 are the components we can have focus on. M is then reduced to a 3×3 matrix.
In analogy with Eq.(3.6) M relates ouput to input via $\hat{\mathbf{s}}_{out} = M\hat{\mathbf{s}}_{in}$

3.1.3 The Poincaré sphere

The Poincaré sphere [Poi92, Jer54] is a useful tool which enables one to represent the SOP and to easily display a transformation of polarization .

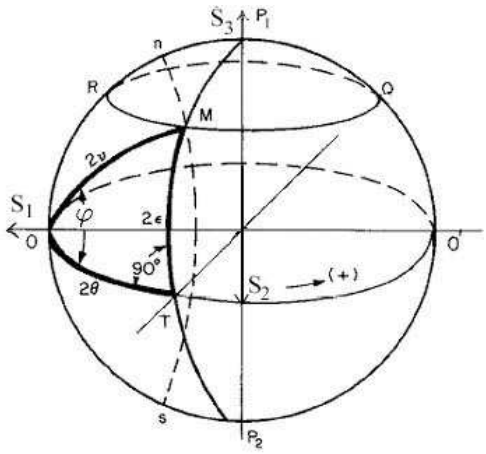

Figure 3.2: *The Poincaré sphere showing the representation of an elliptically polarized vibration by a point M. From the spherical triangle OMT the parameters of the vibration can be found. Points on the equator OO' represent linearly polarized light. The sense of rotation of the ellipse is left and right in the upper and lower hemispheres respectively. The poles P_1 and P_2 represent left and right circularly polarized light respectively [Jer82].*

A given pure SOP is completely characterized on the Poincaré sphere by a point M (see Fig.3.2), whose Cartesian coordinates are the Stokes parameters

$$\hat{\mathbf{s}}(\epsilon,\theta) = \begin{pmatrix} 1 \\ s_1/s_0 \\ s_2/s_0 \\ s_3/s_0 \end{pmatrix} = \begin{pmatrix} 1 \\ \cos 2\epsilon \cos 2\theta \\ \cos 2\epsilon \sin 2\theta \\ \sin 2\epsilon \end{pmatrix} = \begin{pmatrix} 1 \\ \cos 2\nu \\ \sin 2\nu \cos\varphi \\ \sin 2\nu \sin\varphi \end{pmatrix} \tag{3.10}$$

where θ is the azimuth and ϵ the ellipticity.

3.1.4 Degree of polarization and depolarization

When the Mueller matrix M is affected by depolarization the output degree of polarization changes.

The degree of polarization (DOP) , P, is defined by the polarized part of the wave intensity-total intensity ratio,

$$P = \frac{I_{pol}}{I_{tot}} = \frac{\sqrt{s_1^2 + s_2^2 + s_3^2}}{s_0} \, , 0 \leq P \leq 1. \tag{3.11}$$

If $P = 0$, the wave is not polarized and if $P = 1$, the wave is completely polarized.
Partially polarized signals can be represented by augmenting the Poincaré sphere with another sphere whose radius is the total signal power, I_{tot}. The ratio of the radii of the spheres is the DOP. The difference of the radii is the unpolarized power $I_u = I_{tot} - I_{pol}$. By normalizing the total power to unity the inner Poincaré sphere has radius P and will shrink or grow in diameter as the DOP changes. Changes in the polarized part of the signal cause the SOP to move on the surface of the Poincaré sphere.
The term depolarization has come to mean the decrease of the DOP of an incident light beam. DOP is often proposed as an alternative to the BER (bit-error rate) as a feedback parameter in optical communication.

3.1.5 Comparison of Mueller calculus and Jones calculus

The Mueller matrices, which are essentially an offspring of the Jones formalism, give a description of non-pure states with which the Jones calculus is incapable of dealing.
There are many similarities between the two formalisms, but the differences given in [Shu62] is important.

1. Only the Mueller calculus can be used for depolarization problems. the Jones calculus is useful only for completely polarized beams.

2. Only the Jones calculus gives information on absolute phase.

3. The Stokes vector used with Mueller calculus gives intensity directly. In the Jones calculus, intensity is obtained as the sum of the squares of the elements.

4. Jones matrices and Mueller matrices are associated with amplitude transmittance and intensity transmittance respectively

5. The Mueller matrix of a train of polarizing devices contains redundant information, the Jones matrix does not.

6. The Jones calculus allows the result of the passage of light through n devices to be expressed in terms of n, the Mueller calculus does not.

3.2 Fiber Modes experiencing birefringence

Light propagation in optical fibers is described by propagation modes [SL83], based on solutions of Helmholtz's equation[1], which is derivable from Maxwell's equations. See appendix A for derivation of the Helmholtz's equation. Modes as TE, TM, HE and EH are exact solutions of the Helmholtz's equation and LP modes, which are approximations are linearly polarized modes.
In a single mode fiber designed to have a cutoff[2] just below the wavelength of operation only the HE_{11} mode propagates which corresponds to the LP_{01} mode. Having determined a radial orientation for this mode there exists a similar mode with orthogonal polarization and the same propagation constant β.
This means that we have two degenerated modes which usually is denoted LP_{0x} and LP_{0y} in the literature.
However, in a real fiber, the degeneration between the linearly polarized modes LP_{0x} and LP_{0y} is removed and the fiber shows the phenomenon of *birefringence*. Following the formalism of Eq.(3.1) the expression of the electrical field of the LP_0 modes can be written as

[1]Solving Helmholz's equations for any possible combination of fiber parameters is a difficult task but necessary to do in order to design a fiber with the characteristics required.

[2]See Appendix A.1 for an overview of the different modes that can exist in a single- or multimode (MMF) fiber. As the number of modes increase, the effects of modal dispersion increase. Modal dispersion (intermodal dispersion) means that modes arrive at the fiber end at slightly different times. This time difference causes the light pulse to spread. Modal dispersion affects system bandwidth.

$$\mathbf{E} = \begin{pmatrix} E_x(z,t) \\ E_y(z,t) \end{pmatrix} = \begin{pmatrix} E_{ox}e^{i(\omega t - \beta_x z + \varphi_x)} \\ E_{oy}e^{i(\omega t - \beta_y z + \varphi_y)} \end{pmatrix} \tag{3.12}$$

where $\Delta\beta = \beta_x - \beta_y$ measures the fibers birefringence. Due to birefringence, the polarization of a monochromatic field shows periodic evolution during propagation with a period equation equal to $L_b = 2\pi/(\Delta\beta)$, called beat length. In other words the fiber shows the same SOP at z and $z + L_b$. Birefringence is the origin to Polarization mode dispersion, treated in the next chapter (section 4.2).
In a model fiber where the refractive index profile is radially symmetric and the direction of propagation is linear, plane polarized light launched into the fiber is not disturbed. It may be thought to split into two components in the arbitrary polarization modes which travel at the same velocity and can be recombined at any point to be plane polarized in the same direction. Eq.(3.12) does not take into account mode coupling, as there is no mechanism that would cause coupling between the LP_0-modes. If the model fiber is disturbed such that the refractive index profile is changed then mode coupling can be considered.

Chapter 4

Linear effects

This chapter gives a brief introduction to linear effects that leads to system degradation in optical communication, where the main focus will be on the effects that somehow change the input polarization (ISOP). The theory of polarization mode dispersion, which will be applied in calculations in chapter 6 and 7 will be treated in detail.
The basic principles of the linear effects treated in this chapter is covered in several books such as [MS01, Kar03b].

4.1 Chromatic dispersion

Chromatic dispersion is a variation in the velocity of light according to wavelength. This variation causes the pulses of a modulated laser source to broaden when travelling through the fiber; up to a point where pulses overlap and bit error rate increases.

Mathematically, the effects of chromatic dispersion are accounted for by expanding the mode-propagation constant β from Eq.(3.1) in a Taylor series about the frequency ω_0 at which the pulse spectrum is centered[1]

$$\beta(\omega) = n(\omega)\frac{\omega}{c} = \beta_0(\omega_0)+\beta_1(\omega-\omega_0)+\frac{1}{2}\beta_2(\omega-\omega_0)^2+\frac{1}{6}\beta_3(\omega-\omega_0)^3..., \quad (4.1)$$

[1]The scalar approach of Eq.(4.1) only deal with one mode. Due to refractive index fluctuations in different directions the propagation constants of the different LP_0-modes, $\beta_x(\omega)$ and $\beta_y(\omega)$, needs to be treated separately. The vector nature is treated in the next section.

where

$$\beta_m = \left(\frac{d^m\beta}{d\omega^m}\right)_{\omega=\omega_0} \quad \text{where } m = 0, 1, 2... \tag{4.2}$$

The parameters β_1 and β_2 are related to the refractive index n and its derivatives through the relations

$$\beta_1 = \frac{1}{v_g} = \frac{n_g}{c} = \frac{1}{c}\left(n + \omega\frac{dn}{d\omega}\right) \tag{4.3}$$

$$\beta_2 = \frac{1}{c}\left(2\frac{dn}{d\omega} + \omega\frac{d^2n}{d\omega^2}\right) \tag{4.4}$$

where n_g is the group index and v_g is the group velocity. A pulse envelope move at the group velocity $v_g = 1/\beta_1$ while β_2 represents dispersion of the group velocity and it corresponds to pulse broadening due to frequency dependent group velocity. This is known as group-velocity dispersion (GVD). β_3 accounts for the third order dispersion (TOD) which distort ultrashort pulses.
The more commonly used dispersion parameter is given by

$$D = \frac{d\beta_1}{d\lambda} = -\frac{2\pi c}{\lambda^2}\beta_2 \approx \frac{\lambda}{c}\frac{d^2n}{d\lambda^2}\left[\frac{\text{ps}}{\text{nmkm}}\right] \tag{4.5}$$

For standard single mode fibre $D = 0$ near 1.3 μm. Above 1.3 μm, where $D > 0$ ($\beta_2 < 0$) is called anomalous dispersion while the region where $D < 0$ is called normal dispersion. The third order dispersion parameter can be expressed as

$$\beta_3 = \frac{\lambda^4}{(2\pi c)^2}\left(\frac{dD}{d\lambda} + \frac{2}{\lambda}D\right) \tag{4.6}$$

and can be neglected except very close to the wavelength where $D = 0$.

4.2 Polarization mode dispersion

A pulse can broaden even in the case of no chromatic dispersion. Polarization mode dispersion (PMD) [FP91] is a problem associated with difference arrival time of light in different polarizations. Today's fiber exhibits PMD that can be smaller by orders of magnitude than older, currently laid-out fiber, which is mostly due to a much improved manufacturing process.

Replacing old fiber, however, is very costly. Therefore understanding and compensating PMD is of great importance.

The asymmetries in circular geometry and stresses in the fiber core lead to a polarization dependent refractive index n, and propagation constant β. This propagation difference between the LP_0 modes corresponds to the birefringence, which varies randomly along the fibre and leads to pulse spreading.

In a short section of fiber the birefringence can be considered uniform. The difference between the propagation constants of the fast and slow modes can be defined as

$$\Delta\beta_0(\omega_0) = \beta_{0x}(\omega_0) - \beta_{0y}(\omega_0) = \frac{\omega_0 n_s}{c} - \frac{\omega_0 n_f}{c} = \frac{\omega_0 \Delta n}{c} \tag{4.7}$$

where $\Delta n = n_s - n_f$ is the differential effective refractive index between the slow and the fast mode where LP_{0x} is chosen as the slow mode and LP_{0y} as the fast mode.

When a linearly polarized input wave is launched 45° to the birefringent axis into a short fiber, the SOP evolves in a cyclic fashion as the light propagate down the fiber to a linear state orthogonal to the launch state. In Stokes space this means that if e.g. an average input Stokes vector lies along the S_2 axis, $\hat{\mathbf{s}} = (0, 1, 0)^T$ (as is the case for a PDM scheme with two orthogonal input Stokes vectors $\hat{\mathbf{s}}_A = (1, 0, 0)^T$ and $\hat{\mathbf{s}}_B = (-1, 0, 0)^T$) and is 90° opposed to the birefringent axe which lies along the S_1-axis, the polarization will evolve through the circular polarizations and the orthogonal polarization,$\hat{\mathbf{s}} = (0, -1, 0)^T$.
Analogously, for fixed-input SOP, if the frequency is varied, the output SOP will cycle in the same way through the various states. The frequency-domain picture of PMD is shown in Fig.(4.1), for a launch state near the birefringent axis. The output polarization traces out a circle on the surface of the Poincaré sphere. This cycle trace corresponds to the beat length $L_b = \frac{\lambda}{\Delta n}$ (defined in chapter 3.2), or the propagation distance for which a 2π phase difference accumulates between the two LP_0 modes.
In the time-domain picture, for a short fiber section, the different group delay (DGD), $\Delta\tau$, which is defined as the group-delay difference between the slow and fast modes can be expressed as

$$\frac{\Delta\tau}{L} = \beta_{1x}(\omega_0) - \beta_{1y}(\omega_0) = \frac{d}{d\omega}\left(\frac{\omega\Delta n}{c}\right) = \frac{\Delta n}{c} + \frac{\omega}{c}\frac{dn}{d\omega} \tag{4.8}$$

where $\frac{\Delta\tau}{L}$ is often expressed in units of picoseconds per kilometer of fiber length[2]. The time domain effect of PMD in a short fiber is illustrated in

[2]From a statistical viewpoint $\Delta\tau$ has a Maxwellian probability distribution and the mean DGD, $\overline{\Delta\tau}$, increases with $\sqrt{z}$ [FP91]. See section 4.2.1.

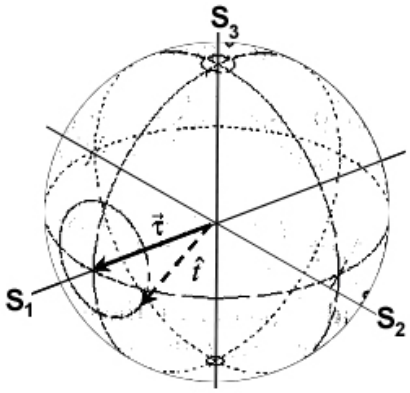

Figure 4.1: *Frequency-domain picture of PMD for a launch state on the azimuth near the birefringent S_1-axis.*

Fig.(4.2). We can write DGD for a single beat length, L_b as

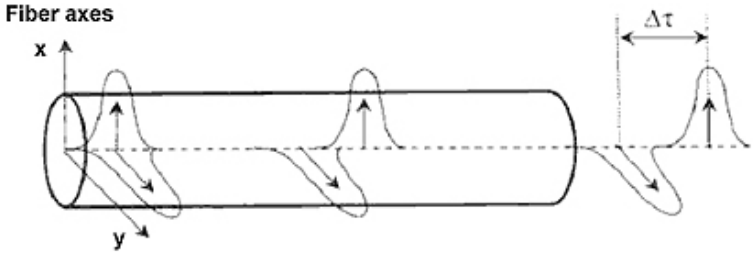

Figure 4.2: *Schematic of how PMD behaves in the time-domain. A pulse launched with equal power on the two birefringent axes results in two pulses at the output separated by the differential group delay $\Delta\tau$.*

$$\Delta\tau_b = L_b \frac{\Delta n}{c} = \frac{\lambda}{c} = \frac{1}{\upsilon} \tag{4.9}$$

which is equal to an optical cycle.

4.2.1 Polarization mode coupling

It is the random variations in the axes of birefringence along the fiber length that causes polarization-mode coupling (treated in [FYP90, FYP85])

wherein the fast and slow polarization modes from one segment each decompose into both the fast and slow modes of the next segment.
This coupling results from localized stress during spooling/cabling/deployment from splices and components, from variations in the fiber drawing process and from intentional spinning during drawing, which induces mode coupling at "meter" length. Long fibers are usually modeled as a concatenation of birefringent sections whose birefringence axes and magnitude change randomly along the fiber. This is illustrated in Fig.(4.3) The concatenation

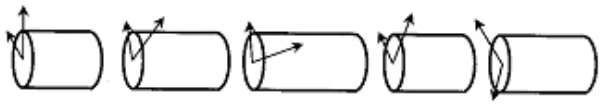

Figure 4.3: *A concatenation of fiber elements with varying birefringence axes.*

model which indicates that fiber can be represented by a 2×2 frequency-dependent complex transformation matrix in Jones space of the form

$$\mathbf{T}(\omega) = e^{k(\omega)}\mathbf{J}(\omega) = e^{k(\omega)} \begin{pmatrix} J_1 & J_2 \\ -J_2^* & J_1^* \end{pmatrix} \tag{4.10}$$

where $\omega = \omega_0 + \Delta\omega$ represents the angular frequency deviation from the carrier ω_0.
To simulate $J(\omega)$, the fiber is modelled as a concatenation of N polarization-maintaining fibers with varying group delays and orientations of the principal axes. Generally N larger than 100 is required to get realistic PMD statistics. Mathematically $J(\omega)$ is given by

$$J(\omega) = \prod_{i=1}^{N} P_i(\omega) \cdot R_i, \tag{4.11}$$

where

$$P_i(\omega) = \begin{pmatrix} e^{i\frac{\Delta\tau_i}{2}\omega} & 0 \\ 0 & e^{-i\frac{\Delta\tau_i}{2}\omega} \end{pmatrix}, \tag{4.12}$$

and

$$R_i = \begin{pmatrix} \cos(\theta_i)e^{i\frac{\phi_i}{2}} & \sin(\theta_i)e^{i\frac{\phi_i}{2}} \\ -\sin(\theta_i)e^{-i\frac{\phi_i}{2}} & \cos(\theta_i)e^{-i\frac{\phi_i}{2}} \end{pmatrix} \tag{4.13}$$

Here $\Delta\tau_i$ represent the group delay induced by the i^{th} section, and is generated following a uniform distribution. R_i gives a frequency-independent

coordinate transformation of the principal axes where θ_i and ϕ_i denote the random polarization and phase angle respectively. These are randomly generated following a uniform distribution with $\theta_i \in [0; 2\pi\rangle$ and $\phi_i \in [-\pi/2; \pi/2]$ Due to the mode coupling the DGD accumulates as a three dimensional random walk and on average increases with square of the fiber length[3], $\sqrt{z}$. Since the mode coupling is determined by the environment, variations in external stresses will change the mode coupling and fiber's DGD. Therefore, a statistical treatment of PMD must be developed.
The correlation length L_c (sometimes denoted the coupling length in the literature) parameter categorizes a fiber in the short- or long-length regime. The random coupling between two LP_0-modes of a fiber with mostly uniform birefringence subject to random perturbation or weak random coupling between two fiber sections are described by this parameter. The evolution of the polarizations as a function of length in an ensemble of fibers with statistically equivalent perturbations is considered. While the ISOP is fixed, it is equally probable to observe any SOP at large length. The difference of the ensemble averages of the power in the x and y polarization characterize the evolution. The statistical PMD theory expresses the linking between the mean square DGD of the fiber to L_b and L_c as

$$\langle \Delta\tau^2 \rangle = 2 \left(\Delta\tau_b \frac{L_c}{L_b} \right)^2 \left(\frac{L}{L_c} + e^{\frac{-L}{L_c}} - 1 \right). \tag{4.15}$$

.

4.2.2 Principal States of Polarization

As the local birefringence axes changes randomly at each section, the mode propagation in a long fiber length is very complicated.
However, two special orthogonal SOP at the fiber input that result in an input pulse that is undistorted to first order can still be found. The Principal States Model developed by Poole and Wagner[4] [CR86] was the first used to

[3] In the statistic theory of PMD the mean DGD ,$\overline{\Delta\tau}$ increases with the square root of the link length z. The mean DGD and standard deviation are given by

$$\overline{\Delta\tau} = \sqrt{\frac{8zL_h}{3\pi}} \Delta\beta_1, \ \sigma_{\Delta\tau} = \sqrt{\frac{(3\pi - 9)zL_h}{3\pi}} \Delta\beta_1 \tag{4.14}$$

where L_h defines the characteristic length of the random mode coupling (the inverse distance over which the power is scrambled over two modes) and $\Delta\beta_1 = \beta_{1x} - \beta_{1y}$. $\overline{\Delta\tau}/\sqrt{\text{z}}$ $\left[\frac{\text{ps}}{\sqrt{\text{km}}}\right]$ is referred to as PMD coefficent which will be useful in Optsim simulations later.

[4] See Appendix B for derivation of the PSPs.

explained this phenomena. The Principle States Model, which provides both a time and a frequency domain, is used for the characterization of PMD, including random mode coupling.
It states that for every frequency component of the field, there are two special SOPs, called the principal states of polarization (PSPs). And for each pairs of PSPs at the fiber input, there is a corresponding PSPs at the fiber output. A PSP is defined as that ISOP for which the output SOP is independent of frequency to first order, i.e. over a small frequency range. The PSPs are orthogonal in the absence of polarization-dependent loss. There is a corresponding pair of orthogonal PSPs at the fiber output for each pair of input PSPs, which are related by the fiber's transformation matrix from Eq.(4.10). The Jones transformation can of course also be converted to a Mueller rotation Matrix to take into account depolarization effects.

4.2.3 The PMD vector

Using the Principal States model, PMD can be described more concisely by the PMD vector:

$$\boldsymbol{\tau}(\omega) = \Delta\tau(\omega) \cdot \hat{\mathbf{q}}(\omega) \tag{4.16}$$

where, in the time domain,$|\boldsymbol{\tau}| = \Delta\tau$ indicates the DGD between light polarized along the two PSPs, and the direction $\hat{\boldsymbol{q}}$, a Stokes vector, represents the slow output PSP. The PMD vector is also very often denoted as $\boldsymbol{\Omega}$ in the literature [FP91].
Given a constant ISOP to the fiber, PMD will manifest as a change in output polarization Stokes vector $\hat{\mathbf{s}}$ with frequency according to [ACDM87]

$$\frac{d\hat{\mathbf{s}}(\omega)}{d\omega} = \boldsymbol{\tau} \times \hat{\mathbf{s}}(\omega) \tag{4.17}$$

This equation might be taken as the definition of the PMD-vector, but it should be noted that the equation is restricted to the case of fibers with negligible PDL.

The direction of $\hat{\mathbf{s}}(\omega)$ relative to $\boldsymbol{\tau}(\omega)$ determines the angle of precession, whereas we can conclude that the the length of the PMD vector determines the rate of polarization change with frequency. As we can see from Eq.(4.17), the SOPs parallel and antiparallel with the PMD-vector will (to first order in ω) not change with wavelength, and those states correspond principal states of polarizations.
A length of polarization-maintaining fiber (PMF) has a constant PMD vector where DGD and the direction do not change with frequency. As illustrated in Fig.(4.1), the output vector will trace out a circle on the Poincaré

sphere as the frequency is varied for this simple case. However, both the direction and magnitude of $\boldsymbol{\tau}$ will change with frequency in a conventional fiber. The frequency-dependence of the magnitude, $\Delta\tau$, and the components[5] which indicate the direction of $\boldsymbol{\tau}$ is shown in Fig.(4.4) Using the

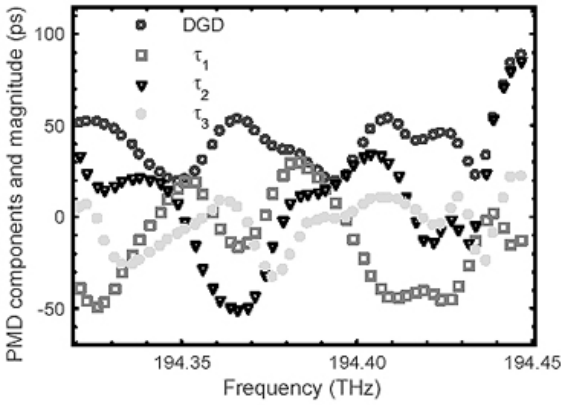

Figure 4.4: *Output PMD vector $\boldsymbol{\tau}(\omega)$ of a fiber with a mean DGD of* 35 *ps as a function of frequency [NGJK00]. The figure shows the three vector components of $\boldsymbol{\tau} = [\tau_1\ \tau_2\ \tau_3]^T$. As indicated, the measurement is done over a* 130 *Ghz spectral range .*

PSPs as an orthogonal basis set, any input or output polarization can be expressed as the vector sum of two components, each aligned with a PSP. Within the realm of first-order PMD, the output electric field from a fiber with PMD has the form

$$\mathbf{E}_{out}(t) = a|q\rangle E_{in}(t - \tau_0 - \frac{\Delta\tau}{2}) + b|q_-\rangle E_{in}(t - \tau_0 + \frac{\Delta\tau}{2}) \qquad (4.18)$$

where $E_{in}(t)$ is the input electric field, a and b are the complex weighting coefficients indicating the field amplitude launched along the slow and fast PSPs, $|q\rangle$ and $|q_-\rangle$, and τ_0 is the polarization independent transmission delay.
The dynamical PMD-equation which describe the evolution of the PMD-

[5]The components of τ_i are $\tau_1 = 2i\left(\frac{dJ_1}{d\omega}J_1^* + \frac{dJ_2}{d\omega}J_2^*\right)$, $\tau_2 = 2\mathrm{Im}\left(\frac{dJ_1}{d\omega}J_2 - \frac{dJ_2}{d\omega}J_1\right)$ and $\tau_3 = 2\mathrm{Re}\left(\frac{dJ_1}{d\omega}J_2 - \frac{dJ_2}{d\omega}J_1\right)$

vector with distance can be written [GK00]

$$\frac{\partial \boldsymbol{\tau}}{\partial z} = \frac{\partial \boldsymbol{\beta}}{\partial \omega} + \boldsymbol{\beta} \times \boldsymbol{\tau} \tag{4.19}$$

where $\boldsymbol{\beta}(\omega, z)$ represent the local birefringence. This equation represent the basis for statistical treatment of PMD.

4.2.4 Higher order PMD

For larger signal bandwidths, a Taylor series expansion of $\boldsymbol{\tau}(\omega)$ about the carrier frequency is needed. Expanding the PMD vector to nth order we can write

$$\boldsymbol{\tau}(\omega) = \boldsymbol{\tau}(\omega_0) + \boldsymbol{\tau}_\omega \Delta\omega + \frac{1}{2}\boldsymbol{\tau}_{\omega\omega}\Delta\omega^2 + ... + \frac{1}{n!}\boldsymbol{\tau}^{(n)}\Delta\omega^n \tag{4.20}$$

By now substituting Eq.(4.16) into Eq.(4.20) we get

$$\begin{aligned} \boldsymbol{\tau}(\omega) &= \Delta\tau\hat{\mathbf{q}}_0 + \left[\Delta\tau_\omega\hat{\mathbf{q}} + \Delta\tau\hat{\mathbf{q}}_\omega\right]\Delta\omega \\ &+ \frac{1}{2}\left[\Delta\tau_\omega\hat{\mathbf{q}} + 2\Delta\tau_\omega\hat{\mathbf{q}}_\omega + \Delta\tau\hat{\mathbf{q}}_{\omega\omega}\right]\Delta\omega^2 + ... + \frac{1}{n!}((\Delta\tau)\hat{\mathbf{q}})^{(n)}\Delta\omega^n \end{aligned} \tag{4.21}$$

where the second term $\tau_\omega = \Delta\tau_\omega\hat{\mathbf{q}} + \Delta\tau\hat{\mathbf{q}}_\omega = \boldsymbol{\tau}_{\omega\parallel} + \boldsymbol{\tau}_{\omega\perp}$ is called the second-order PMD and the subscript ω indicates differentiation.The component parallel to the PMD vector $\boldsymbol{\tau}_{\omega\parallel}$ is often called polarization dependent chromatic dispersion (PSD) and the orthogonal component $\boldsymbol{\tau}_{\omega\perp}$ is frequently referred to as depolarization, apparently because this is the vector that causes relative depolarization both in a PDM and polarization interleaving scheme. PCD however, does not change the direction of the PMD vector itself. Fig.(4.5) shows a vector diagram of the principal parameters and the interrelationships.

$\boldsymbol{\tau}_{\omega\parallel}$ can be considered as a polarization-dependent change in the chromatic dispersion, D from Eq.(4.5), characterized by an effective dispersion $D_{eff} = D \pm \tau_\lambda$. In accordance with customary dispersion measure, the PCD can be defined as

$$\tau_\lambda = -\left(\frac{\pi c}{\lambda^2}\right)\Delta\tau_\omega = \frac{1}{2}\frac{d\Delta\tau}{d\lambda} \tag{4.22}$$

where τ_λ is expressed in ps/nm. The theoretical scaling rule for the root mean square value of $\Delta\tau_\omega$ is [FJNK99]

$$\text{rms } \Delta\tau_\omega = \frac{\pi}{8\sqrt{3}}\overline{\Delta\tau}^2 \tag{4.23}$$

and for the rms value of the depolarization rate $|\hat{\mathbf{q}}_\omega|$ we have [FJNK01]

$$\text{rms } |\hat{\mathbf{q}}_\omega| = \sqrt{\frac{\pi}{6}}\overline{\Delta\tau} \tag{4.24}$$

As shown in [PB98], the angular speed of PSP rotation $\hat{\mathbf{q}}_\omega$ decreases with DGD $\Delta\tau$.

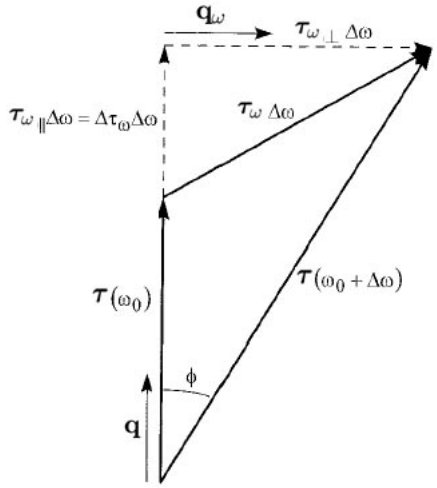

Figure 4.5: *Schematic diagram of the PMD vector $\boldsymbol{\tau}_{\omega_0}$ and the second-order PMD components showing the change of $\boldsymbol{\tau}_{\omega_0}$ with frequency. Note that $\mathbf{q}_\omega$ is perpendicular to $\mathbf{q}$. The angular rotation rate $d\phi/d\omega$ of the PMD vector $\boldsymbol{\tau}_{\omega_0}$ with ω is described by the depolarization rate $|\mathbf{q}_\omega|$.*

4.2.5 Bandwidth of the Principal states

The bandwidth of the principal state is an important concept providing guidance on the change of the PMD vector $\boldsymbol{\tau}(\omega)$ of the fiber with frequency. It is the bandwidth, $\Delta\omega_{PSP} = 2\pi\Delta\nu_{PSP}$ or the corresponding wavelength range, $\Delta\lambda_{PSP}$, over which the PMD vector is reasonably constant.
Fig.(4.6) shows different wavelengths λ_2,λ_2 and λ_3 where the PMD-vector is determined. Polarization rotation measurements at two or more frequencies are required, and these frequencies have to be confined to the range $\Delta\lambda_{PSP}$ as indicated in order to reduce inaccuracy caused by higher-order PMD. Nevertheless measured samples of $\boldsymbol{\tau}(\omega)$ seem to be statistically independent if

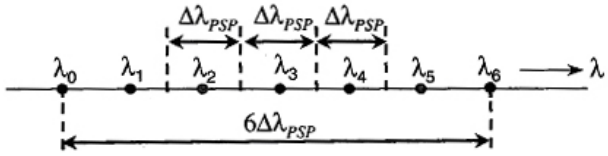

Figure 4.6: *Wavelength intervals for measurement of PMD. To avoid inaccuracy from higher order psp, $\Delta\lambda_{psp}$ should be bigger than the wavelength interval.*

their wavelengths are at least $6\lambda_{PSP}$ apart in statistical PMD measurements. This means that $\boldsymbol{\tau}(\omega_0)$ and $\boldsymbol{\tau}(\omega_6)$ from Fig.(4.6) is considered statistically independent A number of statistically independent samples, $N_{samples}$ will be yield by measurements over a spectral range from λ_{min} to λ_{max} which is given by

$$N_{samples} = \frac{\lambda_{max} - \lambda_{min}}{6\Delta\lambda_{PSP}} \tag{4.25}$$

A good practical estimate for $\Delta\omega_{PSP}$ is given by the relation [KNJ02]

$$\Delta\omega_{PSP}\overline{\Delta\tau} = \frac{\pi}{4} \tag{4.26}$$

where $\overline{\Delta\tau}$ is the mean DGD of the fiber.

4.2.6 Concatenation of PMD vectors

Using the simple but powerful concatenation rules, the total PMD vector of a series of two or more elements with known PMD vectors can be determined. The concatenation rules have been used in the analysis of how the PMD vector grows with fiber length and for statistical PMD modeling. The concatenation rules have appeared in sum, differential, and integral formulations for both first-and second-order PMD vectors [GK00].
In this section we consider only the sum rules.

To obtain the total PMD vector we transform the PMD vectors of each individual section to common reference point and take the vector sum.
The fiber in Fig.(4.7) consist of m sections, each with known Mueller matrix M_n and output PMD vector $\boldsymbol{\tau}_n$, for the first order, the sum rules, of the assembly are

$$\boldsymbol{\tau} = \sum_{n}^{m} M(m, n+1)\boldsymbol{\tau}_n \tag{4.27}$$

and for second-order PMD

$$\boldsymbol{\tau}_\omega = \sum_{n=1}^{m} M(m, n+1)(\boldsymbol{\tau}_{n\omega} + \boldsymbol{\tau}_n \times \boldsymbol{\tau}(n)) \tag{4.28}$$

where we define the Mueller matrix of the last $m - n + 1$ sections as $M(m, n) = M_m M_{m-1} ... M_n$ where $M(m, m) =$M$_m$ and $M(m, m + 1)$ is the identity matrix.

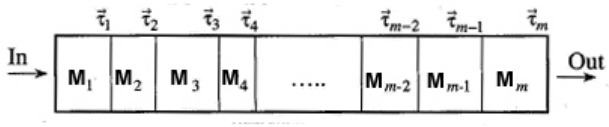

Figure 4.7: *Concatenation of PMD-vectors divided in m sections.The Mueller matrices M_n, and output PMD vectors $\boldsymbol{\tau}_n$ are known.*

4.3 Polarization dependent effects in in-line devices

When the signal spectrum is wider than the PSP's bandwidth and depolarization occurs, the presence of polarization-dependent in-line devices further decreases the DOP [IMMS96]. These effects will only be stressed qualitatively in this report, but their effects should not be underestimated in a PDM and interleaving scheme. Although a *nonlinear* polarization rotation of the Stokes vectors have to be studied in e.g. optical amplifiers [YLKD03b, YLKD03a], the effects are reviewed in this chapter due to the strong connection to PMD. All the effects should be considered in combination with PMD.

4.3.1 Polarization-dependent loss

The more complex a network become, the more important polarization-dependent loss (PDL) will be. The statistics of PDL is studied in e.g. [MS02a, MS02b]. PDL is caused by the strong polarization dependence in optical components such as WDM couplers, isolators and optical switches. A generic optical element can be described as $1 + \boldsymbol{\Gamma} \cdot \hat{\mathbf{s}}$ where $\boldsymbol{\Gamma}$ is the PDL vector and $\hat{\mathbf{s}}$ represent the unit Stokes vector corresponding to the polarization of the incident optical field. Similar to PMD, PDL is also wavelength-dependent and refers to the ratio between the highest and lowest gains of

the system expressed in decibels

$$\rho \equiv 10 \log \frac{1+\Gamma}{1-\Gamma} \tag{4.29}$$

and the evolution of ρ is Maxwellian.
The dynamical PDL equation is [BCN00]

$$\frac{\partial \mathbf{\Gamma}}{\partial z} = \boldsymbol{\beta} \times \mathbf{\Gamma} + \vec{\alpha} - \mathbf{\Gamma}(\boldsymbol{\alpha} \cdot \mathbf{\Gamma}) \tag{4.30}$$

where $\boldsymbol{\alpha}$ is the local vector of polarization-dependent loss. A good analysis of Eq.(4.30) can be found in [MS02b], which concludes that the PDL-distribution remains Maxwellian within all the relevant ranges of parameters. In [GH00] it is stressed that adding PDL to PMD is similar to adding higher-order PMD. The mean broadening of light pulses are unaffected, but the probability of occurrence of a broadening significantly larger as the mean is largely increased. PDL-induced Crosstalk in a PDM scheme is quantified by using a Jones vector approach in [GZ01].

4.3.2 Polarization-dependent gain

Polarization-dependent gain (PDG) arises when optical amplifiers are used whose gain depends on the signal polarization. A certain amount of PDG is often present in semiconductor amplifiers, while erbium-doped amplifiers[6] (EDFAs) are almost immune by the problem. An analysis of the gain dependence on the signal polarization and a good reference list can be found in [SM91].

4.3.3 Polarization hole burning

Polarization hole burning (PHB) is due to the different physical mechanisms in semiconductor amplifiers and EDFAs [BMD94]. In quantum well semiconductor amplifiers the PHB is due to the fact that the valence band is split into two bands. The two-hole populations are coupled differently with the field polarizations, so when a polarized field saturates the amplifier, a gain asymmetry is created even if the linear amplifier gain is polarization independent. The asymmetry has a duration related to the characteristic time for the equilibrium between the two valence bands.

[6]The erbium-doped amplifier is based on a single-mode fiber suitably doped with erbium ions that constitute optically active elements [BOS99].

In EDFAs, the polarization hole burning is generated by the spatial asymmetry of the emission cross section of the erbium ion. Since the ions have random orientation inside the glass matrix, a polarized optical field introduces a selective saturation, causing a gain asymmetry. Differently from the case of semiconductor amplifiers, this asymmetry is not removed by the presence of the other population and remains until the presence of the saturating field is removed .

4.4 The autocorrelation function

From an analytical point of view, it is convenient to treat the frequency difference in terms of correlation functions, i.e. to answer the question "how well are two SOPs at frequency ω_1 and ω_2 correlated? Based on the concatenation model it is possible to derive such correlations.

4.4.1 Autocorrelation function for PMD

An autocorrelation function (ACF), A, for PMD has been derived in [KB99], which can be used to calculate a statistical average of pulse broadening that is induced by PMD. A follow-up of this, and a more important result for our purpose was derived by Karlsson et al. in 2000 [KB00] where the focus is set on the temporal drift of a SOP and the decorrelation of the SOP due to frequency difference.
Based on the results in [KB00] the decorrelation time in a polarization division-multiplexing scheme, where $\omega_1 = \omega_2$, will be

$$A_{time} = E(\hat{\mathbf{s}}(t_1) \cdot \hat{\mathbf{s}}(t_2)) = -e^{-\frac{|\Delta t|}{t_d}} \tag{4.31}$$

where $\Delta t = t_1 - t_2$, and t_d is the typical drift time for the absolute polarization states which decreases with $\Delta\tau$. This is a coefficient that is unique for each fiber, and has to be measured.
In a polarization interleaving case, assuming $t_1 = t_2$, the decorrelation in wavelength is

$$A_{PMD} = E(\hat{\mathbf{s}}_A(\omega_1) \cdot \hat{\mathbf{s}}_B(\omega_2)) = -e^{-\frac{\pi\Delta\omega^2 E(\Delta\tau)^2}{8}} \tag{4.32}$$

where $\Delta\omega = \omega_1 - \omega_2$, and we have assumed $\hat{\mathbf{s}}_A^{in} \cdot \hat{\mathbf{s}}_B^{in} = -1$. Hence the larger $\Delta\tau$ or wavelength spacing, the faster is the decorrelation ($A_{PMD} \to 0$).

4.4.2 Autocorrelation function for PMD and PDL

From earlier we know that PDL also influences the orthogonality between the Stokes vectors, and is a major potential crosstalk source especially for polarization division-multiplexing.
PDL is not taken into consideration in Eq.(4.32). By using the results from [GZ04], also based on the concatenation model, we can derive an explicit ACF which consider both PMD and PDL. Assuming anti-parallell input Stokes vectors the decorrelation in wavelength is

$$A_{PMD\&PDL} = E(\hat{\mathbf{s}}_A(\omega_1) \cdot \hat{\mathbf{s}}_B(\omega_2)) = A_n^2 \left(\frac{E(\Gamma^2)}{K}(1 - e^K) - e^K \right) \quad (4.33)$$

where A_n is the global attenuation, $E(\Gamma^2)$ is the mean-square PDL and $K = \frac{1}{3}\left[E(\Gamma^2) - E((\Delta\tau)^2 - \eta^2)\Delta\omega^2\right]$ where η represents the relative attenuation of the polarization mode[7].
To compare the effect on orthogonality with and without PDL we have plotted the normalized ACFs of SOP against $\Delta\omega$ in Fig.(4.8)[8]. The figure show

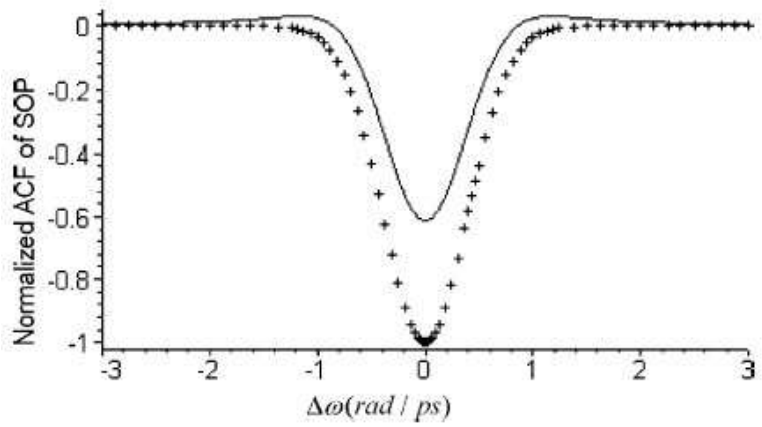

Figure 4.8: *Comparison between a normalized ACF of SOP without PDL (crossline) and a normalized ACF with PDL (solid line).*

that the ACF with PDL changes from negative to positive and approaches to zero as $|\Delta\omega|$ becomes larger - and it is always larger than the ACF without

[7]The concatenation model assumes constant birefringence and loss for each element, that is [HG97] $\beta_i \equiv \beta = \sqrt{\frac{E((\Delta\tau)^2 - \eta^2)}{n}}$ and [MS02a] $\alpha_i \equiv \alpha = \sqrt{\frac{E(\Gamma^2)}{n}}$

[8]See appendix C for Maple calculation details

PDL. Thus the combination effect of PDL and PMD can effect the orthogonality more seriously than the case without PDL. The ACF curve of SOP of the case with PDL has two positive peak points at $\pm\Delta\omega_{max}$, which can be found by numerical methods. This mean that when the channel spacing is equal to $\Delta\omega_{max}$ a polarization interleaving scheme is degraded the worst.The benefit of using polarization interleaving for suppressing crosstalk induced from four-wave mixing would also be reduced, which will be understood in chapter 5.2.2.

Chapter 5

Nonlinear effects

This chapter gives a brief introduction to nonlinear effects that leads to system degradation in optical communication. In a polarization multiplexing scheme there are mainly two important nonlinear effects which impair the transmission quality - cross-phase modulation (XPM) and four-wave mixing (FWM). The effectiveness of both of these depends on the relative polarization of the affected waves, and will be treated in the following sections.
A good overview of the nonlinear effects can be found in [Agr95, IMMS98]. In order to understand these effects properly, one needs to see how light waves interact with matter on a more fundamental level. A proper discussion of the effects uses quantum mechanics, but a classical picture is sufficient to describe a qualitative model. Brillouin and Raman scattering will not be taken into account since they are not directly related to polarization rotation.

5.1 Origin of nonlinear birefringence

The last chapter considered polarization evolution in small fiber elements where the birefringence, caused by the change in the refractive index between the LP_0-modes, can be treated linearly, and in long fibers where the birefringence experience a stochastic behavior and causes a random coupling between the modes. This effect can be modelled by applying unitary transformations on the SOP (See Eq.(4.11)).
However, when the field intensity becomes relevant, which is common for WDM systems with many channels, the nonlinearities become important and a nonlinear birefringence is induced.
The response of any optical fiber to light becomes nonlinear for intense

electromagnetic fields. Mathematically this can be described by the susceptibility $\boldsymbol{\chi}$ [Blo77] as

$$\mathbf{P} = \epsilon_0 \left(\boldsymbol{\chi}^{(1)} \cdot \mathbf{E} + \boldsymbol{\chi}^{(2)} \cdot \mathbf{EE} + \boldsymbol{\chi}^{(3)} \vdots \mathbf{EEE} + ... \right) \tag{5.1}$$

where $\mathbf{P}$ is the induced polarization[1] of the medium, $\mathbf{E}$ is the electric field and ϵ_0 is the vacuum permittivity. In general $\boldsymbol{\chi}^{(j)}$ is a tensor of rank $j+1$. The first term, $\boldsymbol{\chi}^{(1)}$, describes the linear behavior of the system whereas quadratic effects such as second-harmonic generation and sum frequency generation [She84] is described by the second term $\boldsymbol{\chi}^{(2)}$. The third term $\boldsymbol{\chi}^{(3)}$ is responsible for phase modulation and FWM. $\boldsymbol{\chi}^{(2)}$ can normally be ignored in optical fibres since SiO_2 is a symmetric molecule. However, second harmonic generation have been observed in optical fibres [Agr95].
In optical fibres at telecommunication wavelengths, the $\boldsymbol{\chi}^{(3)}$ nonlinearity is a nonresonant electronic nonlinearity, which is extremely fast, in the order of the electron round trip time 10^{-16}s [Boy92] and is dependent on the field polarization.
$\boldsymbol{\chi}^{(3)}$ is the origin of nonlinear birefringence, and following [Agr95] the nonlinear contribution to the change in the refractive indeces in each mode are given by[2]

$$\Delta n_x = n_2 \left(|E_x|^2 + \frac{2}{3}|E_y|^2 \right) \tag{5.2}$$

$$\Delta n_y = n_2 \left(|E_y|^2 + \frac{2}{3}|E_x|^2 \right) \tag{5.3}$$

where n_2 is the nonlinear refractive index respectively and $|E_{(x,y)}|^2$ is the optical intensity of the mode. When the optical field is assumed linear polarized, the relation between n_2 and χ is given by

$$n_2 = \frac{3}{8n_0} \mathrm{Re}(\chi^{(3)}_{xxx}) \tag{5.4}$$

where $\chi^{(3)}_{xxx}$ is the only component of the $\chi^{(3)}$ tensor that is involved in this case. Typical values of n_2 in optical fibres are $2.2 - 3.6 \cdot 10^{-20} \frac{\mathrm{m}^2}{\mathrm{W}}$ [PPB00].

[1] Polarization induced inside a fiber by an electromagnetic field should not be confused with the SOP of that field. The terminology is accepted for historical reasons.

[2] Here we have considered that the elements of $\boldsymbol{\chi}^{(3)}$ has the same magnitude, which is a good approximation in silica fibers

The first term in Eqs.(5.2-5.3) is responsible for self-phase modulation[3] (SPM), and the second term results in cross-phase modulation (XPM) which we will have a closer look at in the next sections.

5.2 The coupled Nonlinear Schrödinger equations

Based on [Agr95] the propagation equation for the two principal polarizations in a birefringent fiber can be obtained by factoring out the transverse dependence on the electric field components E_x and E_y

$$E_j(\mathbf{r},t) = F(x,y)A_j(z,t)e^{iB_{0j}z} \tag{5.5}$$

where $F(x,y)$ describes the spatial distribution of the single mode, $A_j(z,t)$ is the slowly varying amplitude envelope and and B_0 is the propagation constant $(j = x, y)$.
$A_j(z,t)$ satisfy the relation $s_i = (\mathbf{A}^\dagger \sigma_i \mathbf{A})$ where s_i represents the Stokes components, which corresponds to Eq.(3.7) where Jones and Stokes vectors are related. A_x and A_y then relates to the components of $|s\rangle$.

Making allowance for PMD (including polarization mode coupling) and PDL, the slowly varying amplitudes, A_x and A_y, are described by the following set of two coupled stochastic nonlinear Schrödinger equations (NLS) [She84]

$$\begin{aligned} \frac{\partial A_x}{\partial z} &+ \beta_{1x}\frac{\partial A_x}{\partial t} + \frac{i\beta_2}{2}\frac{\partial^2 A_x}{\partial t^2} + \frac{\alpha_x}{2}A_x - \frac{1}{6}\beta_3\frac{\partial^3 A_x}{\partial t^3} + i\kappa(z)A_y e^{-i\Delta\beta_0 z} \\ &= i\gamma\left(|A_x|^2 + \frac{2}{3}|A_y|^2\right)A_x + \frac{i\gamma}{3}A_x^* A_y^2 e^{-2i\Delta\beta_0 z} \end{aligned} \tag{5.6}$$

$$\begin{aligned} \frac{\partial A_y}{\partial z} &+ \beta_{1y}\frac{\partial A_y}{\partial t} + \frac{i\beta_2}{2}\frac{\partial^2 A_y}{\partial t^2} + \frac{\alpha_y}{2}A_y - \frac{1}{6}\beta_3\frac{\partial^3 A_y}{\partial t^3} - i\kappa^*(z)A_x e^{+i\Delta\beta_0 z} \\ &= i\gamma\left(|A_y|^2 + \frac{2}{3}|A_x|^2\right)A_y + \frac{i\gamma}{3}A_y^* A_x^2 e^{+2i\Delta\beta_0 z} \end{aligned} \tag{5.7}$$

[3]Self-phase modulation refers to the self-induced phase shift experienced by an optical field during its propagation in the fiber. SPM is responsible for spectral broadening of ultrashort pulses [SL78] and formation of optical solitons in the anomalous-dispersion regime of fibers [HT73].

where $\kappa(z)$ is the random mode coupling coefficient, $\Delta\beta_0$ is the birefringence parameter defined in Eq.(4.7), α_x and α_y are the losses for the two LP_0 modes and the nonlinear parameter γ is given by

$$\gamma = \frac{n_2\omega}{cA_{eff}} \tag{5.8}$$

with the nonlinear index coefficient n_2 and the effective core area A_{eff}.
The average loss is given by $\alpha = (\alpha_x + \alpha_y)/2$, while $\Delta\alpha = \alpha_y - \alpha_x$ represent the PDL.

The term $\frac{2}{3}i\gamma|A_y|^2A_x$ from Eq.(5.6) and the term $\frac{2}{3}i\gamma|A_x|^2A_y$ from Eq.(5.7) show that XPM occur between different polarization components, not only between different frequency components. The frequency dependence is emphazised in chapter 5.2.1.
Another interaction among the polarization components is given by the term $\frac{i\gamma}{3}A_x^*A_y^2exp(-2i\Delta\beta_0 z)$ in the first equation and by an analogous term in the second; this interaction depends on the fiber birefringence, and leads to degenerate (interaction on the same frequency) FWM.

However, if the fiber length $L >> L_b$, the last term in Eqs.(5.6-5.7) changes sign often and its contribution averages out to zero. In highly birefringent fibers ($L_b \sim 1$ cm typically), the FWM term can often be neglected for this reason. The non-degenerate case of FWM is treated in Section 5.2.2.

To get analytical insight of Eqs.(5.6-5.7) more simplifications have to be made. It is now assumed that the fiber is linear birefringent (neglecting the random mode coupling),polarization dependent loss can be neglected ($\alpha_x = \alpha_y$) and that the third-order dispersion β_3 can be neglected since β_2 not equals zero.The reduced equations now become

$$\begin{aligned}&\frac{\partial A_x}{\partial z} + \beta_{1x}\frac{\partial A_x}{\partial t} + \frac{i\beta_2}{2}\frac{\partial^2 A_x}{\partial t^2} + \frac{\alpha}{2}A_x \\ &= i\gamma\left(|A_x|^2 + \frac{2}{3}|A_y|^2\right)A_x\end{aligned} \tag{5.9}$$

$$\begin{aligned}&\frac{\partial A_y}{\partial z} + \beta_{1y}\frac{\partial A_y}{\partial t} + \frac{i\beta_2}{2}\frac{\partial^2 A_y}{\partial t^2} + \frac{\alpha}{2}A_y \\ &= i\gamma\left(|A_y|^2 + \frac{2}{3}|A_x|^2\right)A_y\end{aligned} \tag{5.10}$$

which we will make use of in the analysis of XPM in the next section.

5.2.1 Cross-phase modulation (XPM)

Cross-phase modulation refers to the nonlinear phase shift of an optical field induced by another field having a different wavelength, direction or SOP.
In a WDM-fiber XPM induces a rapid change of the SOP on each channel [WM99].
When analyzing XPM, two co-propagating waves have to be considered. The total optical field can be written

$$\begin{aligned}\mathbf{E}(\mathbf{r},t) &= \frac{1}{2}\left(e^{-i\omega_A t}|s_A\rangle + e^{-i\omega_B t}|s_B\rangle\right) \\ &= \frac{1}{2}\left[(E^A_{ox}(t)+E^A_{oy}(t))e^{-i\omega_A t} + (E^B_{ox}(t)+E^B_{oy}(t))e^{-i\omega_B t}\right]\end{aligned} \tag{5.11}$$

and following the method of Eq.(5.5) by using Eqs.(5.9-5.10) this result in four coupled NLS equations for the amplitude envelopes A^A_x, A^A_y, A^B_x and A^B_y.

$$\begin{aligned}&\frac{\partial A^A_{(x,y)}}{\partial z} + \beta^A_{1\,(x,y)}\frac{\partial A^A_{(x,y)}}{\partial t} + \frac{i\beta_{BA}}{2}\frac{\partial (A^A_{(x,y)})^2}{\partial t^2} + \frac{\alpha^A}{2}A^A_{(x,y)} \\ &= i\gamma_A\left(|A^A_{(x,y)}|^2 + 2|A^B_{(x,y)}|^2 + \frac{2}{3}|A^A_{(y,x)}|^2 + \frac{2}{3}|A^B_{(y,x)}|^2\right)A^A_{(x,y))}\end{aligned} \tag{5.12}$$

$$\begin{aligned}&\frac{\partial A^B_{(x,y)}}{\partial z} + \beta^B_{1\,(x,y)}\frac{\partial A_{B(x,y)}}{\partial t} + \frac{i\beta_{BB}}{2}\frac{\partial (A^B_{(x,y)})^2}{\partial t^2} + \frac{\alpha_B}{2}A^B_{(x,y)} \\ &= i\gamma_B\left(|A^B_{(x,y)}|^2 + 2|A^A_{(x,y)}|^2 + \frac{2}{3}|A^B_{(y,x)}|^2 + \frac{2}{3}|A^A_{(y,x)}|^2\right)A^B_{(x,y)}\end{aligned} \tag{5.13}$$

The normal terms on the right-hand sides of Eqs.(5.12-5.13) describe the effects of SPM and XPM. In particular, of our interest, the terms describing XPM for the parallel polarized ($A^A_y = A^B_y = 0$) and orthogonally polarized ($A^A_y = A^B_x = 0$) cases are

- Parallel waves ($A^A_y = A^B_y = 0$) :2i$\gamma_A|A^B_x|^2A^A_x$ and $2i\gamma_B|A^A_x|^2A^B_x$
- Orthogonal waves ($A^A_y = A^B_x = 0$) :2/3 i$\gamma_A|A^B_x|^2A^A_x$ and $\frac{2}{3}i\gamma_B|A^A_x|^2A^B_x$

Comparing these terms it leads to the conclusion that XPM between two co-propagating waves is reduced by a factor of $\frac{2}{3}$ if both waves are orthogonally polarized compared to parallel polarization.

Following [CB00a] it can also be shown, by neglecting linear effects as PMD and PDL, that no polarization evolution takes place between orthogonally polarized signals. This can be understood from

$$\frac{\partial \hat{\boldsymbol{s}}_A}{\partial z} = \frac{8}{9}\gamma s_0(\hat{\boldsymbol{s}}_A \times \hat{\boldsymbol{s}}_B) \text{ and } \frac{\partial \hat{\boldsymbol{s}}_B}{\partial z} = \frac{8}{9}\gamma s_0(\hat{\boldsymbol{s}}_B \times \hat{\boldsymbol{s}}_A) \tag{5.14}$$

where $\hat{\boldsymbol{s}}_A$ and $\hat{\boldsymbol{s}}_B$ represent the Stokes vectors of the two channels, and it is assumed, for simplicity, the same optical power, s_0. By reformulating Eq.(5.14) it can be also be shown that there is no polarization evolution for co-polarized signals.
This indicates that the Stokes vectors of both fields precess at the same rate. The length of fiber required for a complete precession is given by the XPM-beat length

$$L_B = \frac{9\pi}{8\gamma s_0 \cos\xi} \tag{5.15}$$

where 2ξ is the angle between the Stokes vectors $\hat{\boldsymbol{s}}_A$ and $\hat{\boldsymbol{s}}_B$.

In long transmission lines, however, PMD eventually spoils the initial relative polarization alignment of channels of different wavelengths. This effect triggers XPM induced depolarization in systems where channels are orthogonally launched.

The study of depolarization due to the interaction of XPM, SPM and PMD has been tackled in several experimental works and some theoretical works [Kik01, MCB01, CB00b]. In [Kik01],the focus is on the analysis by simulation of the depolarization induced by SPM and its dependence on the transmitted pulse chirp, and in [CB00b] it is experimentally shown that if the SOPs of the WDM channels are launched in such a way that the overall input DOP is minimized, the effects of XPM are also minimized and the output DOP is maximized.

5.2.2 Four wave mixing (FWM)

In every WDM system, it is important to eliminate the effect of four-wave mixing (FWM[4]).
FWM induces channel crosstalk which limits the capacity of WDM transmission, particulary over optical dispersion shifted fibers (DSF). FWM is a parametric process, in which three optical fields, propagating at different frequencies (non-degenerate case) in the same direction along a fiber, producing a fourth field, propagating in the same direction, which drains power

[4]In the field of Quantum Optics, four wave mixing is referred to as four photon mixing, which is a four photon process which photons are annihilated and created.

from the originating three fields.
The effectiveness of FWM depends on a phase-matching condition to be fulfilled, but like XPM, also on the polarizations of the affected waves.
Due to chromatic dispersion, the phase-matching condition requires the frequency separation of the originating waves bo be relatively small, in order for FWM to reach significant proportions.
As will be shown, proper alignment of channel polarizations can further reduce FWM efficiency.
For an extensive theoretical treatment of FWM in fiber with random birefringence, [MKJ+04] is a good reference.

Suppression of Four-wave mixing employing orthogonal polarizations

Analysis of the FWM process requires a lot of algebra - this has been accomplished in [Ino92]. We allow us to reproduce the results in this section.

The nonlinear light amplitude E^{NL} is used to describe the FWM light at frequency ω_D, which relates to the originating frequencies as $\omega_D = \omega_A + \omega_B - \omega_C$. The total nonlinear amplitude vector is found to be

$$\mathbf{E}^{NL} = \eta |E_1(0)||E_2(0)||E_3(0)| \cdot (\langle s_C|s_B\rangle |s_A\rangle + \langle s_C|s_A\rangle |s_B\rangle) \tag{5.16}$$

where η satisfy

$$\eta = i\frac{2\pi\omega}{nc} D\xi^{(3)}_{1122} \frac{1-e^{-\alpha L}}{\alpha} e^{-(\alpha/2)L} \tag{5.17}$$

where D is a degeneracy factor, $\xi^{(3)}_{1122}$ is the tensor component of the third-order nonlinear susceptibility and α is the fiber loss coefficient. $|E_j(0)|$ where $(j = A, B, C)$ are the amplitudes at $z = 0$ and the relative polarization states are represented by normalized Jones vectors $|s\rangle_j$, which is assumed to be maintained throughout the fiber.
For the case where all waves are identically polarized ($\langle s_i|s_j\rangle_{i\neq j} = 1$ for $i, j = A, B, C$) Eq.(5.16) can be rewritten as

$$\mathbf{E}^{NL} = 2\eta |E_1(0)||E_2(0)||E_3(0)| \cdot |s_A\rangle \tag{5.18}$$

and

$$|\mathbf{E}^{NL}|^2 = 4|\eta|^2 |E_1(0)|^2 |E_2(0)|^2 |E_3(0)|^2. \tag{5.19}$$

Similarly, one can obtain the result for the case of two waves being co-polarized, and the third being orthogonal polarized ($|s_A\rangle \perp |s_B\rangle = |s_C\rangle$

which means $\langle s_C|s_B\rangle = 1$ and $\langle s_C|s_A\rangle = 0$) The square of the nonlinear amplitude now becomes

$$|\mathbf{E}^{NL}|^2 = |\eta|^2|E_1(0)|^2|E_2(0)|^2|E_3(0)|^2. \tag{5.20}$$

and FWM efficiency drops to 1/4 compared to the case of all waves having identical polarization.
For the case $|s_A\rangle = |s_B\rangle \perp |s_C\rangle$ both $\langle s_C|s_B\rangle = 0$ and $\langle s_C|s_A\rangle = 0$, and FWM efficiency becomes zero.
If the situation is $|s_A\rangle = |s_C\rangle \perp |s_B\rangle$, as in a polarization interleaving case, FWM efficiency will also become 1/4, but the output polarization of the generated wave will be $|s_B\rangle$ instead of $|s_A\rangle$.
Based on these results an orthogonal polarization launch scheme seems like a good approach to reduce FWM crosstalk when the channel spacing is tight in WDM systems.
For both nonlinear effects, XPM and FWM, to be effectively reduced, it is necessary for the waves to remain orthogonally polarized throughout the fiber. PMD, however, not only alters the SOP of each wave as it propagates along the fiber, but its frequency-dependence also leads to a non-uniform change of each channel SOP which causes relative polarizations to vary as the waves propagate the optical fiber. The ACF for PMD (Eq.(4.32)) shows clearly that polarization multiplexing is is less effective for suppressing FWM-crosstalk in long transmission links (with high DGD) and links with high channel spacings. Fig.(5.1) shows how FWM efficiency changes with fiber distance with the influence of PMD for orthogonal polarizations. The PMD coefficient is relatively small in these cases. Another method to reduce nonlinear effects allowing higher bit rates, is to suppress SPM-GVD interplay and reducing power transfer between adjacent bits [HKPW03].

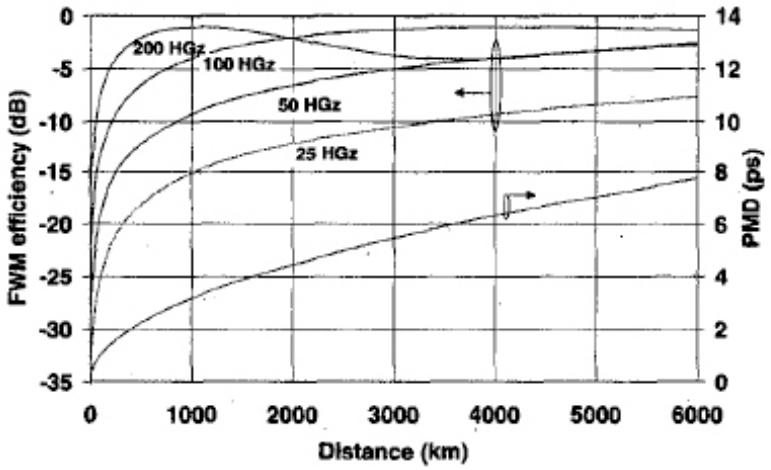

(a) PMD coefficient: 0.1 ps/(km)$^{1/2}$

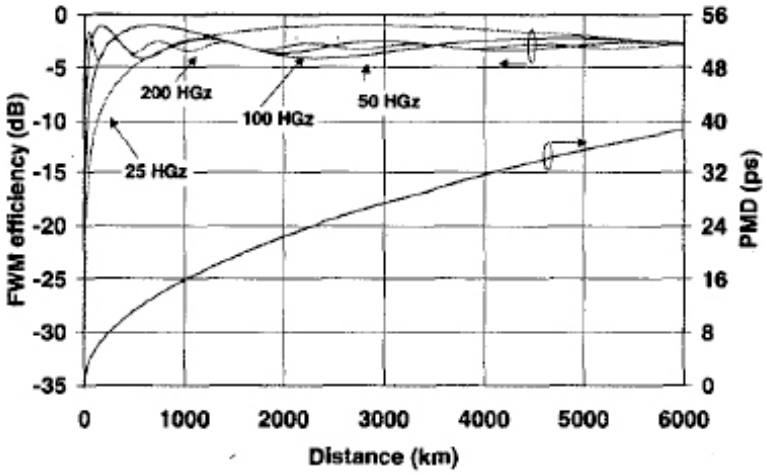

(b) PMD coefficient: 0.5 ps/(km)$^{1/2}$

Figure 5.1: *Four-wave mixing efficiency vs transmission distance for two initially orthogonally polarized signals with different channel spacing for increasing transmission distances [Son00].*

Chapter 6

Depolarization of orthogonal waves

The last two chapters emphasized how linear and nonlinear effects influence states of polarizations. In a PDM and interleaving scheme with two initial orthogonal polarizations it is important to preserve this orthogonality to distinguish the signals at the fiber end and reduce the crosstalk.
Based on our own calculations we will in this chapter first attempt to quantify the depolarization of two general orthogonal states and investigate how PMD affect their states with respect to frequency assuming a Gaussian frequency spectrum.
In the next section we will state a general theory, by using the properties of the Poincare sphere, which can be used to quantify crosstalk in a in a PDM scheme , and clarify how the various effects influence the orthogonality between the SOPs. We will also use a geometric approach to relate the relative depolarization to the angle between the two SOPs.

6.1 Depolarization of orthogonal polarized channels

Any signal can be described naturally as a function of time, which can be written $f(t)$ [New93, Boa03]. This representation leads immediately to the instantaneous power, given by $|f(t)|^2$, which shows how the energy of the signal is distributed over time; the total signal energy is

$$E = \int_{-\infty}^{+\infty} |f(t)|^2 dt \tag{6.1}$$

This time-domain representation tends to hide information about frequency, because it assumes that the two variables t and ω are mutually exclusive. In problems related to depolarization it is therefore convenient to represent the signal $f(t)$ in the frequency domain by its Fourier transform $f(\omega)$, given by

$$f(\omega) = \mathcal{F}\{f(t)\} \equiv \int_{-\infty}^{+\infty} f(t)e^{-i\omega t}dt. \tag{6.2}$$

where $f(\omega)$ represent the fiber input spectrum which is normalized to satisfy the condition

$$\frac{1}{2\pi}\int_{-\infty}^{+\infty} |f(\omega)|^2 d\omega = 1. \tag{6.3}$$

We will denote the ISOPs of two orthogonal signals as $|s_A\rangle = \begin{pmatrix} a \\ b \end{pmatrix}$ and $|s_B\rangle = \begin{pmatrix} a_2 \\ b_2 \end{pmatrix}$ where each satisfy Eq.(3.5). They are orthogonal if their inner product is zero, which can be expressed as $\langle s_A|s_B\rangle_{in} = a_1^* a_2 + b_1^* b_2 = 0$ in Jones space or $\hat{\mathbf{s}}_A = -\hat{\mathbf{s}}_B$ in Stokes space.

By neglecting chromatic dispersion and attenuation, considering PMD only, the field vector at the output of a channel A can be expressed as

$$\begin{pmatrix} E_{ox} \\ E_{oy} \end{pmatrix} = \mathbf{J}(\omega) \begin{pmatrix} a \\ b \end{pmatrix} f(\omega) \tag{6.4}$$

where we operate with the fiber Jones matrix from Eq.(4.10).The field components of Eq.(6.4) can be expressed as follows

$$E_{ox} = (aJ_1 + bJ_2)f(\omega) \tag{6.5}$$
$$E_{oy} = (-aJ_2^* + bJ_1^*)f(\omega) \tag{6.6}$$

By now substituting Eq.(6.5) into the relations from Eq.(3.7) the three components of the output Stokes vector for the whole spectrum can be found

$$\begin{aligned} s_1 &= \int \left(|E_{ox}(\omega)|^2 - |E_{oy}(\omega)|^2\right) \mathrm{d}\omega \qquad (6.7)\\ &= \int \left[\left(|a|^2 - |b|^2\right)\left(|J_1|^2 - |J_2|^2\right) + 2ab^* J_1 J_2^* + 2a^* b J_1^* J_2\right] |f(\omega)|^2 \mathrm{d}\omega \\ &= \int (M_{11}s_{in_1} + M_{12}s_{in_2} + M_{13}s_{in_3})|f(\omega)|^2 \mathrm{d}\omega \end{aligned}$$

$$
\begin{aligned}
s_2 &= \int 2\mathrm{Re}\left(E_{ox}(\omega)E_{oy}^*(\omega)\right)\mathrm{d}\omega \qquad (6.8)\\
&= \int \left[\left(|b|^2-|a|^2\right)\left(J_1J_2+J_1^*J_2^*\right)+a^*b(J_1^*J_1^*-J_2^2)+ab^*(J_1^2-u_2^*J_2^*\right]|f(\omega)|^2\mathrm{d}\omega\\
&= \int (M_{21}s_{in_1}+M_{22}s_{in_2}+M_{23}s_{in_3})|f(\omega)|^2\mathrm{d}\omega
\end{aligned}
$$

$$
\begin{aligned}
s_3 &= \int -2\mathrm{Im}\left(E_{ox}(\omega)E_{oy}^*(\omega)\right)\mathrm{d}\omega \qquad (6.9)\\
&= \int i\left[\left(|b|^2-|a|^2\right)\left(J_1J_2-J_1^*J_2^*\right)+ab^*(J_1^2+J_2^*J_2^*)-a^*b(J_2^2+J_1^*J_1^*\right]|f(\omega)|^2\mathrm{d}\omega\\
&= \int (M_{31}s_{in_1}+M_{32}s_{in_2}+M_{33}s_{in_3})|f(\omega)|^2\mathrm{d}\omega
\end{aligned}
$$

where M_{ij} $(i,j=1,2,3)$ are the elements of a Mueller matrix which have been converted[1] from the Jones matrix using the relationship in Eq.(3.9).

Considering only first order PMD, the PSP orientation is constant along the S_1-axis in Stokes space. The fiber Jones matrix, $\mathbf{J}(\omega)$, is given by Eq.(4.12). However it is the second-order effects that are interesting. The second order fiber Jones matrix can be written [Bru96, ZZCY04]

$$
\mathbf{J}(\omega)=\begin{pmatrix} \cos\frac{\xi}{2}\omega - i\sin\frac{\xi}{2}\cos 2k\omega & -i\sin\frac{\xi}{2}\sin 2k\omega \\ -i\sin\frac{\xi}{2}\sin 2k\omega & \cos\frac{\xi}{2}\omega + i\sin\frac{\xi}{2}\cos 2k\omega \end{pmatrix} \qquad (6.10)
$$

where $\xi=\Delta\tau\omega$ is the phase shift induced by DGD and $k=\frac{|\hat{q}_\omega|}{4}$ where $\hat{q}_\omega$ is the PSP rotation rate from Eq.(4.21). Eq.(6.10) relates to Eq.(4.11) with $N=1$. The difference is that the PSP rotation rate from chapter 4.2.4 is included, which seems like a more intuitive parameter to use . Polarization dependent chromatic dispersion is here neglected.

To find the decrease of the DOP of two orthogonal polarizations we assume that all the incident states are pure, $P_{in}=1$, and the incident channel polarizations are linear and lies along the S_1-axis in Stokes space, that is

$$
\hat{\mathbf{s}}_{A_0}=\begin{pmatrix} s_{1_A} \\ s_{2_A} \\ s_{3_A} \end{pmatrix}=\begin{pmatrix} 1 \\ 0 \\ 0 \end{pmatrix} \text{ and } \hat{\mathbf{s}}_{B_0}=\begin{pmatrix} s_{1_B} \\ s_{2_B} \\ s_{3_B} \end{pmatrix}=\begin{pmatrix} -1 \\ 0 \\ 0 \end{pmatrix} \qquad (6.11)
$$

where $\hat{\mathbf{s}}_A$ is 180° opposed to $\hat{\mathbf{s}}_B$.

[1] The M_{ij}-values are calculated in Maple-source in Appendix $D.1$ and $D.2$

Before attempting to find the output Stokes parameters a derivation of the Mueller Matrix values M_{ij} using the relationship in Eq.(3.9) inserting the Jones matrix from Eq.(6.10) and the pauli matrices Eq.(3.8) is needed. The elements are calculated in Appendix D.3.
Assuming linear ISOPs, Eq.(6.11) implies that the components $s_{2_{(A,B)}}$ and $s_{3_{(A,B)}}$ is zero in both channels. This means that only terms containing s_{in1} are relevant in Eqs.(6.7)-(6.9), which implies that M_{11}, M_{21} and M_{31} are the terms we can concentrate on. Assuming a gaussian frequency spectrum and using the Mueller values calculated in Appendix D the output Stokes components of channel A, $\hat{\mathbf{s}}_A$, become

$$\begin{aligned}
s_{1_A}(\omega) &= \int M_{11} s_{1_A} |f(\omega)|^2 d\omega \\
&= \int M_{11} \left[\frac{1}{\sqrt{2\pi}\sigma^2} \exp\left(-\frac{(\omega-\omega_0)^2}{2\sigma^2} \right) \right]^2 \\
&= \int \left(\frac{1}{2} \left(\cos\frac{\xi}{2} - i \sin\frac{\xi}{2} \cos 2k\omega \right) \left(\cos\frac{\xi}{2} + i \sin\frac{\xi}{2} \cos 2k\omega \right) \right. \\
&\quad - \sin^2\frac{\xi}{2} \sin^2 2k\omega - \frac{1}{2} \left(-\cos\frac{\xi}{2} - i \sin\frac{\xi}{2} \cos 2k\omega \right) \\
&\quad \left. \cdot \left(\cos\frac{\xi}{2} - i \sin\frac{\xi}{2} \cos 2k\omega \right) \right) \left[\frac{1}{\sqrt{2\pi}\sigma^2} \exp\left(-\frac{(\omega-\omega_0)^2}{2\sigma^2} \right) \right]^2 d\omega
\end{aligned} \tag{6.12}$$

$$\begin{aligned}
s_{2_A}(\omega) &= \int M_{21} s_{1_A} |f(\omega)|^2 d\omega \\
&= \int M_{21} \left[\frac{1}{\sqrt{2\pi}\sigma^2} \exp\left(-\frac{(\omega-\omega_0)^2}{2\sigma^2} \right) \right]^2 \\
&= \int \left(i \left(\cos\frac{\xi}{2} - i \sin\frac{\xi}{2} \cos 2k\omega \right) \sin\frac{\xi}{2} \sin 2k\omega \right. \\
&\quad - \frac{1}{2} i \sin\frac{\xi}{2} \sin 2k\omega \left(\cos\frac{\xi}{2} + i \sin\frac{\xi}{2} \cos 2k\omega \right) \\
&\quad \left. + \frac{1}{2} \left(-\cos\frac{\xi}{2} - i \sin\frac{\xi}{2} \cos 2k\omega \right) \sin\frac{\xi}{2} \sin 2k\omega \right) \left[\frac{1}{\sqrt{2\pi}\sigma^2} \exp\left(-\frac{(\omega-\omega_0)^2}{2\sigma^2} \right) \right]^2 d\omega
\end{aligned} \tag{6.13}$$

$$
\begin{aligned}
s_{3_A}(\omega) &= \int M_{31} s_{1_A} |f(\omega)|^2 d\omega \\
&= \int M_{31} \left[\frac{1}{\sqrt{2\pi}\sigma^2} \exp\left(-\frac{(\omega-\omega_0)^2}{2\sigma^2} \right) \right]^2 \\
&= -\int \Bigg[\left(\cos\frac{\xi}{2} - i \sin\frac{\xi}{2} \cos 2k\omega \right) \sin\frac{\xi}{2} \sin 2k\omega \\
&\quad - \frac{1}{2} i \left(-\sin\frac{\xi}{2} \sin 2k\omega \left(\cos\frac{\xi}{2} + i \sin\frac{\xi}{2} \cos 2k\omega \right) i \right. \\
&\quad \left. + \left(-\cos\frac{\xi}{2} - i \sin\frac{\xi}{2} \cos 2k\omega \right) i \sin\frac{\xi}{2} \sin 2k\omega \right) \Bigg] \left[\frac{1}{\sqrt{2\pi}\sigma^2} \exp\left(-\frac{(\omega-\omega_0)^2}{2\sigma^2} \right) \right]^2 d\omega
\end{aligned}
\tag{6.14}
$$

The stokes components for the orthogonal channel B look the same except for having negative sign in front.
The integral-equations Eq.(6.12-6.14) seem impossible to solve analytically, but with numerical calculations it should be possible to plot the DOP after the element as a function of frequency deviation, ω, from the carrier ω_0.
With help from Maple and the DOP-relation in Eq.(6.15),

$$
P = \frac{\sqrt{s_1(\omega)^2 + s_2(\omega)^2 + s_3(\omega)^2}}{s_0} \tag{6.15}
$$

we now attempt to plot[2] DOP versus ω of $\hat{\mathbf{s}}_A$. The carrier frequency, ω_0, is set to $\omega = 0$.
Fig.(6.1b) shows the result for two different $\Delta\tau$ holding the PSP rotation rate, $|\hat{q}_\omega|$ constant. The figure shows that DOP move towards zero when we move away from carrier frequency and become unpolarized.
When we plot the DOP for the other channel, using the same carrier frequency, this will be shown as overlaps of the graphs in Fig.(6.1b)

[2]Maple calculations in Appendix D.7.

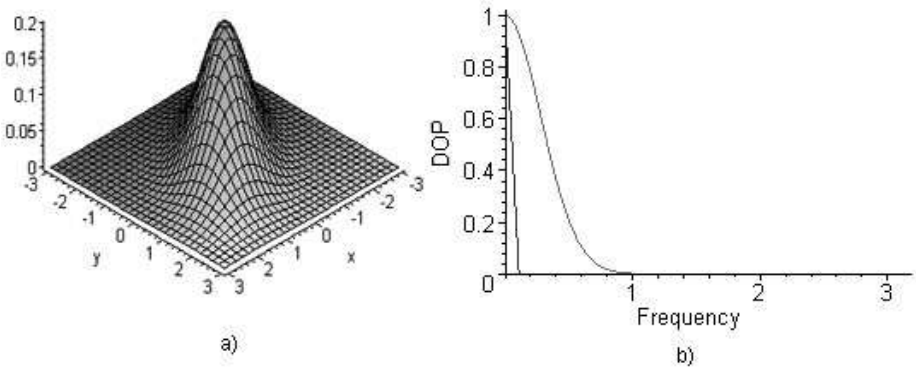

Figure 6.1: *(a) Plot of the gaussian frequency spectrum used in the calculation (b) DOP versus frequency for* $\hat{\mathbf{s}}_A$*. The inner curve is calculated for a lower DGD value* $\Delta\tau$*.*

From these results we can conclude that the two initial orthogonal polarizations experience the same pulse depolarization when lying on the same carrier frequency and will remain orthogonal. The transmission along the fiber will however still be impaired by first-order PMD, and both SOPs are rigidly rotated on the Poincaré as we keep adding fiber elements. In chapter 7.2 we will defend this analysis by simulation.

6.2 Relative depolarization

It has been recently demonstrated that orthogonal SOPs can be transmitted over up to 3 km of graded index 50μm multimode fibres [RW03, RWP04], keeping their relative orthogonal natures, and that polarization orthogonality is available over the complete C-band. This indicate the possibility to double the bandwidth of existing MMF in access networks.
In long transmission however, using single-mode fibers, the desire of preservation of orthogonality seems like a hard nut to crack due to higher order PMD effects, polarization effects in in-line devices and non-linear effects.
We will now try to quantize what we call the relative depolarization and crosstalk based on the formalism suggested in [RWP04] for MMF.
Analogous to chapter 6.1 we still assume that the two input fields are orthogonally linear polarized which can be described by the two anti-parallel

Stokes vectors along the S_1-axis

$$\hat{\mathbf{s}}_{A_0} = \begin{pmatrix} 1 \\ 0 \\ 0 \end{pmatrix} \text{ and } \hat{\mathbf{s}}_{B_0} = \begin{pmatrix} -1 \\ 0 \\ 0 \end{pmatrix} \tag{6.16}$$

At the fiber output the Stokes vectors are unknown and can be denoted as

$$\hat{\mathbf{s}}_A = \begin{pmatrix} s_{1_B} \\ s_{2_B} \\ s_{3_B} \end{pmatrix} \text{ and } \hat{\mathbf{s}}_2 = \begin{pmatrix} s_{1_A} \\ s_{2_A} \\ s_{3_A} \end{pmatrix} \tag{6.17}$$

where their intensities are given by s_{0_A} and s_{0_B}, and where the relative orthogonality, 2ξ, can be found by the scalar product

$$\arccos(\hat{\boldsymbol{s}}_A \cdot \hat{\boldsymbol{s}}_B) = 2\xi \tag{6.18}$$

In the launch case $\xi = 90°$ and $\hat{\mathbf{s}}_{A_0} \cdot \hat{\mathbf{s}}_{B_0} = -1$.
Fig.(6.2) shows the position of two instantaneous SOP and their relative angle. It also shows the ellipticity, 2ϵ, and orientation, 2θ, for $\hat{\mathbf{s}}_A$ which

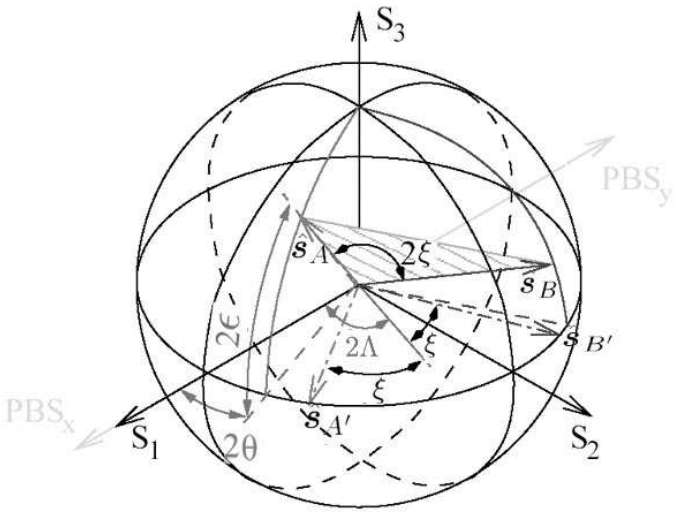

Figure 6.2: *Arbitrary SOP's represented on the Poincare sphere.* $\hat{\boldsymbol{s}}_A$ *and* $\hat{\boldsymbol{s}}_B$ *represent the polarizations before realignment to the azimuth, and* $\hat{\boldsymbol{s}}_{A'}$ *and* $\hat{\boldsymbol{s}}_{B'}$ *after the realignment.*

can be related to the Stokes components through $s_3 = \sin 2\epsilon$ and $s_2 = \sin 2\theta \cos 2\epsilon$.

As mentioned in Section 3.1.3 this relationship is only true when the states are pure, which means not depolarized. However $\hat{\mathbf{s}}_A$ and $\hat{\mathbf{s}}_B$ represent the average Stokes vectors, and not the instantaneous ones and therefore can be considered as pure states.
Another consideration we can introduce is the relative DOP, $\mathbf{P}_r$, between the two SOP. P_r is essentially the length of a vector which represents the average of two other vectors - one for each polarization - so it is half the vector sum of these vectors. When 2ξ is the angle between these vectors, each of which are defined as being vectors of unit length, the following relation exists between ξ and $\mathbf{P}_r$

$$|\mathbf{P}_r| = \frac{1}{2}\sqrt{2 + 2\cos 2\xi} \text{ where } \xi \in [0; 90^\circ] \tag{6.19}$$

which also holds in Jones space. The relation is pictured in Fig.(6.3).

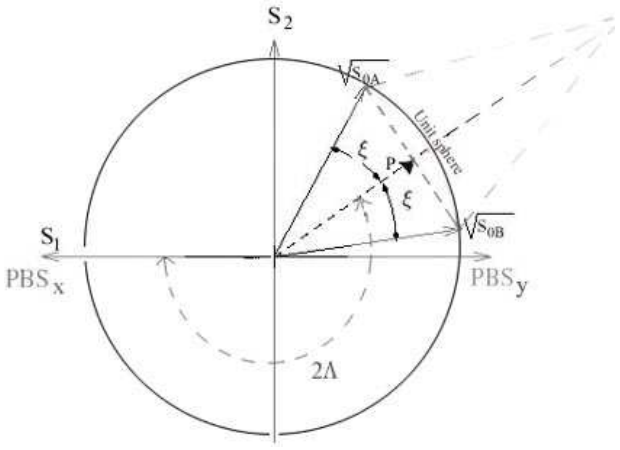

Figure 6.3: *Arbitrary SOP's projected on the plane of linear polarizations of the Poincare sphere.*

If orthogonality is perfectly maintained, the average polarization vector in Stokes space, $|\mathbf{P}_r|$, would have zero length, since the alternating antiparallel Stokes vectors cancel each other out, therefore causing the light to be (on average) unpolarized. We make use of Eq.(6.19) in the simulations in the next chapter.

6.2.1 Crosstalk between states of polarizations

As mentioned in chapter 2.3 polarization multiplexed signals are demultiplexed using a combination of polarization controller and polarization beam

splitter (PBS). The isolation between the demultiplexed channels depends on ξ, where the polarization orientation angles $\delta_A = \Lambda + \xi/2$ and $\delta_B = \lambda - \xi/2$ are defined with respect to the PBS. See Fig.(6.4b) for details.
Computing the crosstalk between two SOPs is equivalent to calculating their projections on the x-and y-axis of the PBS. The projection of $\sqrt{s_{0_A}}$ is equivalent to computing the two transmissions through the PBS. The projections

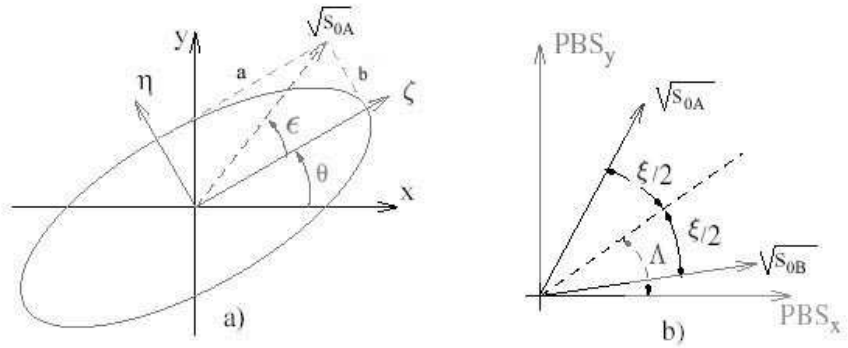

Figure 6.4: *(a) Projection of $\hat{\boldsymbol{s}}_A$ on the axis of PBS for polarization demultiplexing. The amplitude length $\sqrt{s_{0A}}$ can be understood from Fig.(3.1) where the length of the semiminor axis a and the length of the semimajor axis b have the property that $E_{ox}^2 + E_{oy}^2 = a^2 + b^2$ (b) Schematic of the orientations of two multiplexed signals with respect to the PBS. The PBS are assumed aligned to the x-axis.*

on the equator of the Poincaré sphere for $\hat{\boldsymbol{s}}_A$ become

$$\sqrt{s_{0A}}^{(x)} = \sqrt{s_{0A}} \cos(\theta_A + \varepsilon_A) \quad (6.20)$$
$$\sqrt{s_{0A}}^{(y)} = \sqrt{s_{0A}} \sin(\theta_A + \varepsilon_A). \quad (6.21)$$

The intensities seen by the photodetector then become

$$s_{0A}^{(x)} = s_{0A} \cos^2(\theta_A + \varepsilon_A) \quad (6.22)$$
$$s_{0A}^{(y)} = s_{0A} \sin^2(\theta_A + \varepsilon_A). \quad (6.23)$$

and similarly for the intra-channel $\hat{\boldsymbol{s}}_B$

$$s_{0B}^{(x)} = s_{0B} \cos^2(\theta_B + \varepsilon_B) \quad (6.24)$$
$$s_{0B}^{(y)} = s_{0B} \sin^2(\theta_B + \varepsilon_B). \quad (6.25)$$

If we assume that channel $\hat{\boldsymbol{s}}_A$ is detected on the x-axis and channel $\hat{\boldsymbol{s}}_B$ on the y-axis, we can define the crosstalk between the channels as

$$Xt^{(x)} = 10\log\left(\frac{s_{0B}\cos^2(\theta_b+\varepsilon_b)}{s_{0A}\cos^2(\theta_A+\varepsilon_A)}\right) \tag{6.26}$$

$$Xt^{(y)} = 10\log\left(\frac{s_{0A}\sin^2(\theta_A+\varepsilon_A)}{s_{0A}\sin^2(\theta_B+\varepsilon_B)}\right) \tag{6.27}$$

Due to the variation of the PMD vector, $\boldsymbol{\tau}(\omega)$, with frequency and different depolarization rates, $|\mathbf{q}(\omega)|$, at different frequencies the SOP's at different carrier wavelengths is affected randomly, which causes the ellipticity ε and orientation θ to vary randomly. This means that by using a single PBS demultiplexer optimized for one wavelength will not necessarily demultiplex polarization channels at other wavelengths. In chapter 7.2.2 we will attempt to quantify the polarization separation angle numerically.

Assuming that the PBS is aligned with S_1-axis as indicated in Fig.(6.3) we can experimentally use a combination of quarter and-half wave plates to rotate the SOP's to the equator of the Poincaré sphere. The 2ξ angle is conserved by this transformation so that we have $\epsilon_a = \epsilon_b = 0$ and $\theta_b = \theta_a + \xi$. As shown in Fig.(6.4b) the bisector of the two realigned SOP's is oriented at an angle Λ with respect to the PBS. The resulting crosstalk are now

$$Xt^{(x)} = 10\log\left(\frac{s_{0B}\cos^2(\Lambda+\frac{\xi}{2})}{s_{0A}\cos^2(\Lambda-\frac{\xi}{2})}\right) \tag{6.28}$$

$$Xt^{(y)} = 10\log\left(\frac{s_{0A}\sin^2(\Lambda-\frac{\xi}{2})}{s_{0A}\sin^2(\Lambda+\frac{\xi}{2})}\right) \tag{6.29}$$

When the crosstalk is the same for both channels, that is when $\Lambda = 45^\circ$ the transmission is optimized. The above equations then reduces to

$$Xt^{(x)} = Xt^{(y)} = 20\log\left(\tan\left(45^\circ - \frac{\xi}{2}\right)\right) \tag{6.30}$$

assuming equal channel powers $s_{0A} = s_{0B}$ and is minimized when $\xi = 90^\circ$ as expected, and zero when $\xi = 0$.

Chapter 7

Simulations

Computer modelling of the physical layer (i.e. optical transport) of multi-wavelength optical networks is a challenging task, due to the large number of network components and reconfigurable links.
Several products for the study of point-to-point optical communication systems and optical networks are commercially available (e.g. LinkSim [httb], COMSIS [BGC98], FOCUSS [GEV97, htta], OptSim [httc], HP EEsof [Elr93] and PTDS [httd]).
For the numerical calculations OptSim from RSoft is used, which is capable of calculating more than 15000 km of nonlinear fiber, including polarization related effects, with the highest precision in a finite time. It is the fastest simulator among the one mentioned, essentially because of its proprietary time domain simulation technology [ea97]. Based on the NLS-equations from chapter 5.2, the general strategy for solution is to take alternating fiber steps of size dz, solving the dispersive linear part of the problem in the frequency domain, and the nonlinear part of the problem in the time domain.
This chapter is divided into two parts : polarization interleaving and polarization-division multiplexing where the main focus will be on the evolution of the separation angle between the polarizations and its dependence on channel spacing and PMD.

7.1 WDM Polarization interleaving

7.1.1 Verifying the polarization angle dependence on FWM

As mentioned in chapter 5.2.1 and 5.2.2 launching orthogonal neighboring channels seems advantageous for suppressing XPM and FWM.
We will start by verifying how the initial polarizations affect the channel performance, and have prepared a setup as shown in Fig.(E) in the appendix. The topology setup consist of 8 channels launched into a single fiber span of 50 km. Channel spacing is 50 GHz and they are generated in groups by odd and even channels by two PRBS generators, electrical signal generators, and CW laser sources. Fig.(7.1) shows a schematic of the setup.

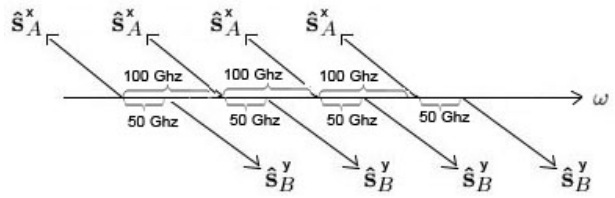

Figure 7.1: *Principle sketch of the initial stokes vectors.* $\hat{\mathbf{s}}_A^y$ *and* $\hat{\mathbf{s}}_B^x$ *are anti-parallel and* $180°$ *opposed to each other in Stokes space.*

The polarizations for the even laser sources source are rotated all around the S_2-axis of the Poincaré sphere through parametric runs ($0°$ to $180°$ with $10°$ step in Jones space), and at the end of the fiber the performance of each channel is tested. This is done by measuring the BER and the Q-factor[1].

The Q-factor performance for one channel is shown in Fig.(7.2a). The Q-factor is minimal for parallel polarization angles ($0°$ and $180°$), and maximum when the neighbor channels are orthogonal to each other ($90°$). Difference between Q's is ~ 0.6 dB. Fig.(7.2b) shows the Q-factor performance for the same channel with the presence of PMD and a DGD coefficient of $D_p = 1$ ps/ km$^{\frac{1}{2}}$. We see that both the total channel performance and Q-factor difference for parallel and orthogonal polarization is reduced. However orthogonal polarizations are still favorable.
As reviewed in chapter 5.2.2 the FWM products are maximized when the polarizations are aligned and nearly completely reduced to zero when the

[1]The BER improves as Q increases and can be approximated with the formula BER $\approx \exp(-Q^2/2)/(Q\sqrt{2\pi})$ [Agr97]. When $Q^2 = 26.7$ BER is $\sim 10^{-7}$. A commonly used criterion for optical receivers requires BER $< 10^{-9}$.

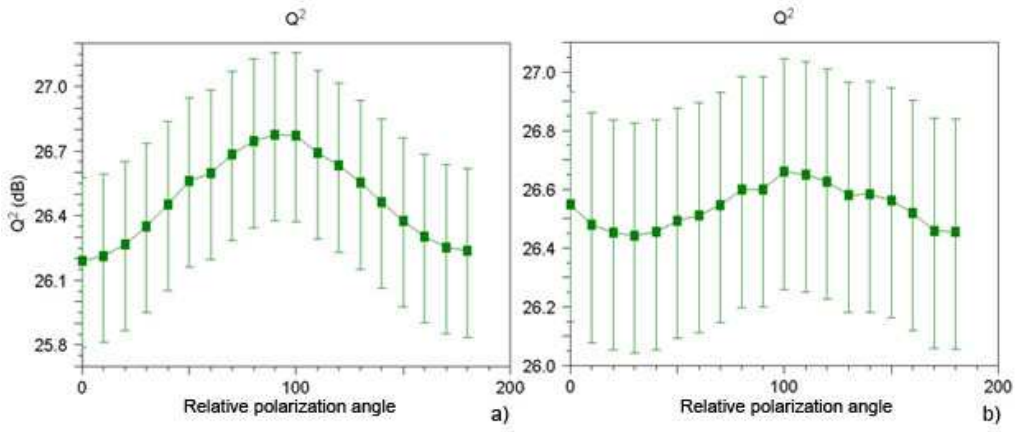

Figure 7.2: (a) *Channel performance versus polarization angle between adjacent channels in absence of PMD* **(b)** *Channel performance versus polarization angle between adjacent channels with PMD present. The angle is taken in Jones space.*

two polarizations are orthogonal, which Fig.(7.2a) reflects. Eq.(5.14) manifests that XPM has no effect when the adjacent channels are orthogonal, but due to PMD-induced XPM the channel performance is further reduced, as shown in Fig.(7.2b). However it seems like it is the PMD itself that is the worst source for orthogonality degradation.

7.1.2 Verifying the bandwidth of the principles states in Polarization interleaving

It is known from chapter 4.2.5 that the bandwidth of the principal states defines the spectral area where $\boldsymbol{\tau}$ is reasonably constant. We will is this section check the viability of the PSP bandwidth from Eq.(4.26).

In the setup two orthogonal polarization channels $\hat{\mathbf{s}}_A$ and $\hat{\mathbf{s}}_B$ are multiplexed, where both laser sources transmit a wavelength on 1537.4 nm, and PRBS-NRZ[2] modulation is used. The wavelength of channel B is then var-

[2]On-off keying (OOK) is a modulation method according to which a logic "one" is manifested by the presence of light;similarly, logic "zero" is manifested by the absence of light. When the logic "one" is lighted for the full period ($T = 1/\Delta\nu$), this OOK is termed nonreturn to zero (NRZ), and when for a fraction of the period (such as 1/3 or 1/2, it is termed return to zero (RZ). Pseudo-random bit sequences (PRBS) are generated using a binary shift register with taps that are modulo-2 added together and fed back to the register's input.

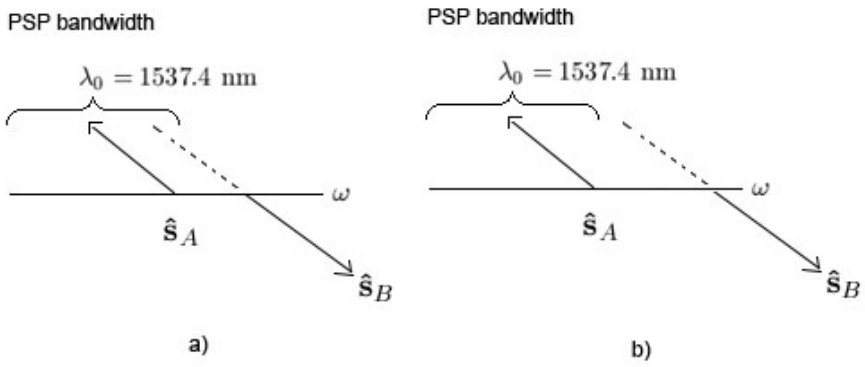

Figure 7.3: (a) $\hat{\mathbf{s}}_B$ *is inside the half PSP bandwidth of* $\hat{\mathbf{s}}_A$. **(b)** $\hat{\mathbf{s}}_B$ *is outside the half PSP bandwidth of* $\hat{\mathbf{s}}_A$.

ied by steps of 5 Ghz, up to 50 Ghz away from the reference wavelength (corresponding to 1537.8 nm) By now using a polarization monitor at the end of the fiber we can read of the DOP for each frequency step. Fig.(7.3) explains the steps. When $\hat{\mathbf{s}}_B$ is inside the half PSP bandwidth of $\hat{\mathbf{s}}_A$, that is $1537.4 + \Delta\lambda_{PSP}/2$ the orthogonality between the Stokes vectors will be reasonably constant as only first order PMD occur. Outside the half PSP bandwidth, depolarization occurs, and the vectors looses their intra-relationship.

Fig.(7.4) shows the DOP versus channel spacing for two mean DGD values, $\Delta\overline{\tau}_1 = 14.85$ ps and $\Delta\overline{\tau}_2 = 2.1$ ps. By reformulating Eq.(4.26),

$$\Delta\nu_{PSP} = \frac{1}{8 \cdot \Delta\overline{\tau}} \tag{7.1}$$

we calculate the half PSP bandwidths to $\Delta\nu_{PSP/2} = 4.2$ Ghz and $\Delta\nu_{PSP/2} = 29.7$ Ghz (for $\Delta\overline{\tau}_1$ and $\Delta\overline{\tau}_2$ respectively).
The simulation results in Fig.(7.4) shows that the analysis of PSP bandwidth agree also for orthogonal polarizations. It is observed that the depolarization occur around these bandwidths, which mean that the PSPs can only be used as an orthogonal basis set up to this point (ref. Eq.(4.18)) .
It is also observed how PMD induces XPM which leads to the conclusion that the field depolarizes faster. In the further sections we will try to quantify the decrease of the orthogonality.

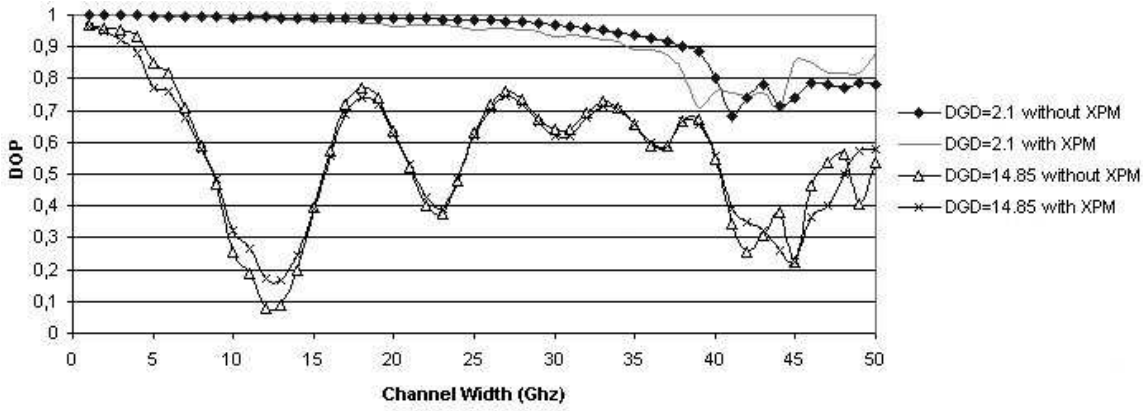

Figure 7.4: *DOP versus bandwidth for two initial orthogonal channels* $\hat{\mathbf{s}}_A$ *and* $\hat{\mathbf{s}}_B$*. The apparently random behavior of the DOP is the result of the random behavior of PMD, and only one seed value is used for each frequency step.*

7.1.3 Relative depolarization using alternating bits

In this section the focus will be on the relative depolarization and the analysis of the evolution of the separation angle 2ξ between the stokes vectors pictured in Fig.(7.5).
The topology setup consist of a transmitter section, a PMD fiber and a SOP evaluation section.

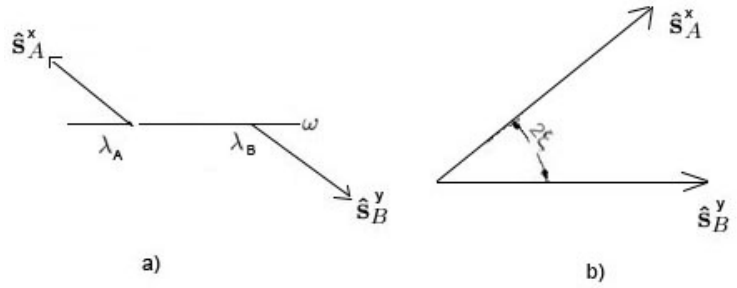

Figure 7.5: *(a) Before fiber propagation the Stokes vectors are orthogonal,* $\hat{\mathbf{s}}_A^y \cdot \hat{\mathbf{s}}_B^x = -1$*. (b) After propagating a distance z the Stokes vectors are separated by a polarization angle* 2ξ*.* λ_B *is varied relative to* $\lambda_A = 1537.4$ *nm to check the frequency dependence of* $\xi(\omega)$ *which is related to* $\boldsymbol{\tau}_\omega$*.*

Transmitter section

The transmitter section, shown in Fig.(7.6) consist of 2 channels launched into a single fiber span. To ensure that the SOP of the two channels could

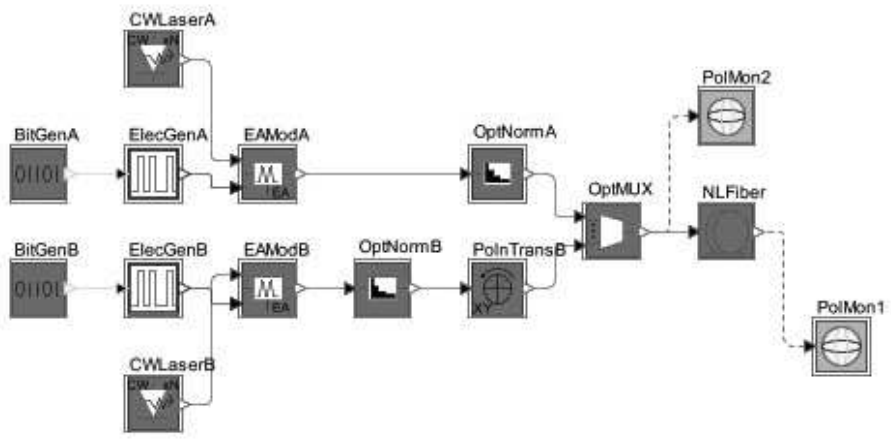

Figure 7.6: *The topology setup of channel A and B.*

be determined at any time, the bit sequences consist of two parametric bit sequences, transmitted with different polarizations which alternately contained ones. The multiplexed stream would then consist of a series of ones with alternating polarizations which are distinguishable by the receiver due to their parametric nature. The SOP analyzer at the fiber end will then produce a set of stokes coordinates $(s_1, s_2, s_3)^T$ for each parametric signal, which allows for computation of the angle separating the polarizations at the fiber end.
Signals from the continuous-wave laser sources (each with a peak power of 10 mW) are modulated by external modulators giving a 10 Gb/s NRZ pattern.

Initially the two channels have linear polarization along the x-axis, that is $\hat{\mathbf{s}}_A = \begin{pmatrix} 1 & 0 & 0 \end{pmatrix}^T$. Before being multiplexed into the fiber channel B channel are rotated 180° on the Poincaré sphere by a polarization controller, which corresponds to $\hat{\mathbf{s}}_B = \begin{pmatrix} -1 & 0 & 0 \end{pmatrix}^T$. As in chapter 7.1.2 channel A's wavelength is set to 1537.4nm while channel B's wavelength is varied 12.5, 25 and 50 Ghz (corresponding to 0.1, 0.2 and 0.4 nm respectively) away from channel A. Using a 10 Gb/s bit rate these spacings correspond to the spectral efficiencies 0.8, 0.4 and 0.2 bit/s/Hz. This particular bit rate and the associated channel separations were chosen, because at 40 Gb/s, PMD

effects already become problematic within a single transmission channel and lower bit rates are generally considered unaffected by PMD.

Fiber section

The chromatic dispersion is modelled with the empirical formula

$$D(\lambda) = \frac{\lambda S_0}{4}\left(1 - \left(\frac{\lambda_0}{\lambda}\right)^4\right) \tag{7.2}$$

in terms of a dispersion slope $S_0 = 90$ s/m^3 and a reference wavelength $\lambda_0 = 1550$ nm. The component parameters n_1, β_2 and β_3 are not used in this dispersion model. To not complicate the setup, there are no components along the fiber giving room for PDL[3], and therefore both modes from the channels experience the same attenuation coefficient which is set to $\alpha = 0.25$ dB/km. The nonlinear parameter n_2 is set to $2.6 \cdot 10^{-20}$ m^2 /W. The non-linear effects XPM/SPM are neglected due to the relatively long simulation times. To defend this decision, the relative low intensity launched into the fiber leads to a low nonlinear birefringence which will not affect the orthogonality between the stokes vectors much compared to PMD. Simulations runs with XPM and PMD present led to only 0.003% more angle deviation compared to the case with only PMD present. To simulate PMD the concatenation model (coarse-step method) is used. The degree of PMD is controlled by the correlation length, L_c and the PMD coefficient, D_p. L_c is set to 10 m, which is common scale in single-mode fibers. The step size is set to 500 m and is 10% of the minimum characteristic length. A minimum of 15 steps will be taken, regardless of the characteristic length in order to obtain randomization of the polarization.
The fiber length was varied from 1 to 40 km in 1 km increments. At each increment a generator was seeded with 50 random numbers, leading to a statistical distribution of the DOP, and a total data set of 2000 values for each simulation. D_p values we used was 1.0, 0.1 and 2.0 ps/ km$^{1/2}$ for each frequency spacing.

Receiver section

At the fiber end a polarization monitor was used to read out the DOP, which from now on is denoted relative depolarization, $|\mathbf{P}_r|$.
Before the simulations we related $|\mathbf{P}_r|$ to the relative angle ξ between the two

[3]Current version of Optsim does not take into account PDL in fiber components.

SOPs, which does not seem possible for PRBS bit sequences. To do this the polarization controller at channel B was scanned from 0° to 180° around the S_3-axis on the Poincaré sphere, relative to the constant polarization angle at channel A on the positive S_1-axis. $|\mathbf{P}_r|$ values was then read off by a polarization monitor after the multiplexer, before entering the fiber span. Fig.(7.7) show the relative angle for different setups. The relationship from

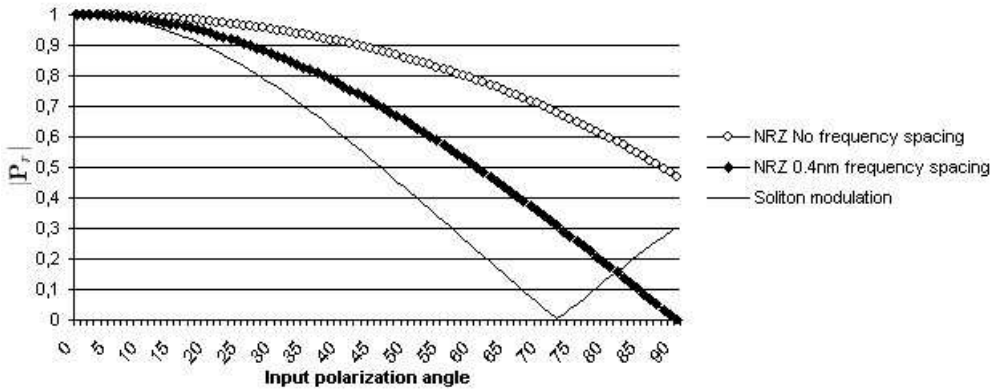

Figure 7.7: *The relation between DOP and relative angle (taken in Jones space) for different modulations.*

Eq.(6.19) agree totally with the curve for the NRZ modulation where there is frequency separation between the channels. By reformulating this equation we obtain

$$\xi = \frac{1}{2}\arccos\left(\frac{4\cdot|\mathbf{P}_r|^2-2}{2}\right) \tag{7.3}$$

which is applicable for arbitrary channel spacings.
For NRZ modulation, when both channels are located at the same frequency and used in chapter 7.2.1, we have done a second order polynomial curve fitting. The relationship here is

$$|\mathbf{P}_r| = -7\cdot10^{-5}\cdot\xi^2 + 0.001\cdot\xi + 0.992. \tag{7.4}$$

The $|\mathbf{P}_r|$-relationship for soliton modulation, which we make use of in chapter 7.1.6, fits to a step function consisting of a 3rd order polynomial and a linear relationship,

$$|\mathbf{P}_r| = \left[(2\cdot10^{-6}\cdot\xi^3 - 0.0003\cdot\xi^2 + 0.0013\xi + 0.9978)\right]H(72-\xi)$$

$$+ \left[0.0171 \cdot \xi + 0.0029\right] H(72 - \xi)(7.5)$$

where $H(\xi)$ is the Heaviside step function[4].

7.1.4 Simulation results

We will now go on and have a look at how the polarization separation angle deviates in an average, low and high PMD fiber, where the PMD coefficients is set to 1.0, 0.1 and 2.0 ps/ $km^{1/2}$ respectively.

Standard PMD fiber

Fig.(7.8) depicts the distribution of the relative polarization angle of the two channels versus the fiber length. The channel spacing is 50 Ghz. The angle is measured in Jones coordinates, where an angle of 90° corresponding to orthogonality.

The orthogonality is lost as early as only a few kilometers into the fiber and the channel separation angle becomes distributed between a decreasing lower bound and orthogonality. A more meaningful presentation is shown in Fig.(7.9) where the angle are normal distributed at 1, 10, 20 and 40 km fiber propagation.

The figure shows that the probability for the channels polarization to be perfectly orthogonal is only small. The mean angle decreases with distance while its variance increases.

Treating the worst case, it is observed that the distribution of the angles after 40 km of fiber extends from 0° to 90°, which means that there is a chance that the benefits or orthogonally polarized channels concerning the reduction of nonlinear interactions to completely vanish at this point. Fig.(7.10) shows the average relative angle for different channel spacings versus fiber length. It is observed that a much greater benefit of using orthogonal channels can be expected at a channel seperation of 12.5 Ghz. This behavior was anticipated, since the contribution of 1st order PMD dominate higher-order PMD, and the two channels seems to have more similar DGDs. This can be understood from the continuous DGD-curve versus frequency in Fig.(4.2.3).

[4]In a distribution-theoretic sense the Dirac delta distribution is the derivative of the Heaviside step function. The Heaviside step function has the following properties

$$\mathrm{H}(\xi)=\begin{cases} 0 & \text{when } \xi < 0 \\ 1/2 & \text{when } \xi = 0 \\ 1 & \text{when } \xi > 0 \end{cases}$$

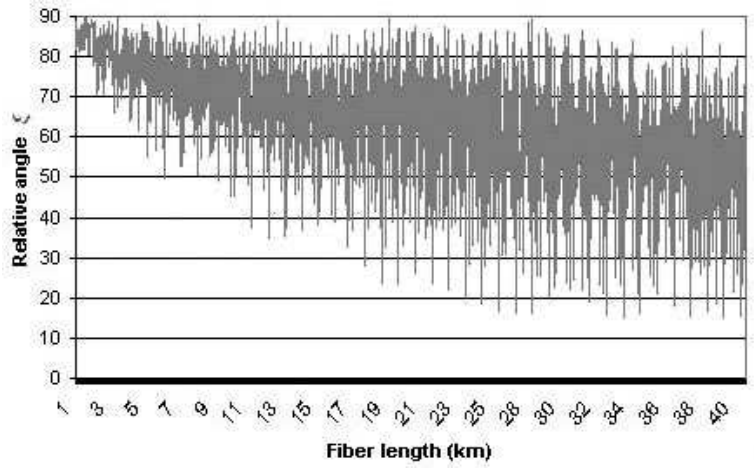

Figure 7.8: *Relative angle ξ versus fiberlength, z, between channels at* 50 *Ghz apart. Fiber PMD coefficient is* 1.0 $ps/km^{\frac{1}{2}}$*.There are* 50 *simulation runs at each km fiber increment.*

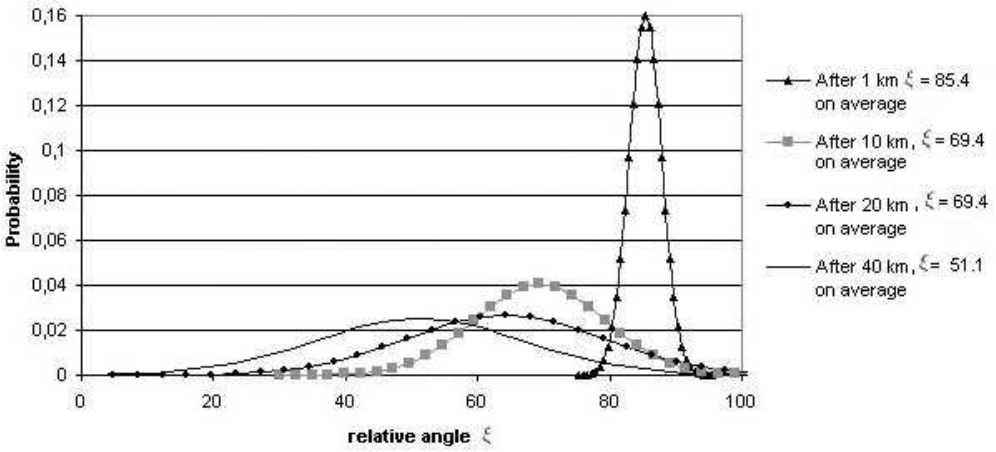

Figure 7.9: *Probability distributions of relative angles ξ. Channels are spaced* 50 *Ghz and fiber PMD coefficient is* 1.0 $ps/km^{\frac{1}{2}}$*. The angles are normal distributed at* 1, 10 20 *and* 40 *km.*

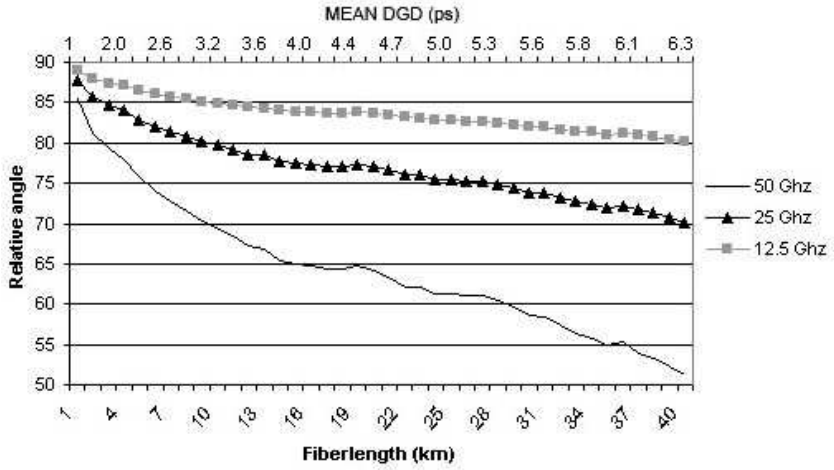

Figure 7.10: *Average relative angle ξ versus fiberlength, z, between channels at* 12.5 *Ghz,* 25 *Ghz and* 50 *Ghz apart. Fiber PMD coefficient is* 1.0 *ps/km*$^{\frac{1}{2}}$

Fig.(7.11) shows that the standard deviation of ξ at different channel spacings increases with increasing fiber length. The larger channel spacing, the larger standard deviation.
Fig.(7.12) visualizes the polarization separation angles on the Poincaré sphere, where the angles for increasing fiber lengths are measured.
We observe how the initial anti-parallel vectors $\hat{\mathbf{s}}_A^x$ and $\hat{\mathbf{s}}_B^y$ precess around $\boldsymbol{\tau}_1(\omega)$ and $\boldsymbol{\tau}_2(\omega+\Delta\omega)$ respectively. Using our mathematical machinery from the PMD-theory the precess equations can be written (Eq.(4.17))

$$\frac{d\hat{\mathbf{s}}_A^x}{d\omega} = \boldsymbol{\tau}_1 \times \hat{\mathbf{s}}_A^x \quad \text{and} \quad \frac{d\hat{\mathbf{s}}_B^y}{d\omega} = \boldsymbol{\tau}_2 \times \hat{\mathbf{s}}_B^y, \tag{7.6}$$

and following Eq.(4.19) the change of $\boldsymbol{\tau}_1(\omega)$ and $\boldsymbol{\tau}_2(\omega+\Delta\omega)$ with fiber length can be written as

$$\frac{\partial\boldsymbol{\tau}_1}{\partial z} = \frac{\partial\boldsymbol{\beta}}{\partial\omega} + \boldsymbol{\beta} \times \boldsymbol{\tau}_1 \quad \text{and} \quad \frac{\partial\boldsymbol{\tau}_2}{\partial z} = \frac{\partial\boldsymbol{\beta}}{\partial\omega} + \boldsymbol{\beta} \times \boldsymbol{\tau}_2. \tag{7.7}$$

Qualitatively we can say that τ_ω and $\hat{\mathbf{q}}_\omega$ changes the magnitude and the direction of $\boldsymbol{\tau}_2$ relative to $\boldsymbol{\tau}_1$ and cause degradation of the relative polarization angle 2ξ (taken in stokes space) between $\hat{\mathbf{s}}_A^x$ and $\hat{\mathbf{s}}_B^y$.

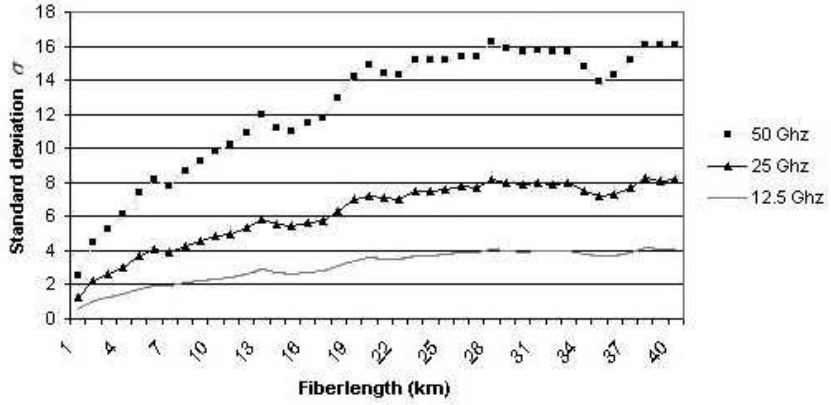

Figure 7.11: *Standard deviation versus fiberlength for channels spaced* 12.5 *Ghz,* 25 *Ghz and* 50 *Ghz. Fiber PMD coefficient is* 1.0 $ps/km^{\frac{1}{2}}$

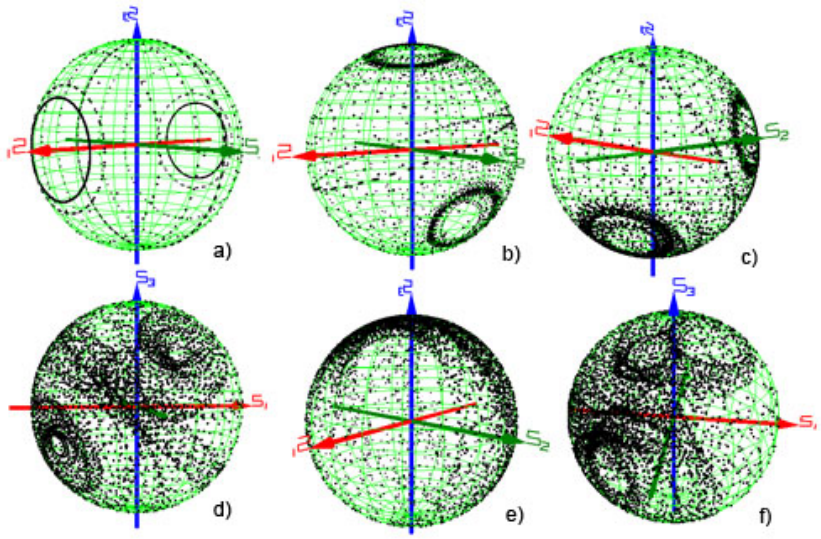

Figure 7.12: *DOP shown on the Poincaré surface in the average PMD case for increasing fiber distances.* **(a)** $z = 0$ *km,* $\Delta\overline{\tau} = 0$ *ps,* $\xi = 90°(180°)$ **(b)** $z = 20$ *km,* $\Delta\overline{\tau} = 4.47$ *ps,* $\xi = 68°(136°)$ **(c)** $z = 40$ *km,* $\Delta\overline{\tau} = 6.32$ *ps,* $\xi = 55°(110°)$ **(d)** $z = 80$ *km,* $\Delta\overline{\tau} = 8.95$ *ps,* $\xi = 41°(82°)$ **(e)** $z = 200$ *km,* $\Delta\overline{\tau} = 14.14$ *ps,* $\xi = 39°(78°)$ **(f)** $z = 500$ *km,* $\Delta\overline{\tau} = 22.36$ *ps,* $\xi = 32°(64°)$ *The polarization separation angle in Stokes space is emphasized in parenthesis.*

Low PMD fiber

Newer fibers exhibit D_p as low as 0.1 ps/km$^{\frac{1}{2}}$, and these fibers should be less affected by both first and higher order PMD. The difference between the second-order PMD vectors at different wavelengths will still be there, but the difference is much smaller. Fig.(7.17) shows the decrease of orthogonality for two initial orthogonal polarizations separated 50 Ghz with PMD coefficient 0.1 ps/km$^{\frac{1}{2}}$. It is observed that both the angle deviation and the standard deviation is much smaller compared to the case with higher D_p in Fig.(7.8). As shown in Fig.(7.14) the polarizations remain almost orthogonal after 40 km fiber propagation with 12.5 Ghz channel spacing - the standard deviation is only 0.5° as observed in Fig.(7.15).

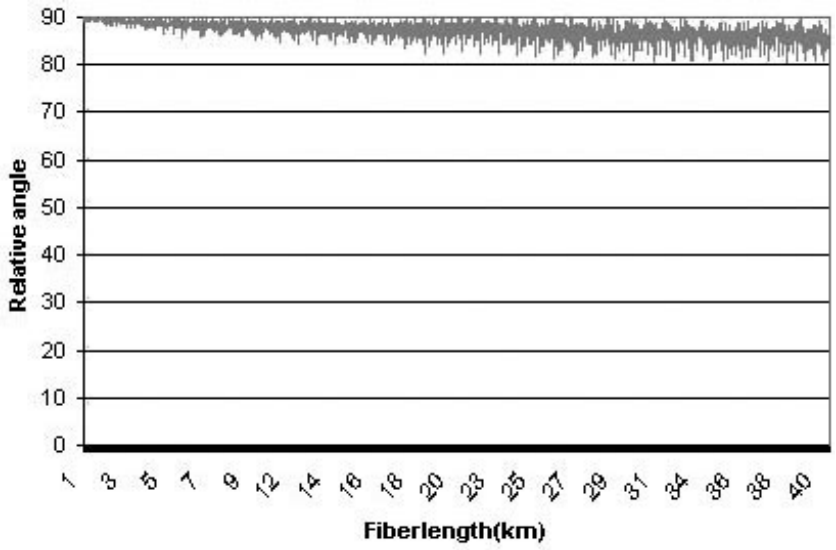

Figure 7.13: *Relative angle ξ versus fiberlength, z, between channels at* 50 *Ghz apart. Fiber PMD coefficient is* 0.1 *ps/km$^{\frac{1}{2}}$. There are* 50 *simulation runs at each km fiber increment*

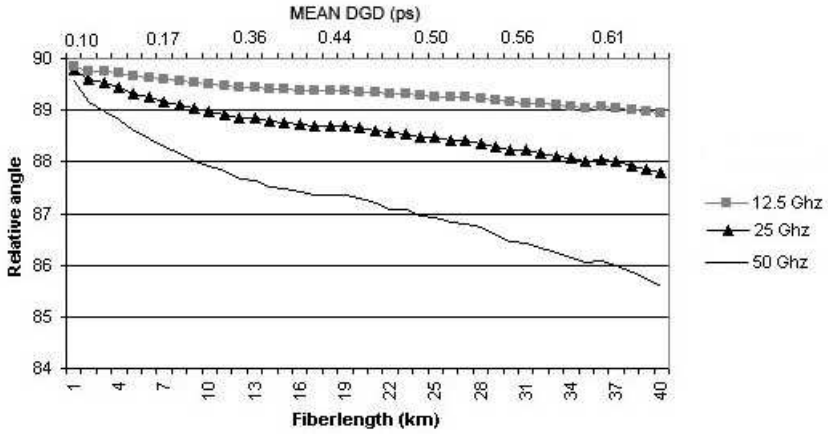

Figure 7.14: *Average relative angle ξ versus fiberlength, z, between channels at* 12.5 *Ghz,* 25 *Ghz and* 50 *Ghz apart. Fiber PMD coefficient is* 0.1 $ps/km^{\frac{1}{2}}$.

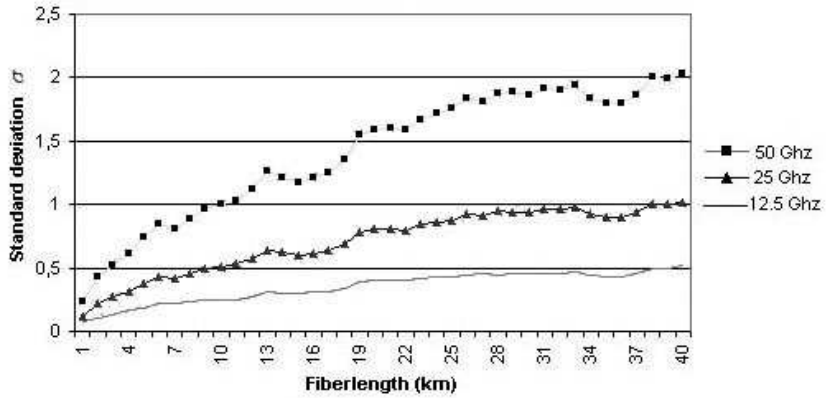

Figure 7.15: *Standard deviation versus fiberlength for channels spaced* 12.5 *Ghz,* 25 *Ghz and* 50 *Ghz. Fiber PMD coefficient is* 0.1 $ps/km^{\frac{1}{2}}$

High PMD fiber

Many of the fibers installed before the 1990s have relatively high-PMD coefficients. In Fig.(7.16) the angle deviations and the corresponding standards deviations for each channel spacing are plotted as a function of fiber length with $D_p = 2.0$ ps/km$^{\frac{1}{2}}$.
We find that the gradients for both the angle deviation and the standard deviation is almost twice as large in the beginning compared to an average PMD fiber, but levels out at the fiber end.

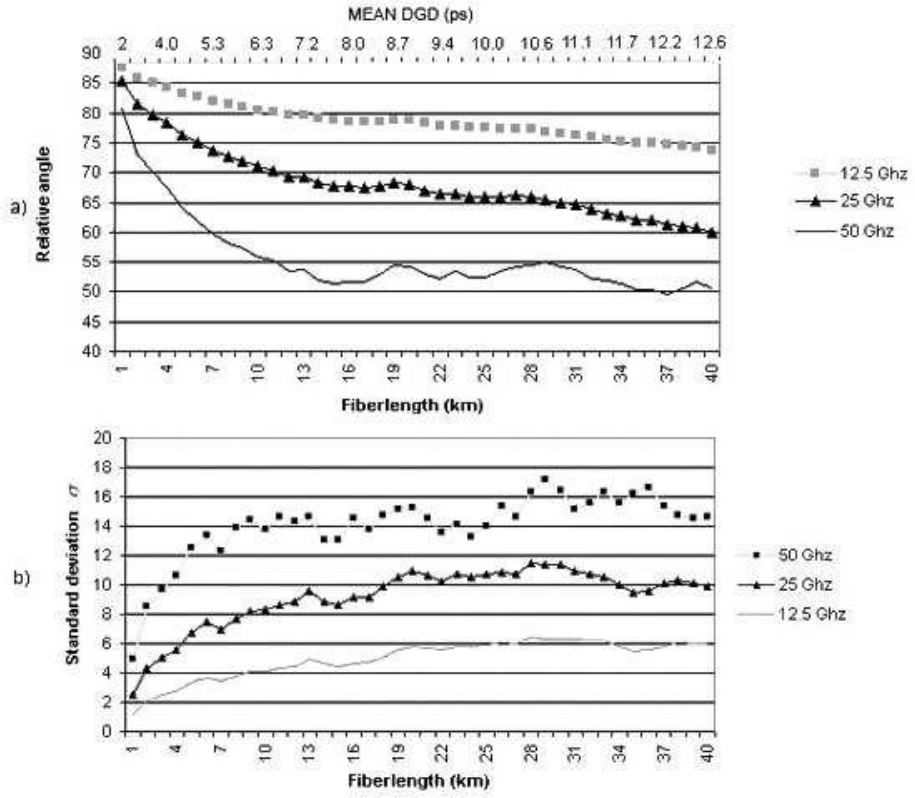

Figure 7.16: **(a)** *Average relative angle ξ versus fiberlength, z, between channels at* 12.5 *Ghz,* 25 *Ghz and* 50 *Ghz apart. Fiber PMD coefficient is* 2.0 *ps/km*$^{\frac{1}{2}}$.**(b)** *Standard deviation of ξ.*

7.1.5 Influence of XPM on orthogonality

When the field intensity becomes large enough, we remember from chapter 5.1 that nonlinear birefringence becomes important.
In the low power simulations in the former chapters XPM/SPM-effects are disabled due to the small influence on SOPs and long simulation time.
To illustrate how the relative angle between the two SOPs get affected by XPM, each laser intensity is increased and the powers are normalized 158 mW in each channel, producing a total power of 316 mW in an average PMD fiber.
Fig.(7.17) shows the relative angle versus fiber length, where the channels are separated by 50 Ghz.
When XPM and PMD are present at the same time it seems like the average relative polarization angle splits at $\sim$ 10 km compared to the case where XPM is isolated and only PMD is present in the fiber. However, the standard

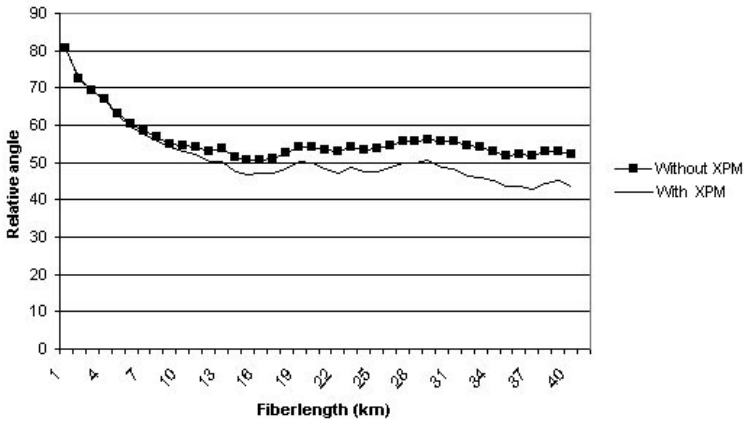

Figure 7.17: *High intensity fiber. Relative angle versus fiber length.* 50 *Ghz channel spacing,* 1.0 $ps/km^{\frac{1}{2}}$.

deviation difference between the two cases remain zero throughout the fiber, so it seems like the angle distributions remain same for all fiber lengths, but the average angle for the XPM-case deviate more from orthogonality at long fiber lengths. At smaller fiber lengths XPM has no influence and is overlapping the other graph. However as the DGD increases the PMD effect triggers XPM induced depolarization as explained in chapter 5.2.1.

7.1.6 Polarization interleaved solitons

Orthogonally polarized soliton pulses was also simulated. Solitons are known for maintaining a high DOP throughout the whole fiber link, even though the presence of random variations of the fiber birefringence and PMD. In fact, it is considered that the typical length scale where birefringence and PMD fluctuations occur is much shorter than the soliton period, so that the fluctuating PMD vector, $\boldsymbol{\tau}$, may be averaged over all polarization states. The soliton robustness of the temporal pulse is caused by so-called "self-trapping". A PMD-induced temporal pulse break-up of linear pulses is counteracted in solitons through a spectral change such that GVD cancels out the effect of PMD. Thus, the temporal distortion in linear pulses is traded for a small spectral distortion in solitons.
Polarization multiplexing of solitons are e.g. studied in [ea92, CCD98] as special solutions of the coupled NLS-equations. In our simulation the con-

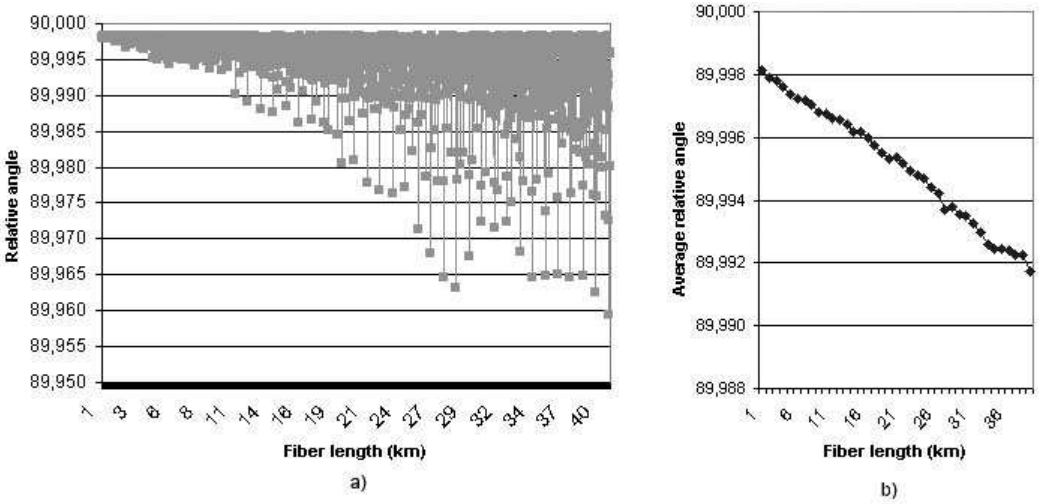

Figure 7.18: *Soliton transmission.* **(a)** *Relative angle ξ versus fiberlength with* 50 *Ghz spacing and* 50 *simulation runs at each km.* **(b)** *Average angle versus fiberlength. . Fiber PMD coefficient is* 1.0 *ps/km$^{\frac{1}{2}}$.*

tinuous wave lasers are substituted with two mode-locked laser sources, in conjunction with the external modulators to produce soliton pulses with pulse widths $t_p = 20$ ps. Parameterized bit-sequences and the same dispersion/loss model as in former chapters were used. An average PMD fiber is used for the setup.

The polarization angle for polarizations spaced 50 Ghz is plotted in Fig.(7.18). It is observed that solitons preserve orthogonality extremely well - the angle deviated only by 0.008° on average after 40 km fiber propagation, and the angle was deviated 0.041° in the worst case. However, as in the other cases the standard deviation increased along the fiber, and reach 0.007° at 40 km - which is again extremely small. With our model assumptions the conclusion is that orthogonally polarized solitons remain so as they traverse the system. In [ea92] it is revealed that orthogonally polarized solitons can be spaced as close as $\sim 2.5t_p$ apart without significant interaction over transoceanic distances. By contrast, in a single-polarization soliton system, the solitons must be spaced at least $5t_p$ apart to avoid significant soliton-soliton interaction over the same distances [Mol90]. However, resistance of solitons PMD break down for large amount of PMD. The breakdown limit has been estimated to [MSGM89]

$$D_p \leq 0.3D^{1/2} \tag{7.8}$$

where D is the dispersion parameter from Eqs.(4.5, 7.2). In practice this relation is often satisfied and PMD should therefore be a minor problem in most soliton systems.

7.2 Polarization-division multiplexing

In this section we will first try to quantify the evolution of the polarization angle separating two independent polarizations on one frequency, and then continue on looking at two frequencies each containing two orthogonal independent signal polarizations.

7.2.1 Relative depolarization of one PDM signal

When using alternating polarizations to modulate a standard single-channel NRZ or RZ bitstream, it is expected that the orthogonality will be maintained in the presence of PMD, since the frequency dependence of all PMD effects is avoided.
However the propagation along the fiber will be impaired by first-order PMD, which causes the bits at one polarization to have a greater group velocity than those at the other polarization. On average both polarizations will experience the same distortions due to PMD as mentioned in chapter 6.1. However these effects are not considered here as the quality of the transmission link is disregarded and emphasis is placed solely on the evolution of the polarization angle ξ. These statements will first be verified with simulations, making use of an almost identical setup as in Fig.(7.6). The two wavelengths used are now both $\lambda_{A,B} = 1537.4$ nm. By solving the 2nd order compound quantity of Eq.(7.4) with respect to ξ the DOP values at the end of the fiber can be converted to the relative angle. The average relative angle for each increment in length is plotted in Fig.(7.19).
Using the parameterized signals approach, the results confirm that the or-

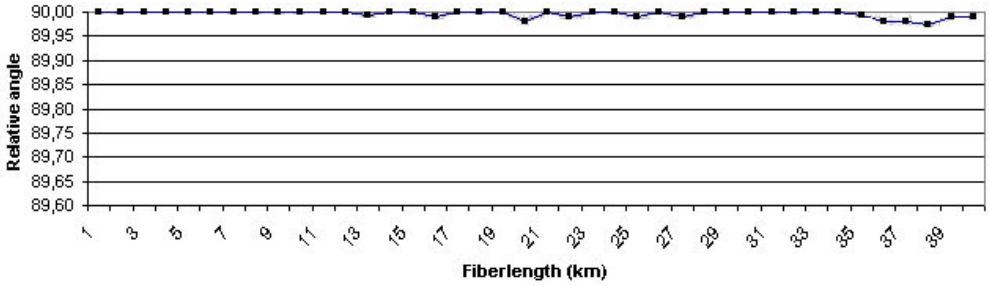

Figure 7.19: *Relative angle ξ between intra-channels $|s_A^x\rangle$ and $|s_A^y\rangle$ versus fiber length. $D_p = 1.0$ $ps/km^{\frac{1}{2}}$.*

thogonality of intra-channel polarization alternation is affected very little by

PMD. Fig.(7.19) shows that ξ after propagation of 40 km of fiber is $< 90°$, but still very small in almost all of the 2000 simulation runs. When both $\lambda_{A,B}$ are displaced the same amount in frequency and more simulations are done there is no significant angle deviation.

7.2.2 Relative depolarization between two PDM signals.

Now we move on treating the polarization angle separating two channels each containing two orthogonal polarizations. Our intra-channel setup from the last section then have to be expanded. Fig.(7.20a) illustrate a schematic of the situation before fiber propagation. Two orthogonal linearly polarizations $\hat{\mathbf{s}}_A^x = (1\ 0\ 0)^T$ $\hat{\mathbf{s}}_A^y = (-1\ 0\ 0)^T$ lie on the same wavelength λ_A along the S_1-axis on the equator of the Poincaré sphere. Using the superposition

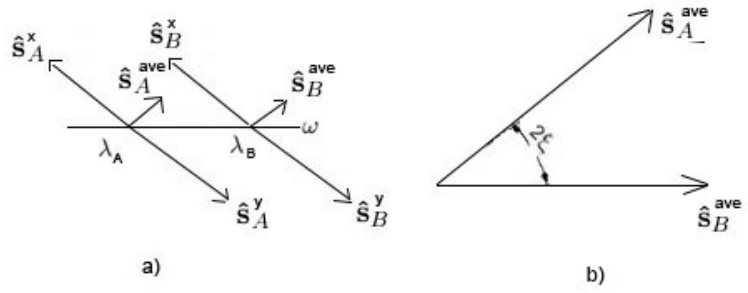

Figure 7.20: *(a) Before fiber propagation the Average Stokes vectors are parallel,* $\hat{\mathbf{s}}_A^{ave} \cdot \hat{\mathbf{s}}_B^{ave} = 1$. *(b) After propagating a distance x the Stokes vectors are separated by a polarization angle* 2ξ. λ_B *is varied relative to* $\lambda_A = 1537.4$ *nm to check the frequency dependence of* $\xi(\omega)$ *which is related to* $\boldsymbol{\tau}_\omega$.

principle in Stokes space[5] we can "add" these vectors together obtaining the average polarization $\hat{\mathbf{s}}_A^{ave} = (0\ 1\ 0)^T$ lying along the S_2-axis - also on the equator.
The same rules applies for channel B which is displaced $\lambda_A + \Delta\lambda$ away from signal A as shown in the figure.
While assuming that the relative angle between the intra-channels is rela-

[5]The Jones vectors form a vectorial space, whereas the Stokes vectors do not. Thus we can not just take the sum of the stokes vectors. The superposition in Jones space is represented by $|s_A^{ave}\rangle = a|s_A^x\rangle + b|s_A^y\rangle$ where $a = b = 1/\sqrt{2}$. The corresponding stokes vector will be $\hat{\mathbf{s}}_A^{ave} = (aa^* - bb^*)\hat{\mathbf{s}}_1 + (ab^* + a^*b)\hat{\mathbf{s}}_2 + i(ab^* - a^*b)\hat{\mathbf{s}}_3$ representing a 3D superposition in Stokes space. We know that aa^*/bb^* have equal power split which indicates that only the term $(ab^* + a^*b)\hat{\mathbf{s}}_2$ is relevant, obtaining $\hat{\mathbf{s}}_A^{ave} = (0\ 1\ 0)^T$.

tively constant throughout the fiber,we can concentrate on the angle separating $\hat{\mathbf{s}}_A^{ave}$ and $\hat{\mathbf{s}}_B^{ave}$, which also is denoted 2ξ (in Stokes space). Before being multiplexed into the fiber the average polarizations are parallel, that is $\hat{\mathbf{s}}_A^{ave} \cdot \hat{\mathbf{s}}_B^{ave} = 1$, which means that $\xi = 0$ at launch.

The setup

The PDM-setup is shown in Fig.(7.21). The bit generators $BitGenA_x$ and $BitGenA_y$ use parameterized signals (101010... and 010101... respectively) where $BigGenA_y$ is offset by one bit, each consisting of a 128-bit sequence. Similar relations applies for channel B. The signal wavelengths for the NRZ-modulated laser source in channel A is $\lambda_{Laser_{A_x}} = \lambda_{Laser_{A_y}} = 1537.4$ nm while the wavelengths in channel B are 1537.8 nm, corresponding to a 50 Ghz ($\Delta\lambda = 0.4$ nm) channel spacing. 12.5 and 25 Ghz channel spacing was also simulated. Two multiplexers, denoted $OptMux_A$ and $OptMux_B$ on

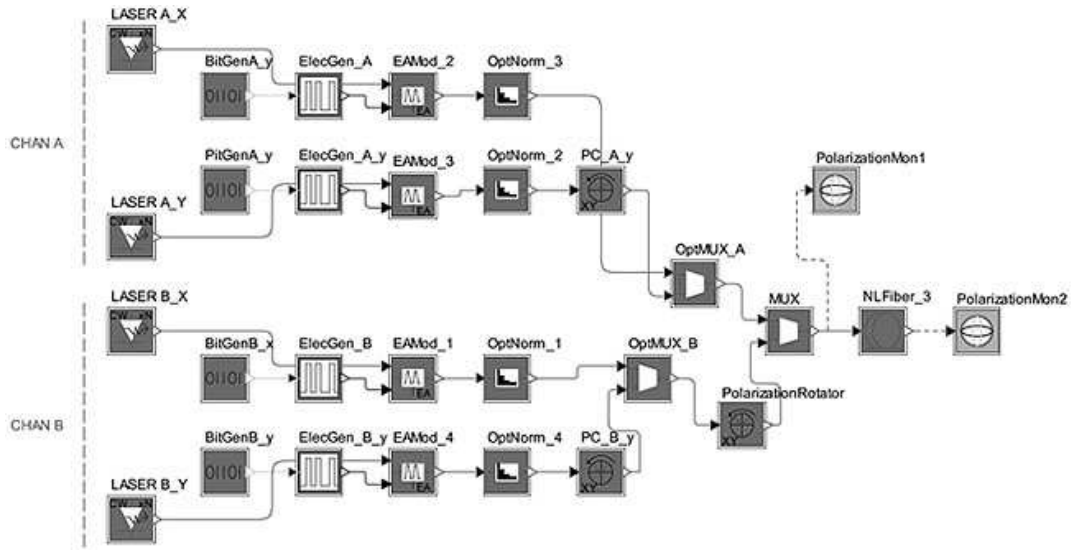

Figure 7.21: *The setup for polarization-division multiplexing of* 2 *channels. The polarization rotator is only used to find the relationship between the DOP and the average angle* ξ *between* $\hat{\mathbf{s}}_A^{ave}$ *and* $\hat{\mathbf{s}}_B^{ave}$.

the figure, multiplex the two orthogonal intrachannels in each channel, and gives us the average polarizations $\hat{\mathbf{s}}_A^{ave}$ and $\hat{\mathbf{s}}_B^{ave}$.
To find the relationship between the relative angle ξ and the length of DOP-vector,$|\mathbf{P}_r|$, we use a polarization rotator which rotate $\hat{\mathbf{s}}_B^{ave}$ around the S_3-

axis on the Poincaré sphere with 1° increments, keeping $\hat{\mathbf{s}}_B^{ave}$ constant. The relation is then plotted using the results from $PolarizationMon1$.
Fig.(7.22) shows $|\mathbf{P}_r|$ versus ξ in Jones space. The relation is well fitted by

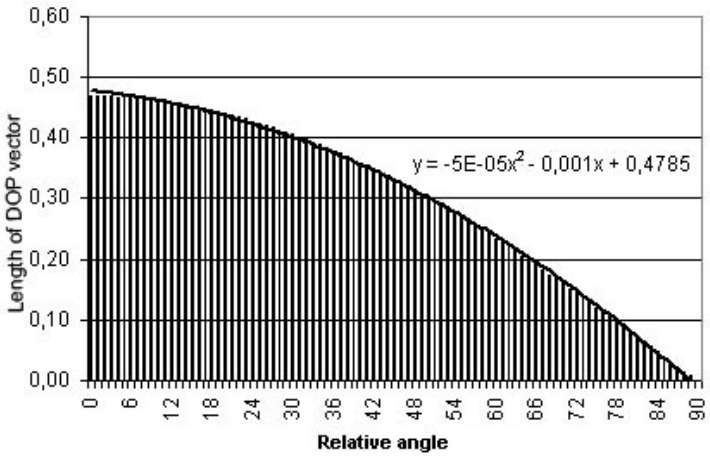

Figure 7.22: *Length of DOP vector versus relative angle ξ.*

a 2nd order compound quantity, shown in the figure, which is solved with respect to ξ, obtaining

$$\xi = \sqrt{100 + 20000 \cdot (0,4785 - |\mathbf{P}_r|)} - 10 \tag{7.9}$$

which is used in the results section.

Results

To make the results comparable with the polarization interleaving scheme we have plotted ξ for the three respective frequency separations both for an average PMD fiber, with $D_p = 1.0$ ps/km$^{\frac{1}{2}}$, and for a low PMD fiber with $D_p = 0.1$ ps/km$^{\frac{1}{2}}$.
Fig.(7.23a) shows the instantaneous ξ versus fiber length in an average PMD fiber with channels spaced 50 Ghz. We see that the variance increases with fiber distance as in the interleaving case.
Angle probability distributions for selected lengths is plotted in Fig.(7.23b), which shows that the distributions after 40 km extends from 0° to almost 90°. The average relative angles for all the cases are plotted in Fig.(7.24) for the two different fiber types.

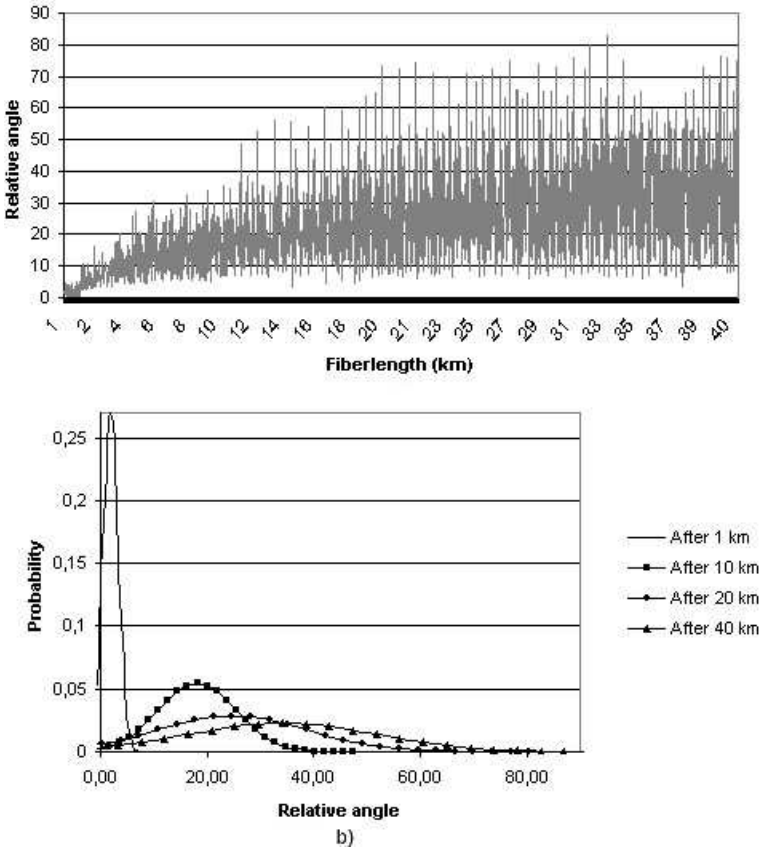

Figure 7.23: *(a) ξ versus fiberlength for 2 PDM channels spaced* 50 *Ghz. $D_p = 1.0$ ps/km$^{\frac{1}{2}}$. (b) Probability distributions of relative angles ξ. The angles are normal distributed at* 1, 10 20 *and* 40 *km.*

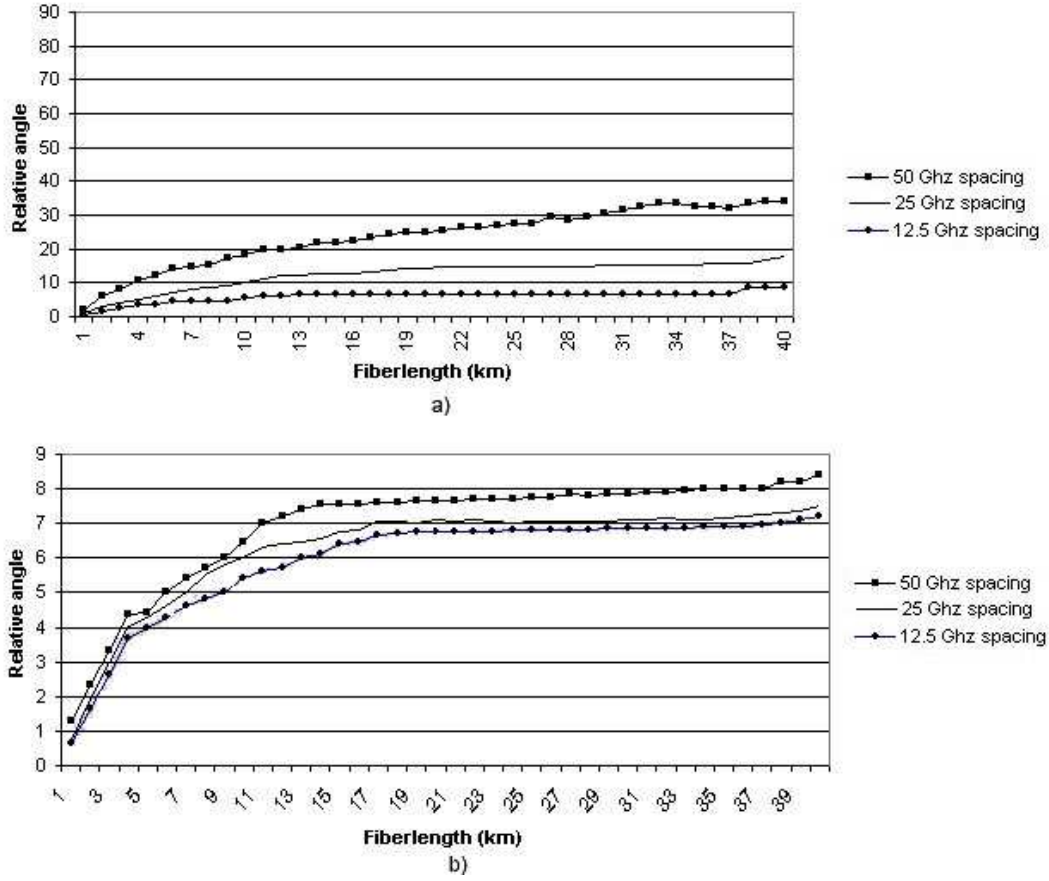

Figure 7.24: *(a) Average relative angle ξ versus fiber length. $D_p = 1.0\ ps/km^{\frac{1}{2}}$. (b) Average relative angle ξ versus fiber length. $D_p = 0.1\ ps/km^{\frac{1}{2}}$.*

D_p	$\Delta\omega$ [Ghz]	Concept	$\Delta\xi$ after 1 km	$\Delta\xi$ after 10 km	$\Delta\xi$ after 20 km	$\Delta\xi$ after 40 km
0.1	12.5	PI	$0.17° \pm 0.023°$	$0.25° \pm 0.07°$	$0.64° \pm 0.11°$	$1.0° \pm 0.14°$
0.1	12.5	PDM	$0.66° \pm 0.0007°$	$5.40° \pm 0.002°$	$6.75° \pm 0.003°$	$7.2° \pm 0.004°$
0.1	25	PI	$0.2° \pm 0.03°$	$1.02° \pm 0.14°$	$1.33° \pm 0.22°$	$2.22° \pm 0.28°$
0.1	25	PDM	$0.76° \pm 0.0001°$	$6.04° \pm 0.05°$	$7,11° \pm 0.07°$	$7.5° \pm 0.09°$
0.1	50	PI	$0.44° \pm 0.07°$	$2.03° \pm 0.28°$	$2.7° \pm 0.44°$	$4.4° \pm 0.56°$
0.1	50	PDM	$1.32° \pm 0.005°$	$6.48° \pm 0.04°$	$7.65° \pm 0.10°$	$8.4° \pm 0.24°$
1.0	12.5	PI	$1.13° \pm 0.16°$	$5.04° \pm 0.65°$	$6.35° \pm 0.98°$	$9.9° \pm 1.14°$
1.0	12.5	PDM	$0.65° \pm 0.004°$	$5.48° \pm 0.03°$	$6.43° \pm 0.10°$	$8.9° \pm 0.47°$
1.0	25	PI	$2.3° \pm 0.34°$	$10.32° \pm 1.34°$	$12.93° \pm 1.99°$	$19.9° \pm 2.25°$
1.0	25	PDM	$0.9° \pm 0.20°$	$10.01° \pm 1.2°$	$14.1° \pm 2.05°$	$18° \pm 2.4°$
1.0	50	PI	$4.6° \pm 0.69°$	$20.6° \pm 2.72°$	$25.8° \pm 4.1°$	$39° \pm 4.4°$
1.0	50	PDM	$1.88° \pm 0.41°$	$18.2° \pm 2.03°$	$24.7° \pm 3.86°$	$34.17° \pm 4.9°$

Table 7.1: *Comparison of polarization angle deviations $\Delta\xi$ for PDM and Polarization interleaving (PI) for increasing fiber lengths. The PMD coefficient, D_p, is given in $\frac{ps}{km^{\frac{1}{2}}}$. Angles are given in Jones space.*

7.3 Comparison of the polarization separation angles

Based on the results from chapter 7.1.4 and chapter 7.2.2 we will now compare the mean polarization angle fluctuation $\Delta\xi$ between the nearest neighbor channels from the initial angle ξ for polarization interleaving and PDM at various points in the fiber. The angles we concentrate on are pictured in Fig.(7.5b) and Fig.(7.20b).
In Table 7.1 we have listed $\Delta\xi$ after fiber lengths 1, 10, 20 and 40 km for an average and low PMD fiber with channel spacings 12.5, 25 and 50 Ghz.
Since our PMD calculations are based on random seed-parameters confidence intervals make a reasoned statement about the true mean of $\Delta\xi$. The angle deviations given is estimated with a 95% confidence interval, $\Delta\xi \pm 1.96 \cdot \frac{\sigma}{\sqrt{n}}$, where $n = 50$, since 50 parameters was simulated at each fiber length increment.

Chapter 8

Conclusions

8.1 Discussion

The study, and understanding of polarization of light is becoming increasingly important in a number of disciplines in the optical sciences. A sound knowledge of the subject is needed, for example in the study of laser physics, nonlinear optics and optical waveguides.
In this report we have shown how light fields are depolarized due to the mixture of spectral modes with different polarizations.
When $|s_A\rangle_\omega$ and $|s_B\rangle_\omega$ lie on the same carrier wavelength (1 channel) they will never depolarize, since any fiber Jones matrix $J(\omega)$ will change the absolute states of polarization, but they will remain orthogonal. Both SOPs are rigidly rotated on the poincaré sphere.
Exceptions to this happen if you have PDL, PDG and PHB in the fiber or, even in the absence of these effects, you are in the nonlinear-propagation regime [BVO$^+$03]. Also the relative drift causes depolarization as shown in Eq.(4.31).
When $|s_A\rangle_{\omega_1}$ and $|s_B\rangle_{\omega_2}$ lie on two carrier wavelengths (2 channels) they will usually depolarize due to PMD. The amount of mutual depolarization depends (on average) on the autocorrelation of the fiber Jones Matrix, taken at the two carrier wavelengths, or, in other words on how the fiber changes its behaviour (with respect to polarization) from ω_1 to ω_2 [VB02]. $|s_A\rangle_{\omega_1}$ and $|s_B\rangle_{\omega_2}$ will not be depolarized due to PMD if the product $\Delta\omega\Delta\bar{\tau}$ is sufficiently close to zero. i.e. $\langle s_A^x|s_B^y\rangle_{out} = 0$ is satisfied at the output in a polarization interleaving scheme, and $\langle s_A^{ave}|s_B^{ave}\rangle_{out} = 1$ is satisfied in the PDM scheme.
When $\Delta\omega\Delta\bar{\tau}$ is sufficiently higher than zero, exceeding the PSP band-

width, depolarization causes the polarization separation angle $\Delta\xi$ to deviate stochastically from the initial angle.
The topic of chapter 7 was the evolution of $\Delta\xi$ separating initially orthogonal polarized channels and initially orthogonal bits within a single channel. The third part dealt with the angle separation of average polarizations constituted by two neighboring channels each containing two orthogonal polarizations.
It was revealed that launching neighboring channels with orthogonal polarizations effectively suppresses XPM and FWM. However, due to birefringence and the frequency-dependence of PMD initially orthogonally polarized channels do not remain so.
The simulations showed that, depending on the frequency separation and the PMD coefficient, the orthogonality is lost quickly as the optical waves propagate along the fiber.
The larger the channel spacing and the PMD coefficient were chosen, the larger the range over which the polarization angles were distributed at any point in the fiber, in agreement with the ACF from chapter 4.4.1.
With a PMD coefficient of 1.0 ps/km$^{\frac{1}{2}}$ and a channel spacing of 50 Ghz, the distribution covered the entire range from parallel to orthogonal after 40 km propagation, while coefficients of 0.1 ps/km$^{\frac{1}{2}}$ and 12.5 Ghz did not affect the initial orthogonality noteworthy.
Simulations with orthogonal bits on the same wavelength showed that the relative polarization angle is preserved throughout the fiber with hardly any deviation from the input angle. An optical crosstalk ratio between the two SOPs in future calculations can be calculated using the formulaes from chapter 6.2.1. From a practical point of view, an optical crosstalk-ratio of typically 10 dB (corresponding to $\xi = 78.5^\circ$ ($\Delta\xi = 11.5^\circ$) is desirable in order to achieve robust error free transmission [RW03].
Based on these simulations we could focus on the average polarizations constituted by two neighboring channels each containing two orthogonal polarizations. The results reminded much about the polarization interleaving case.
In the *low* PMD fiber case, the comparison between the interleaving and PDM scheme shows that the polarization angle deviates faster for PDM than interleaving - especially for lower channel spacings. The explanation can be that FWM efficiency[1] are more severe when the dispersion and channel spacing is less - in line with Fig.(5.1). The PDM case also have twice as much power, due to the two set of extra modes, which should cause more

[1] In Optsim the phase matching condition is satisfied all the time.

nonlinear interactions inducing PMD. As the initial average Stokes vectors are parallel in the PDM case this should also lead to a higher FWM efficiency in accordance with chapter 5.2.2.
The characteristics are that for larger channel separations D_p plays a smaller role in PDM compared to interleaving. When the two schemes in an *average* PMD fiber are compared it seems like the separation angles are more similar.
However, comparing the two cases with respect to spectral efficiency it is believed that the PDM scheme is affected less by nonlinear impairments such as FWM and XPM than the interleaved scheme. To a first approximation, PDM has two signal channels at the same frequency with orthogonal polarizations and different optical phase. Assuming On/off keying, in any bit slot, there will be one of four states, depending on the bit being sent in each channel. The four states are: signal with only $|s_A^x\rangle$ present, only $|s_A^y\rangle$ present, signal determined by the phase difference between $|s_A^x\rangle$ and $|s_A^y\rangle$ or no signal at all. If there is no dispersion, there will be no FWM or XPM between the two PDM signals. When you add dispersion the pulses spread out and intra-channel XPM and FWM must be considered. For PDM, you will still have FWM and XPM from other frequency channels, but if you preserve spectral efficiency, these other channels are twice as far away compared to polarization interleaving and will have a diminished effect. The polarization of the one-one state will evolve as the relative phase between channels A and B changes, but this will occur slowly, at the coherence time of the source lasers.
For interleaving, the nearest neighbour do not interact in the first approximation and, as in PDM, it is the second channel away that dominates the nonlinear impairment. In the first approximation, it would appear that PDM and interleaving have equal impairment from FWM and XPM. Each is most affected by channels having the same polarization lying two frequency slots away. The next step towards realism would be to assume that the channel clocks are not synchronized . In this case, the PDM case will see twice as many changes in polarization and will experience more SPM.

Further simulations could also be run to evaluate transmission at longer distances to determine at which point polarization angles deviate when using fairly good constellations (low PMD and small channel spacing).
When the channel bit rates exceeds 40 Gb/s, the channel spacings is likely to exceed 100 Ghz, so also simulations at larger channel spacings needs to be run. The efficiency of polarization interleaving for suppressing XPM will become questionable at such spacings since PMD compensation at the

receiver will not solve the problem of the distributed nature of the XPM-induced crosstalk. Optical fibers with ultra-low D_p may become essential for implementation of polarization interleaving.
Since the distribution of the relative polarizations has been determined, follow-up research may also concentrate on quantifying the dependence of the nonlinear effects on the polarization angle between channels to obtain a nonlinear penalty distribution.
Further statistical simulation runs should also be used, to receive better accuracy in the data results. The number of statistical simulation runs was unfortunately limited due to the long simulation times.

8.2 Summary

Due to the statistical nature of PMD and the presence of nonlinear effects it seems hard to quantify depolarization, which induces degradation of the initial polarizations, analytically. A further in-depth investigation of autocorrelation functions is probably the best way to enter PMD and PDL analytically, which could be combined working on the coupled nonlinear Schrödinger equations treating XPM/SPM and FWM.
Analytically we have found expressions for the frequency-dependent stokes parameters at the end of a fiber element influenced by 2nd-order PMD. The expressions are solved numerically finding the DOP versus frequency which also show that orthogonality is preserved using orthogonal polarizations on the same carrier wavelength.
By using simulations the relative depolarization for polarization interleaving and polarization-division multiplexing have been quantized focusing on the evolution of the polarization separation angle when influenced of PMD.
In both cases angle deviation occurred at a early stage in the fiber. The comparison shows that the PMD-coefficient has less influence on larger frequency separations for PDM compared to interleaving in fibers with low polarization-mode dispersion.

Appendix A

From Maxwell equations to Helmholtz equation

Propagation of optical fields in fibers is governed by Maxwells equations. For a nonconducting medium without free charges these equations take the form

$$\nabla \times \mathbf{E} = -\frac{\partial \mathbf{B}}{\partial t}, \tag{A.1}$$

$$\nabla \times \mathbf{H} = \frac{\partial D}{\partial t}, \tag{A.2}$$

$$\nabla \cdot \mathbf{D} = 0, \tag{A.3}$$

$$\nabla \cdot \mathbf{B} = 0, \tag{A.4}$$

$$\tag{A.5}$$

where $\mathbf{E}$ and $\mathbf{H}$ are the electric and magnetic field vectors and $\mathbf{D}$ and $\mathbf{B}$ are the flux densities which are related to the field vectors as

$$\mathbf{D} = \epsilon_0 \mathbf{E} + \mathbf{P}, \tag{A.6}$$

$$\mathbf{B} = \mu_0 \mathbf{H} + \mathbf{M}, \tag{A.7}$$

$$\tag{A.8}$$

where ϵ_0 is the vacuum permittivity, μ_0 is the vacuum permability, and $\mathbf{P}$ and $\mathbf{M}$ are the induced electric and magnetic polarizations. For a nonmagnetic medium, such as fibers, $\mathbf{M} = 0$.

By taking the curl of Eq.(A.2) and using Eqs.(A.3),(A.7) and (A.8) one can eliminate $\mathbf{B}$ and $\mathbf{D}$ in favor of $\mathbf{E}$ and $\mathbf{P}$ and obtain

$$\nabla \times \nabla \times \mathbf{E} = -\frac{1}{c^2}\frac{\partial^2 \mathbf{E}}{\partial t^2} - \mu_0 \frac{\partial^2 \mathbf{P}}{\partial t^2} \tag{A.9}$$

where c is the speed of light in vacuum and the relation $\mu_0\epsilon_0 = 1/c^2$ was used.

The evaluation of $\mathbf{P}$ requires a quantum mechanical approach. The quantum mechanical approach is essential when the optical frequency is near a medium resonance, but a phenomenological relation between $\mathbf{P}$ and $\mathbf{E}$ and can be used far from medium resonances which is the case in fiber-optical communication systems.
In general the relation between $\mathbf{P}$ and $\mathbf{E}$ can be nonlinear. Although the nonlinear effects in optical fibers can be ignored in a discussion of fiber modes. The linear part of $\mathbf{P}$ is related to the general relation

$$\mathbf{P}(\mathbf{r},t) = \epsilon_0 \int_{-\infty}^{\infty} \chi(\mathbf{r}, t-t')\mathbf{E}(\mathbf{r},t')\,dt' \tag{A.10}$$

where the linear susceptibility χ in general is a second-rank tensor but reduces to a scalar for an isotropic medium such as silica glass (neglecting the birefringence of the fiber).
By now introducing the Fourier transform of $\mathbf{E}(\mathbf{r},t)$

$$\tilde{\mathbf{E}}(r,\omega) = \int_{-\infty}^{\infty} \mathbf{E}(r,t)e^{i\omega t}\,dt, \tag{A.11}$$

and a similar relation for $\mathbf{P}(\mathbf{r},t)$, and by using Eq.(A.10), Eq.(A.9) can be written in the frequency domain as

$$\nabla \times \nabla \times \tilde{\mathbf{E}} = -\epsilon(\mathbf{r},\omega)\frac{\omega^2}{c^2}\tilde{\mathbf{E}}. \tag{A.12}$$

The frequency-dependent dielectric constant appearing in Eq.(A.12) is defined as

$$\epsilon(\omega) = 1 + \tilde{\chi}(\mathbf{r},\omega) \tag{A.13}$$

where $\chi(\mathbf{r})$ is the Fourier transform of $\tilde{\chi}(\mathbf{r})$. In general $\epsilon(\mathbf{r},\omega)$ is complex and its real and imaginary parts are related to the refractive index and the absorption coefficient α by the definition

$$\epsilon = (n + i\alpha\frac{c}{2\omega})^2. \tag{A.14}$$

By using Eq.(A.13) and Eq.(A.14) n and α are related to $\tilde{\chi}$ as

$$n = (1 + \text{Re } \tilde{\chi})^{\frac{1}{2}} \tag{A.15}$$

$$\alpha = \frac{\omega}{nc}(\text{Im } \tilde{\chi}). \tag{A.16}$$

The frequency dependence of n is referred to as chromatic dispersion or simply as material dispersion.
Because of low optical losses in fibers in the wavelength region of interest, the imaginary part of ϵ is small i comparison to the real part. We can therefore replace ϵ by n^2. Second, since n is independent of the spatial coordinate $\mathbf{r}$ in both the core and the cladding of a step-index fiber, one can use the identity

$$\nabla \times \nabla \times \mathbf{E} = \nabla(\nabla \cdot \mathbf{E}) - \nabla^2 \mathbf{E} = -\nabla^2 \mathbf{E} \tag{A.17}$$

where we have used Eq.(A.4) and the relation $\tilde{\mathbf{D}} = \epsilon \tilde{\mathbf{E}}$ to set $\nabla \cdot \tilde{\mathbf{E}} = 0$. Eq.(A.17) holdes approximately as long as the index changes occur over a length scale much longer than the wavelength.
By using Eq.(A.17) in Eq.(A.12) we obtain

$$\nabla^2 \tilde{\mathbf{E}} + n^2(\omega) k_0^2 \tilde{\mathbf{E}} = 0, \tag{A.18}$$

where the free-space wave number k_0 is defined as

$$k_0 = \frac{\omega}{c} = \frac{2\pi}{\lambda} \tag{A.19}$$

and λ is the vacuum wavelength of the optical field oscillating at the frequency ω.

A.1 Fiber modes

At any frequency ω, optical fibers can support a finite number of guided modes whose spatial distrubution $\tilde{\mathbf{E}}(\mathbf{r}, r)$ is a solution of Helmholtz's equation (A.18) and satisfy all appropriate boundary coniditions.
A weakly guiding fiber behaves as a single mode waveguide if the optical frequency is smaller than the lowest cutoff frequency, υ_{cutoff} defined as

$$\upsilon_{cutoff} = \frac{Vc}{2\pi\rho_c\sqrt{n_1^2 - n_2^2}} \tag{A.20}$$

where ρ_c is the core radius, n_1 and n_2 is the refractive indexes of the core and the cladding respectively and V is the so-called V-number which restricts the number of modes in the fiber. Looking at Fig.(A.1) we can conclude that if $V < 2.405$ only one fundamental mode, LP_{01}, is supported by the optical fiber. The reader can easily identify cutoff conditions for other modes.

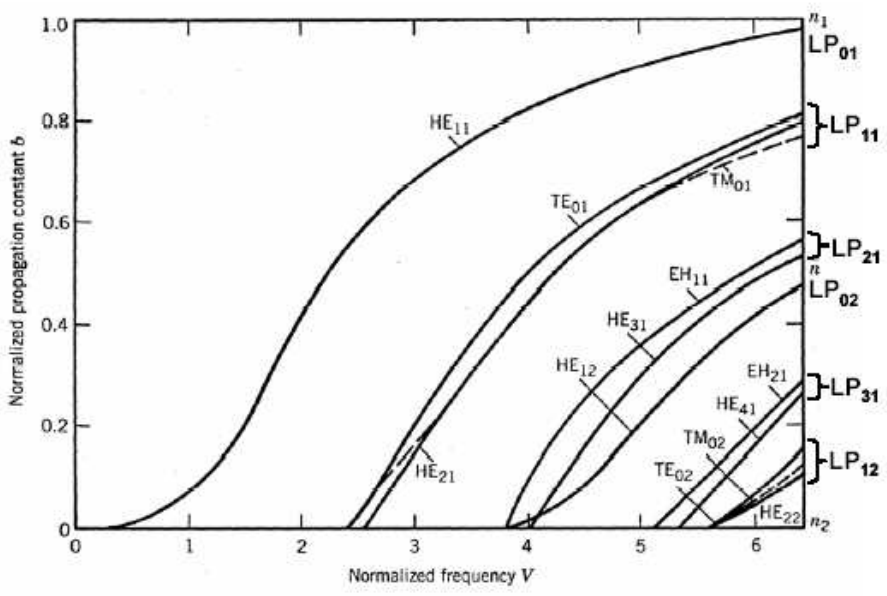

Figure A.1: *LP-modes in step-index fiber. Normalized propagation constant b versus the V-number.*

Appendix B

Principal States of Polarization

Let us consider a single-mode fiber of length L that does not represent polarization-dependent loss.
In the linear regime, if a monochromatic field represented by the complex vector $\mathbf{E}_a$ is coupled to the fiber, the complex vector $\mathbf{E}_b$ related to the output field is given by

$$\mathbf{E}_b = e^{-\alpha(\omega)L/2} e^{i\beta(\omega)L} \mathbf{J}(\omega, t)\mathbf{E}_a \tag{B.1}$$

where $\alpha(\omega)$ is the loss coefficient and $\beta(\omega)$ is the phase term taking into account the chromatic dispersion effect. The Jones Matrix $\mathbf{J}(\omega, t)$ is unitary and can be written

$$\mathbf{J}(\omega) = \begin{pmatrix} J_{11}(\omega) & J_{12}(\omega) \\ J_{21}(\omega) & J_{22}(\omega) \end{pmatrix} = \begin{pmatrix} J_{11} & J_{12} \\ -J_{12}^* & J_{11}^* \end{pmatrix} \tag{B.2}$$

where we have neglected the time dependence because the time evolution is rather slow compared to the polarization fluctuation time. Here $|J_{11}|^2 + |J_{12}|^2 = 1$.
After setting $k(\omega) = (-\alpha(\omega)/2 + i\beta(\omega)L)$ and deriving Eq.(B.1) with respect to ω we obtain

$$\frac{d\mathbf{E}_b}{d\omega} = e^{k(\omega)} \left[\frac{dk(\omega)}{d\omega} [\mathbf{J}(\omega)] + \frac{d[\mathbf{J}(\omega)]}{d\omega} \right] \mathbf{E}_a \tag{B.3}$$

The relation

$$\mathbf{E}^{a,b} = \begin{pmatrix} E_{a,b}^x \\ E_{a,b}^y \end{pmatrix} = A_{a,b} e^{i\phi_{a,b}} \epsilon^{a,b} \tag{B.4}$$

describes the input and output field vectors where $\epsilon^{a,b}$ are two complex unitary vectors representing the polarization state of the fields.
Differentation of Eq.(B.4) with respect to ω gives

$$\frac{d\mathbf{E}_b}{d\omega} = \left[\frac{1}{A_b}\frac{dA_b}{d\omega} + i\frac{d\phi_b}{d\omega}\right]\mathbf{E}_b + A_b e^{i\phi_b}\frac{d\epsilon_b}{d\omega}. \tag{B.5}$$

Since we wish to find the input states of polarization that give zero dispersion in the output state, we set $\frac{d\epsilon_b}{d\omega}$ to zero. By now combining Eq.(B.3) and Eq.(B.5) we obtain the following eigenvalue equation

$$\frac{d[\mathbf{J}(\omega)]}{d\omega}\epsilon_a = ih(\omega)[\mathbf{J}(\omega)]\epsilon_a \tag{B.6}$$

where

$$h(\omega) = \frac{d\phi_a(\omega)}{d\omega} + i\left[\frac{dk(\omega)}{d\omega} - \frac{1}{A_a}\frac{dA_a}{d\omega}\right] \tag{B.7}$$

The eigenvalue problem can be readily solved, obataining two eigenvalues

$$h_\pm = \pm\sqrt{\left|\frac{dJ_{11}}{d\omega}\right|^2 + \left|\frac{dJ_{12}}{d\omega}\right|^2} \tag{B.8}$$

The eigenvectors are expressed as

$$\epsilon_a^\pm = e^{i\rho}\begin{pmatrix} \frac{1}{D_\pm}\left(\frac{dJ_{12}}{d\omega} - ih_\pm J_{12}\right) \\ -\frac{1}{D_\pm}\left(\frac{dJ_{11}}{d\omega} - ih_\pm J_{11}\right) \end{pmatrix} \tag{B.9}$$

where

$$D_\pm = \sqrt{2h_\pm\left[h_\pm - \mathrm{Im}\left(J_{11}^*\frac{dJ_{11}}{d\omega} + J_{12}^*\frac{dJ_{12}}{d\omega}\right)\right]} \tag{B.10}$$

where ρ is an arbitrary phase.
The eigenvectors ϵ_a^+ and ϵ_a^- are an orthogonal pair of unitary complex vectors that represent the principal states of polarization of the medium.

The group delay difference is defined as

$$\Delta\tau = \frac{d\phi_b^+}{d\omega} - \frac{d\phi_b^-}{d\omega} = \tau_+ - \tau_- = 2\sqrt{\left|\frac{dJ_{11}}{d\omega}\right|^2 + \left|\frac{dJ_{12}}{d\omega}\right|^2} \tag{B.11}$$

Appendix C

Autocorrelation functions of PMD and PDL

Plots of the autocorrelation functions for PMD and PDL in Maple

```
> restart:with(linalg):
```

> K:=1/3*(Lambda-Theta*omega^2);
> Gamma=E(Gamma^2), Theta=E(tau^2-eta^2) as shown in the report.

```
K := 1/3*Lambda-1/3*Theta*omega^2
```

> tau:=10;
> DGD = 10 ps

```
tau := 10
```

> Lambda:=0.25;
> Mean-square PDL = 0.25

```
Lambda := .25
```

> Theta:=10;
> Birefringence = 10 ps

```
Theta := 10
```

> A:=0.8;

```
A := .8
```

> ExpectationPDL:=A^2*((Lambda/K)*(1-exp(K))-1*exp(K));
> Autocorrelation function with PDL and PMD.

```
ExpectationPDL :=
.1600/(.8333333333e-1-10/3*omega^2)*(1-exp(.8333333333e-1-10/3*omega^2
))-.64*exp(.8333333333e-1-10/3*omega^2)
```

```
> ExpectationWithoutPDL:=-1*exp(-1/3*Lambda*omega^2);
```

> Autocorrelation function with PMD

```
ExpectationWithoutPDL := -exp(-.8333333333e-1*omega^2)
> plot([ExpectationPDL,ExpectationWithoutPDL],omega,labels=[omega,ACF],
> legend=["With PDL","Without PDL"],title="Autocorrelation function
> of
> SOP",linestyle=[1,3]);
```

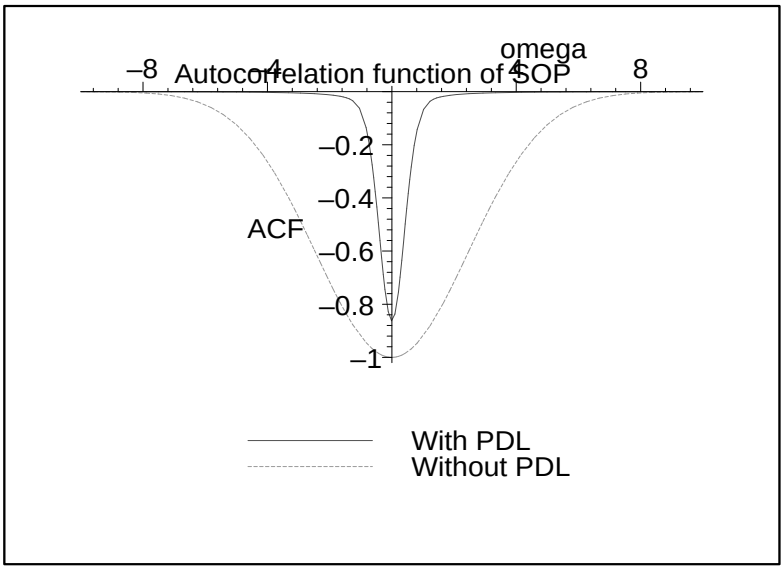


```
> extrema(ExpectationPDL,omega);extrema(ExpectationWithoutPDL,omega);
```

$$\{-0.8624743680\}$$

$$\{-1.\}$$

```
> max(ExpectationPDL,omega);
```

$$\max\left(\omega,\ \frac{0.1600\,(1-e^{(0.08333333333-\frac{10\,\omega^2}{3})})}{0.08333333333-\frac{10\,\omega^2}{3}}-0.64\,e^{(0.08333333333-\frac{10\,\omega^2}{3})}\right)$$

Appendix D

From Jones Matrix to Mueller matrix

Calculation of Mueller matrix from fiber Jones Matrix

```
> with(linalg):
```

D.1 Pauli matrices

```
> p[1]:=Matrix([[1,0],[0,-1]]);
```

$$p_1 := \begin{bmatrix} 1 & 0 \\ 0 & -1 \end{bmatrix}$$

```
> p[2]:=Matrix([[0,1],[1,0]]);
```

$$p_2 := \begin{bmatrix} 0 & 1 \\ 1 & 0 \end{bmatrix}$$

```
> p[3]:=Matrix([[0,-I],[I,0]]);
```

$$p_3 := \begin{bmatrix} 0 & -I \\ I & 0 \end{bmatrix}$$

$$j := 1$$

```
> U:=Matrix([[u[1],u[2]],[-q[2],q[1]]]);
> q2 and q1 is the complexvalued u1 and u2
```

$$U := \begin{bmatrix} u_1 & u_2 \\ -q_2 & q_1 \end{bmatrix}$$

```
> U2:=Matrix([[q[1],-u[2]],[q[2],u[1]]]);
```
> The complex transposed of U:

$$U2 := \begin{bmatrix} q_1 & -u_2 \\ q_2 & u_1 \end{bmatrix}$$

```
> for i from 1 to 3 do for j from 1 to 3 do
> print(R_[i,j]=1/2*trace(multiply(U,p[j],U2,p[i]))) end do
end do;
```

D.2 Calculation of Mueller matrix elements from fiber Jones Matrix

$$R_{-1,1} = u_1\,q_1 - u_2\,q_2$$
$$R_{-1,2} = u_2\,q_1 + u_1\,q_2$$
$$R_{-1,3} = u_2\,q_1\,I - u_1\,q_2\,I$$
$$R_{-2,1} = -u_1\,u_2 - q_2\,q_1$$
$$R_{-2,2} = -\frac{1}{2}\,{u_2}^2 + \frac{1}{2}\,{u_1}^2 + \frac{1}{2}\,{q_1}^2 - \frac{1}{2}\,{q_2}^2$$
$$R_{-2,3} = -\frac{1}{2}\,I\,{u_2}^2 - \frac{1}{2}\,I\,{u_1}^2 + \frac{1}{2}\,I\,{q_1}^2 + \frac{1}{2}\,I\,{q_2}^2$$
$$R_{-3,1} = -u_1\,u_2\,I + q_2\,q_1\,I$$
$$R_{-3,2} = \frac{1}{2}\,I\,(-{u_2}^2 + {u_1}^2) - \frac{1}{2}\,I\,({q_1}^2 - {q_2}^2)$$
$$R_{-3,3} = \frac{1}{2}\,I\,(-{u_2}^2\,I - {u_1}^2\,I) - \frac{1}{2}\,I\,({q_1}^2\,I + {q_2}^2\,I)$$

```
> R:=Matrix([[u[1]*q[1]-u[2]*q[2],u[2]*q[1]+u[1]*q[2],u[2]*q[1]*I-I*u[1
> ]*q[2]],[-u[1]*u[2]-q[2]*q[1],-1/2*u[2]^2+1/2*u[1]^2+1/2*q[1]^2-1/2*q[
> 2]^2,-1/2*I*u[2]^2-1/2*I*u[1]^2+1/2*I*q[1]^2+1/2*I*q[2]^2],[-I*u[1]*u[
> 2]+q[2]*q[1]*I,1/2*I*(-u[2]^2+u[1]^2)-1/2*I*(q[1]^2-q[2]^2),1/2*I*(-I*
> u[2]^2-I*u[1]^2)-1/2*I*(q[1]^2*I+q[2]^2*I)]]);
```
> Inserting the above elements give the General fiber PMD Mueller Matrix

$$R := \begin{bmatrix} u_1\,q_1 - u_2\,q_2\,,\; u_2\,q_1 + u_1\,q_2\,,\; u_2\,q_1\,I - u_1\,q_2\,I \\ -u_1\,u_2 - q_2\,q_1\,,\; -\frac{1}{2}\,{u_2}^2 + \frac{1}{2}\,{u_1}^2 + \frac{1}{2}\,{q_1}^2 - \frac{1}{2}\,{q_2}^2\,,\; -\frac{1}{2}\,I\,{u_2}^2 - \frac{1}{2}\,I\,{u_1}^2 + \frac{1}{2}\,I\,{q_1}^2 + \frac{1}{2}\,I\,{q_2}^2 \\ -u_1\,u_2\,I + q_2\,q_1\,I\,,\; \frac{1}{2}\,I\,(-{u_2}^2 + {u_1}^2) - \frac{1}{2}\,I\,({q_1}^2 - {q_2}^2)\,,\; \frac{1}{2}\,I\,(-{u_2}^2\,I - {u_1}^2\,I) - \frac{1}{2}\,I\,({q_1}^2\,I + {q_2}^2\,I) \end{bmatrix}$$

```
> s[1]:=Matrix([[1],[0],[0]]);
```
> linear input polarization along x-axis

$$s_1 := \begin{bmatrix} 1 \\ 0 \\ 0 \end{bmatrix}$$

```
> s[2]:=Matrix([[-1],[0],[0]]);
```
> linear input polarization

along y axis

$$s_2 := \begin{bmatrix} -1 \\ 0 \\ 0 \end{bmatrix}$$

```
> M:=Matrix([[cos(xi/2)-I*sin(xi/2)*cos(2*k*omega),-I*sin(xi/2)*sin(2*k
> *omega)],[-I*sin(xi/2)*sin(2*k*omega),cos(xi/2)+I*sin(xi/2)*cos(2*k*om
> ega)]]);
```
> 2nd order PMD Jones matrix (included depolarization)

$$M := \begin{bmatrix} \cos(\frac{\xi}{2}) - \sin(\frac{\xi}{2})\cos(2\,k\,\omega)\,I & -I\sin(\frac{\xi}{2})\sin(2\,k\,\omega) \\ -I\sin(\frac{\xi}{2})\sin(2\,k\,\omega) & \cos(\frac{\xi}{2}) + \sin(\frac{\xi}{2})\cos(2\,k\,\omega)\,I \end{bmatrix}$$

```
> M2:=Matrix([[cos(xi/2)+I*sin(xi/2)*cos(2*k*omega),I*sin(xi/2)*sin(2*k
> *omega)],[I*sin(xi/2)*sin(2*k*omega),cos(xi/2)-I*sin(xi/2)*cos(2*k*ome
> ga)]]);
```
> Complex transposed of M

$$M2 := \begin{bmatrix} \cos(\frac{\xi}{2}) + \sin(\frac{\xi}{2})\cos(2\,k\,\omega)\,I & \sin(\frac{\xi}{2})\sin(2\,k\,\omega)\,I \\ \sin(\frac{\xi}{2})\sin(2\,k\,\omega)\,I & \cos(\frac{\xi}{2}) - \sin(\frac{\xi}{2})\cos(2\,k\,\omega)\,I \end{bmatrix}$$

D.3 Finding Mueller matrix elements

```
> for v from 1 to 3 do for w from 1 to 3 do
> print(M_[v,w]=1/2*trace(multiply(M,p[w],M2,p[v]))) end do
end do;
```

$$M_{-1,1} = \frac{1}{2}\left(\cos(\frac{\xi}{2}) - \sin(\frac{\xi}{2})\cos(2\,k\,\omega)\,I\right)\left(\cos(\frac{\xi}{2}) + \sin(\frac{\xi}{2})\cos(2\,k\,\omega)\,I\right)$$
$$- \sin(\frac{\xi}{2})^2\sin(2\,k\,\omega)^2$$
$$- \frac{1}{2}\left(-\cos(\frac{\xi}{2}) - \sin(\frac{\xi}{2})\cos(2\,k\,\omega)\,I\right)\left(\cos(\frac{\xi}{2}) - \sin(\frac{\xi}{2})\cos(2\,k\,\omega)\,I\right)$$

$$M_{-1,2} = -\sin(\frac{\xi}{2})\sin(2\,k\,\omega)\left(\cos(\frac{\xi}{2}) + \sin(\frac{\xi}{2})\cos(2\,k\,\omega)\,I\right)I$$
$$+ \left(\cos(\frac{\xi}{2}) - \sin(\frac{\xi}{2})\cos(2\,k\,\omega)\,I\right)\sin(\frac{\xi}{2})\sin(2\,k\,\omega)\,I$$

$$M_{-1,3} = \sin(\frac{\xi}{2})\sin(2\,k\,\omega)\left(\cos(\frac{\xi}{2}) + \sin(\frac{\xi}{2})\cos(2\,k\,\omega)\,I\right)$$
$$+ \left(\cos(\frac{\xi}{2}) - \sin(\frac{\xi}{2})\cos(2\,k\,\omega)\,I\right)\sin(\frac{\xi}{2})\sin(2\,k\,\omega)$$

$$M_{-2,1} = \left(\cos(\frac{\xi}{2}) - \sin(\frac{\xi}{2})\cos(2\,k\,\omega)\,I\right)\sin(\frac{\xi}{2})\sin(2\,k\,\omega)\,I$$
$$- \frac{1}{2}\,I\sin(\frac{\xi}{2})\sin(2\,k\,\omega)\left(\cos(\frac{\xi}{2}) + \sin(\frac{\xi}{2})\cos(2\,k\,\omega)\,I\right)$$
$$+ \frac{1}{2}\,I\left(-\cos(\frac{\xi}{2}) - \sin(\frac{\xi}{2})\cos(2\,k\,\omega)\,I\right)\sin(\frac{\xi}{2})\sin(2\,k\,\omega)$$

$$M_{-2,2} = \sin(\frac{\xi}{2})^2\sin(2\,k\,\omega)^2 + \frac{1}{2}\left(\cos(\frac{\xi}{2}) - \sin(\frac{\xi}{2})\cos(2\,k\,\omega)\,I\right)^2$$
$$+ \frac{1}{2}\left(\cos(\frac{\xi}{2}) + \sin(\frac{\xi}{2})\cos(2\,k\,\omega)\,I\right)^2$$

$$M_{-2,3} = -\frac{1}{2}\,I\left(\cos(\frac{\xi}{2}) - \sin(\frac{\xi}{2})\cos(2\,k\,\omega)\,I\right)^2 + \frac{1}{2}\,I\left(\cos(\frac{\xi}{2}) + \sin(\frac{\xi}{2})\cos(2\,k\,\omega)\,I\right)^2$$

$$M_{-3,1} = -\left(\cos(\frac{\xi}{2}) - \sin(\frac{\xi}{2})\cos(2\,k\,\omega)\,I\right)\sin(\frac{\xi}{2})\sin(2\,k\,\omega) - \frac{1}{2}\,I($$
$$-\sin(\frac{\xi}{2})\sin(2\,k\,\omega)\left(\cos(\frac{\xi}{2}) + \sin(\frac{\xi}{2})\cos(2\,k\,\omega)\,I\right)I$$
$$+ \left(-\cos(\frac{\xi}{2}) - \sin(\frac{\xi}{2})\cos(2\,k\,\omega)\,I\right)\sin(\frac{\xi}{2})\sin(2\,k\,\omega)\,I)$$

$$M_{-3,2} = \frac{1}{2}\,I\left(\sin(\frac{\xi}{2})^2\sin(2\,k\,\omega)^2 + \left(\cos(\frac{\xi}{2}) - \sin(\frac{\xi}{2})\cos(2\,k\,\omega)\,I\right)^2\right)$$
$$- \frac{1}{2}\,I\left(\left(\cos(\frac{\xi}{2}) + \sin(\frac{\xi}{2})\cos(2\,k\,\omega)\,I\right)^2 + \sin(\frac{\xi}{2})^2\sin(2\,k\,\omega)^2\right)$$

$$M_{-3,3} = \frac{1}{2} I \left(\sin(\frac{\xi}{2})^2 \sin(2\,k\,\omega)^2 I - (\cos(\frac{\xi}{2}) - \sin(\frac{\xi}{2}) \cos(2\,k\,\omega) I)^2 I\right)$$
$$- \frac{1}{2} I \left((\cos(\frac{\xi}{2}) + \sin(\frac{\xi}{2}) \cos(2\,k\,\omega) I)^2 I - \sin(\frac{\xi}{2})^2 \sin(2\,k\,\omega)^2 I\right)$$

$$\int \mathrm{f}(\omega)^2 \, d\omega$$

D.4 Stokes vectors at fiber output

The tree output Stokes vector components for the whole spectrum of
Channel A (assuming linear input polarization (1,0,0)ˆT)

```
> s[(1-chan1)]:=int(1/2*(cos(1/2*xi)-I*sin(1/2*xi)*cos(2*k*omega))*(cos
> (1/2*xi)+sin(1/2*xi)*cos(2*k*omega)*I)-sin(1/2*xi)^2*sin(2*k*omega)^2-
> 1/2*(-cos(1/2*xi)-I*sin(1/2*xi)*cos(2*k*omega))*(cos(1/2*xi)-I*sin(1/2
> *xi)*cos(2*k*omega))*f(omega)^2,omega);
```

$$s_{1-chan1} := \int \frac{1}{2} \left(\cos(\frac{\xi}{2}) - \sin(\frac{\xi}{2}) \cos(2\,k\,\omega) I\right) \left(\cos(\frac{\xi}{2}) + \sin(\frac{\xi}{2}) \cos(2\,k\,\omega) I\right)$$
$$- \sin(\frac{\xi}{2})^2 \sin(2\,k\,\omega)^2$$
$$- \frac{1}{2} \left(-\cos(\frac{\xi}{2}) - \sin(\frac{\xi}{2}) \cos(2\,k\,\omega) I\right) \left(\cos(\frac{\xi}{2}) - \sin(\frac{\xi}{2}) \cos(2\,k\,\omega) I\right) \mathrm{f}(\omega)^2 d\omega$$

```
> s[(2-chan1)]:=int((cos(1/2*xi)-I*sin(1/2*xi)*cos(2*k*omega))*sin(1/2*
> xi)*sin(2*k*omega)*I-1/2*I*sin(1/2*xi)*sin(2*k*omega)*(cos(1/2*xi)+sin
> (1/2*xi)*cos(2*k*omega)*I)+1/2*I*(-cos(1/2*xi)-I*sin(1/2*xi)*cos(2*k*o
> mega))*sin(1/2*xi)*sin(2*k*omega)*f(omega)^2,omega);
```

$$s_{2-chan1} := \int \left(\cos(\frac{\xi}{2}) - \sin(\frac{\xi}{2}) \cos(2\,k\,\omega) I\right) \sin(\frac{\xi}{2}) \sin(2\,k\,\omega) I$$
$$- \frac{1}{2} I \sin(\frac{\xi}{2}) \sin(2\,k\,\omega) \left(\cos(\frac{\xi}{2}) + \sin(\frac{\xi}{2}) \cos(2\,k\,\omega) I\right)$$
$$+ \frac{1}{2} I \left(-\cos(\frac{\xi}{2}) - \sin(\frac{\xi}{2}) \cos(2\,k\,\omega) I\right) \sin(\frac{\xi}{2}) \sin(2\,k\,\omega) \mathrm{f}(\omega)^2 d\omega$$

```
> s[(3-chan1)]:=int(-(cos(1/2*xi)-I*sin(1/2*xi)*cos(2*k*omega))*sin(1/2
> *xi)*sin(2*k*omega)-1/2*I*(-I*sin(1/2*xi)*sin(2*k*omega)*(cos(1/2*xi)+
> sin(1/2*xi)*cos(2*k*omega)*I)+(-cos(1/2*xi)-I*sin(1/2*xi)*cos(2*k*omeg
> a))*sin(1/2*xi)*sin(2*k*omega)*I)*f(omega)^2,omega);
```

$$s_{3-chan1} := \int -(\cos(\frac{\xi}{2}) - \sin(\frac{\xi}{2})\cos(2\,k\,\omega)\,I)\sin(\frac{\xi}{2})\sin(2\,k\,\omega) - \frac{1}{2}\,I($$
$$-\sin(\frac{\xi}{2})\sin(2\,k\,\omega)\,(\cos(\frac{\xi}{2}) + \sin(\frac{\xi}{2})\cos(2\,k\,\omega)\,I)\,I$$
$$+\,(-\cos(\frac{\xi}{2}) - \sin(\frac{\xi}{2})\cos(2\,k\,\omega)\,I)\sin(\frac{\xi}{2})\sin(2\,k\,\omega)\,I)\mathrm{f}(\omega)^2 d\omega$$

The tree output Stokes vector components for the whole spectrum of Channel B (assuming linear input polarization (-1,0,0)ˆT) is orthogonal to channelA

D.5 Frequency spectrum plot

The grid and the contour plots of a 2-D Gaussian density function assuming zero means and unit variances. R is the 2x2 correlation matrix, and E[xy]=0.6

```
> R:=array( [[1.0,0.6],[0.6,1.0]] ); f :=
> (x,y) -> evalf( 1/(2*Pi) * 1/sqrt(det(R)) * exp(-1/2 *
> (evalm([x,y] &* inverse(R) &* [x,y]) )) ); with(plots):
> plot3d(f(x,y), x=-3..3, y=-3..3, grid=[30,30], axes=FRAME);
> contourplot(f(x,y), x=-3..3, y=-3..3, grid=[30,30], axes=FRAME);
```

$$R := \begin{bmatrix} 1.0 & 0.6 \\ 0.6 & 1.0 \end{bmatrix}$$

$$f := (x,\, y) \rightarrow \mathrm{evalf}(\frac{1}{2}\,\frac{e^{(-1/2\,\mathrm{evalm}(\text{`\&*`}(\text{`\&*`}([x,y],\,\mathrm{inverse}(R)),\,[x,y])))}}{\pi\,\sqrt{\det(R)}})$$

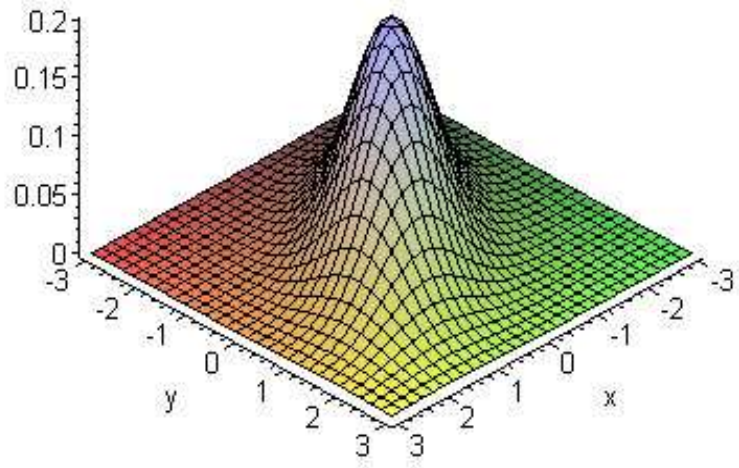

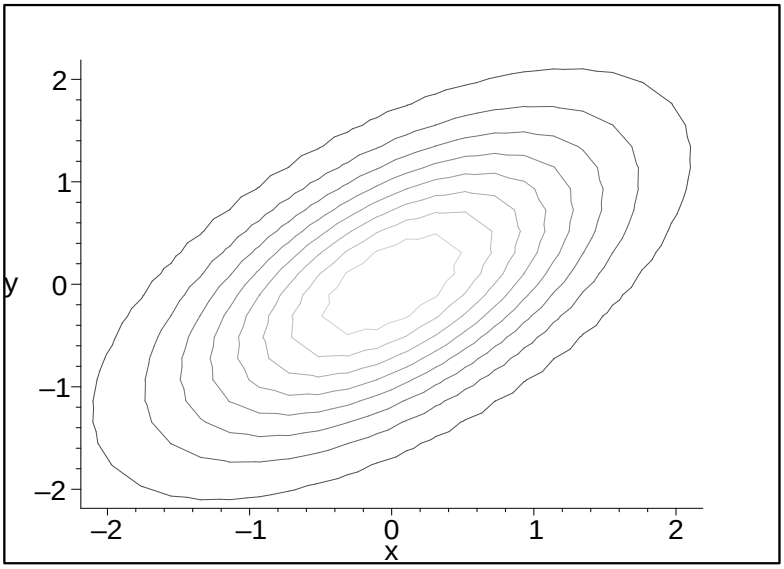


```
> f:=(1/(sqrt(2*pi)*sigma))*exp(-((omega)^2-(omega[carrier])^2)/(2*sigm
> a^2));
```

> Assuming a gaussian frequency spectrum.

```
> l:=f^2;
```

> f squared

$$f := \frac{1.000000000\,\sqrt{2}\,e^{(-2.000000000\,\omega^2+2.000000000\,{\omega_{carrier}}^2)}}{\sqrt{\pi}}$$

$$l := \frac{2.000000000\,(e^{(-2.000000000\,\omega^2+2.000000000\,{\omega_{carrier}}^2)})^2}{\pi}$$

D.6 Stokes components (M_11,M_21 and M_31 multiplied with frequency spectrum (l=fˆ2 above)

```
> s_1:=(omega,tau,k)->evalf(1/2*(cos(1/2*(omega*tau))-I*sin(1/2*(omega*
> tau))*cos(2*k*omega))*(cos(1/2*(omega*tau))+sin(1/2*(omega*tau))*cos(2
> *k*omega)*I)-sin(1/2*(omega*tau))^2*sin(2*k*omega)^2-1/2*(-cos(1/2*(om
> ega*tau)*I)-I*sin(1/2*(omega*tau))*cos(2*k*omega))*(cos(1/2*(omega*tau
> ))-I*sin(1/2*(omega*tau))*cos(2*k*omega)))*((1/(sqrt(2*pi)*sigma))*exp
> (-((omega)^2-(omega[carrier])^2)/(2*sigma^2)))^2 ;
```

Stokes componcent S1*M_11*f(omega)

```
> s_2:=(omega,tau,k)->evalf((cos(1/2*omega*tau)-I*sin(1/2*omega*tau)*co
> s(2*k*omega))*sin(1/2*omega*tau)*sin(2*k*omega)*I-1/2*I*sin(1/2*omega*
> tau)*sin(2*k*omega)*(cos(1/2*omega*tau)+sin(1/2*omega*tau)*cos(2*k*ome
> ga)*I)+1/2*I*(-cos(1/2*omega*tau)-I*sin(1/2*omega*tau)*cos(2*k*omega))
> *sin(1/2*omega*tau)*sin(2*k*omega))*((1/(sqrt(2*pi)*sigma))*exp(-(omeg
> a^2-(omega[carrier])^2)/(2*sigma^2)))^2;
```

Stokes componcent S2*M_21*f(omega)

```
> pi:=Pi;
```

$$\pi := \pi$$

```
> s_3:=(omega,tau,k)->evalf(-(cos(1/2*(omega*tau))-I*sin(1/2*(omega*tau
> ))*cos(2*k*omega))*sin(1/2*(omega*tau))*sin(2*k*omega)-1/2*I*(-I*sin(1
> /2*(omega*tau))*sin(2*k*omega)*(cos(1/2*(omega*tau))+sin(1/2*(omega*ta
> u))*cos(2*k*omega)*I)+(-cos(1/2*(omega*tau))-I*sin(1/2*(omega*tau))*co
> s(2*k*omega))*sin(1/2*(omega*tau))*sin(2*k*omega)*I))*((1/(sqrt(2*pi)*
> sigma))*exp(-(omega^2-(omega[carrier])^2)/(2*sigma^2)))^2;
```

Stokes componcent S3*M_31*f(omega)

D.7 Evaluation of degree of polarization (DOP) for Channel A

Inserting the parameters: (tau=10ps)

```
> sigma:=0.399;k:=1/10;tau:=1*10^(-12);omega[carrier]:=0;
```

```
> plot([evalf(sqrt(abs(s_1(omega,tau,k))^2+abs(s_2(omega,tau,k))^2+abs(
> s_3(omega,tau,k))^2)),evalf(sqrt(abs(s_1(omega,tau+60000,k))^2+abs(s_2
> (omega,tau+60000,k))^2+abs(s_3(omega,tau+60000,k))^2))],omega=0..5,lab
> els=[Frequency,DOP],color=[red,blue]);
```

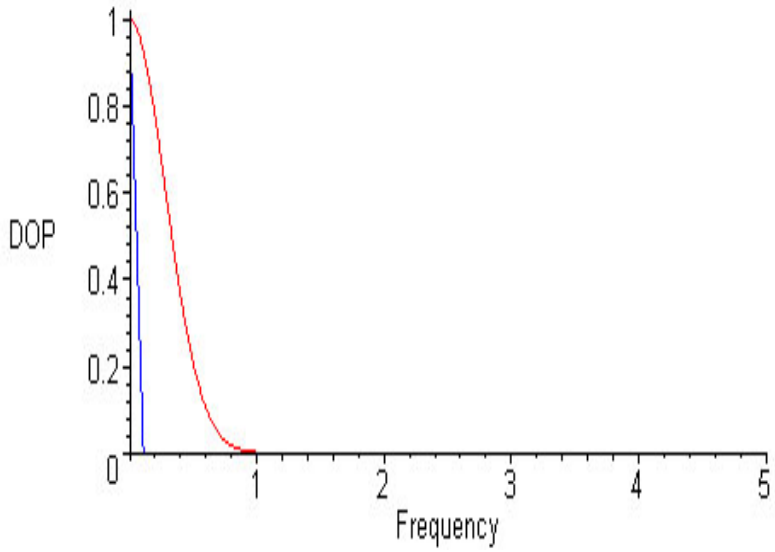

Appendix E

Polarization interleaving setup

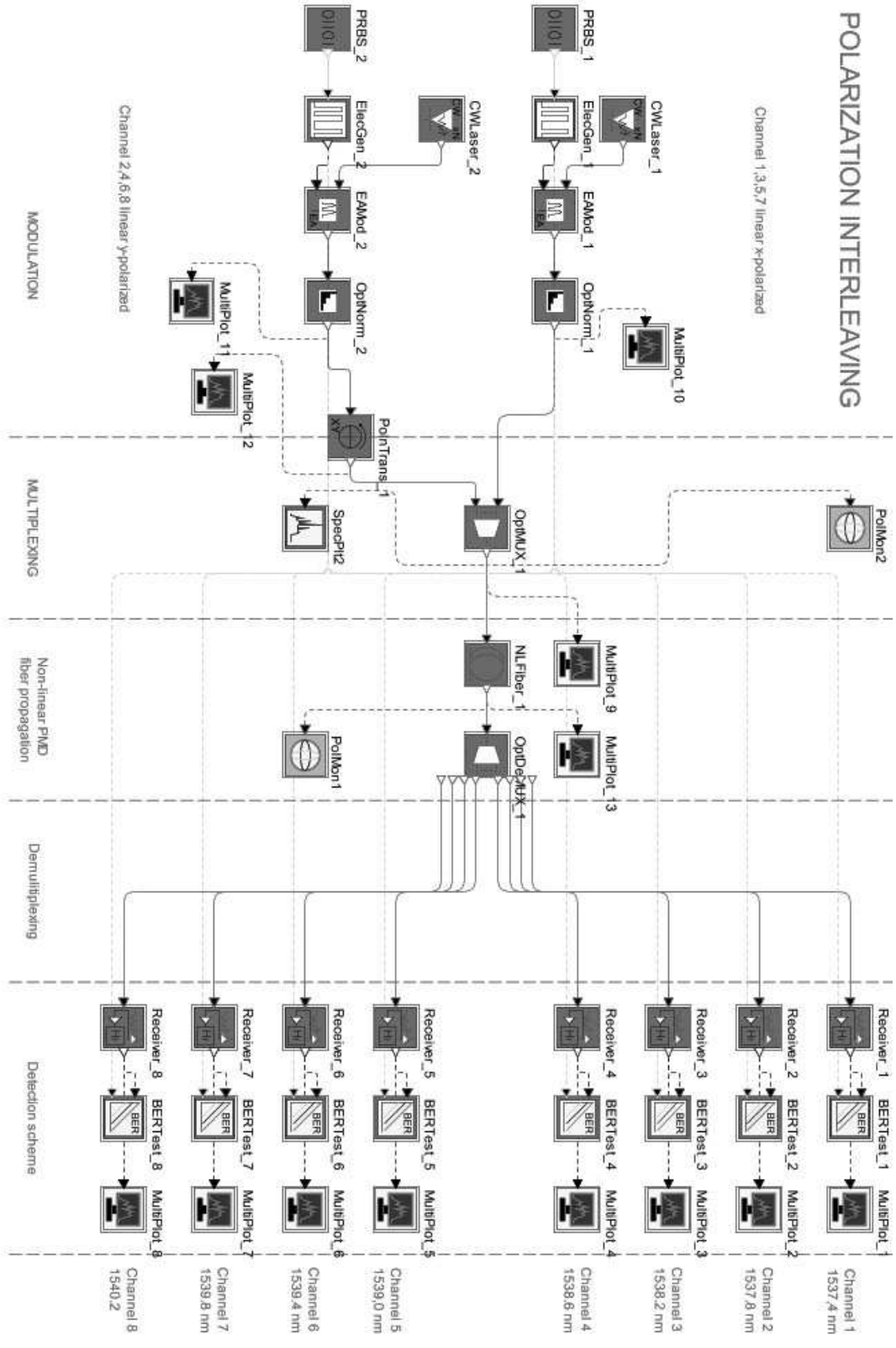

Figure E.1: *Setup for measuring the Q-value for different input angles*

Bibliography

[ACDM87] D. Andresciani, F. Curti, B. Daino, and F. Matera. measurement of the group delay difference between the PSP on a low-terrestrial fiber cable. *Optics letters*, 12:144–146, 1987.

[Agr95] Govind P. Agrawal. *Nonlinear fiber optics*. Academic Press, 3th edition, 1995. ISBN 0120451433.

[Agr97] Govind P. Agrawal. *Fiber-optic communication systems*. John Willey and sons, 2nd edition, 1997. ISBN 0471175404.

[BCN00] B.Huttner, C.Geiser, and N.Gisin. Polarization-induced distortions in optical fiber networks with polarization-mode dispersion and polarization-dependent losses. *IEEE Journal of Quantum Electronics*, 6:317–329, 2000.

[BGC98] C. Le Brun, E. Guillard, and J. Citerne. Communication systems interactive software (comcis): modelling of components and its application to the simulation of optical networks. *Applied Optics*, 37:6059–6065, 1998.

[Blo77] N. Bloembergen. *Nonlinear optics*. World Scientific Publishing Company, 4th edition, 1977. ISBN 9810225997.

[BMD94] N. S. Bergano, V. J. Mazurczyk, and C. R. Davidson. Polarization hole-burning in erbium doped fiber amplifier transmission systems. *Proceedings of ECOC'94*, pages 621–628, 1994.

[Boa03] Boualem Boashash. *Time and Frequency Signal analysis and processing - a comprehensive reference*. Elsevier, 1st edition, 2003. ISBN 0080443354.

[BOS99] P. C. Becker, N. A. Olsson, and J. R. Simpson. *Erbium-doped fiber amplifiers*. Academic Press, 1st edition, 1999. ISBN 0120845903.

[Boy92] R. W. Boyd. *Nonlinear optics*. Academic Press, Boston, 1st edition, 1992. ISBN 0121216802.

[Bru96] F. Bruyere. Impact of first- and second order PMD in optical digital transmission systems. *Optical fiber technology*, 2:269–280, 1996.

[BVO+03] Alberto Bononi, Armando Vannucci, A. Orlandini, E. Corbel, S. Lanne, and S.Bigo. Degree of polarization degradation due to cross-phase modulation and its impact on polarization-mode dispersion compensators. *IEEE Journal of lightwave technology*, 21(9):1903–1913, 2003.

[CB00a] B. Collings and L. Boivin. Nonlinear polarization evoluation induced by cross-phase modulation and its impact on trasmission systems. *IEEE Photonics Technology Letters*, 12(11), 2000.

[CB00b] B. C. Collings and L. Boivin. Nonlinear polarization evolution induced by cross-phase modulation and its impact on transmission systems. *IEEE Photonics technology letters*, 12(1582-1584), 2000.

[CB01] B. C. Collings and L. Boivin. Interference detection enables 2*20 Gbit/s RZ polarization division multiplex transmission. *IEEE Journal of Electronic letters*, 12:511–512, 2001.

[CCD98] Sien Chi, Chi Chen, and Jeng Dung. Multiple soliton interactions in a polarization-division multiplexed system. *Optics communications*, 147(42-46), 1998.

[Coc95] P. Cochrane. *Optical Network technology*. Chapman Hall, 1st edition, 1995.

[CR86] C.D.Poole and R.E.Wagner. Phenomenological approach to polarization dispersion in single mode fibers. *IEEE Journal of Electronic Letters*, 22(19):1029–1030, 1986.

[DDF03a] A. K. Dutta, N. K. Dutta, and M. Fujiwara. *WDM technologies: active optical components*. academic press, 1st edition, 2003. ISBN 0122252616.

[DDF03b] A. K. Dutta, N. K. Dutta, and M. Fujiwara. *WDM technologies: passive optical components*. academic press, 1st edition, 2003. ISBN 0122252624.

[Dir47] Paul Dirac. *The principles of quantum mechanics*. Oxford university press,London, New York, 4th edition, 1947. ISBN 0198512082.

[ea92] S. G. Evangelides et al. Polarization multiplexing with solitons. *IEEE Journal of lightwave technology*, 10:28–35, 1992.

[ea97] A. Carena et al. A time domain optical transmission system simulation package accounting for nonlinear and polarization related effects in fiber. *IEEE Journal on selected areas in communications*, 15(4):751–765, 1997.

[Elr93] A. F. Elrefaie. Computer-aided modeling and simulation of lightwave systems. *IEEE LEOS Newslett*, 7:1, Feb.19-20 1993.

[FJNK99] G. J. Foschini, R. M. Jopson, L. E. Nelson, and H. Kogelnik. The statistics of PMD-induced chromatic fiber dispersion. *IEEE Journal of lightwave technology*, 17:1560–1565, december 1999.

[FJNK01] G. J. Foschini, R. M. Jopson, L. E. Nelson, and H. Kogelnik. Statistics of second order PMD depolarization. *IEEE Journal of lightwave technology*, 19(12):1882–1886, december 2001.

[FP91] G. J. Foschini and C. D. Poole. Statistical theory of polarization dispersion in single mode fibers. *IEEE Journal of lightwave technology*, 9(11):1439–1456, 1991.

[FYP85] Tian Feng, Wu Yizun, and Ye Peida. Polarization mode coupling with a broadband source in birefringent polarization-maintaining fibers. *Optical society of America*, 2(5), 1985.

[FYP90] Tian Feng, Wu Yizun, and Ye Peida. Random mode coupling theory of single-mode optical fibers. *IEEE Journal of lightwave technology*, 8:1235–1242, 1990.

[GEV97] C. Glingener, J. P. Elbers, and E. Voges. Simulation tool for WDM networks. *Colloquium on WDM Technol. Applicat, London;Inst.Elect.Eng.*, 1:2/1–2/4, 1997.

[GH00] N. Gisin and B. Huttner. Influence of polarization dependent loss on birefringent optical fiber networks. *OFC Conference, Baltimore*, 2000.

[GK00] J. P. Gordon and H. Kogelnik. PMD fundamentals: Polarization mode dispersion in optical fibers. *Proc. of the national academy of science*, 97(9):4541–4550, 2000.

[GZ01] Ling-Wei Guo and Ying-Wu Zhou. Crosstalk detection schemes for polarization division multiplex transmission. *IEEE Journal of lightwave technology*, 19(10):1469–1475, 2001.

[GZ04] Ling-Wei Guo and Ying-Wu Zhou. Combined effect of PMD and PDL on four-wave mixing induced crosstalk in WDM system. *Optics communications*, 230:309–312, 2004.

[Hei00] F. Heismann. Autmatic polarization demultiplexer for polarization-multiplexed transmission systems. *IEEE Journal of Electronic letters*, 22:1965–1966, 2000.

[HG97] B. Huttner and N. Gisin. Anomalous pulse spreading in birefringent optical fibers with polarization-dependent losses. *Optics letters*, 22:504, 1997.

[Hil92] P. M. Hill. Optical polarization division multiplexing at 4gb/s. *IEEE Photonics Technology Letters*, 4:500–502, 1992.

[HKPW03] A. Hodzic, B. Konrad, K. Petermann, and M. Winter. Improvement of system performance in nx 40 Gb/s WDM transmission using alternate polarizations. *IEEE Photonics Technology Letters*, 6(1):153–155, 2003.

[HNW00] S. Hinz, D. Sandel R. Noe, and F. Wust. Optical NRZ 2*10 Gb/s polarization division multiplex transmission with endless polarization controll driven by correlation signals. *IEEE Photonics technology letters*, 3:1402–1403, 2000.

[HT73] A. Hasegawa and F. Tappert. Optical solitons in single-mode fibers. *Applied Physics letters*, 23(142), 1973.

[htta] Available: http://focuss.zedo.fuedo.de. *ZEDO.FOCUS (online).*

[httb] Available: http://www.rsoftdesign.com/. *LinkSim (online).*

[httc] Available: http://www.rsoftdesign.com/. *Rsoft OptSim(Online).*

[httd] Available: http://www.virtualphotonics.com/. *Virtual Photonics, Photonic Transmission Design Suite (Online).*

[Hua97] S. Huard. *Polarization of light.* Wiley, New York, 1st edition, 1997. ISBN 0471965367.

[IMMS96] E. Iannone, F. Matera, A. Mecozzi, and M. Settembre. Performance evaluation of very long span direct detection intensity and polarization modulated systems. *IEEE Journal of lightwave technology*, 14:261–272, 1996.

[IMMS98] E. Iannone, F. Matera, A. Mecozzi, and M. Settembre. *Nonlinear optical communication networks.* John Willey and sons, 1st edition, 1998. ISBN 0471152706.

[Ino91] K. Inoue. Arrangement of orthogonal polarized signals for suppressing fiber four-wave mixing in optical multichannel transmission systems. *IEEE Photonics Technology Letters*, 3:560, 1991.

[Ino92] Kyo Inoue. Polarization effect on four-wave mixing efficiency in single-mode fiber. *IEEE Journal of Quantum Electronics*, 28 (4), 1992.

[Jer54] H. G. Jerrard. The poincare sphere. *Journal of Optical society of America*, 44:634–640, 1954.

[Jer82] H. G. Jerrard. Modern desctiption of polarized light: matrix methods. *Optics and laser technology*, 1982.

[Kar03a] Stamatios V. Kartalopoulos. *DWDM.* Wiley interscience, 1st edition, 2003. ISBN 0471269050.

[Kar03b] Stamatios V. Kartalopoulos. *Fiber-optic communications technology.* Prentice Hall, 1st edition, 2003. ISBN 0471269342.

[KB99] Magnus Karlsson and Jonas Brentel. Autocorrelation function of polarization-mode dispersion. *Optics letters*, 24(14):939–941, 1999.

[KB00] Magnus Karlsson and Jonas Brentel. Long-term measurement of PMD and polarization drift in installed fibers. *IEEE Journal of lightwave technology*, 18(7):941–951, 2000.

[KH03] J. M. Kahn and K. Ho. Ultimate spectral efficiency limits in DWDM systems. *Unpublished*, 2003.

[Kik01] N. Kikuchi. Analysis of signal degree of polarization degradation used as control signal for optical polarization mode dispersion compensation. *IEEE Journal of lightwave technology*, 19 (480-486), 2001.

[KNJ02] H. Kogelnik, L. E. Nelson, and R. M. Jopson. Polarization mode dispersion. *Optical fiber telecommunications*, IVB, I.P., 2002.

[Lou73] Rodney Loudon. *The quantum theory of light*. Oxford Science publications, 2nd edition, 1973. ISBN 0198511558.

[MCB01] L. Moller, S. Chandrasekhar, and L. L. Buhl. Dependence of nonlinear depolarization on the overall polarization of PMD distorted WDM signals. *Prof. ECOC'01, Amsterdam, The Netherlands*, 17(214-215), 2001.

[MKJ+04] C. J. McKinstrie, H. Kogelnik, R. M. Jopson, S. Radic, and A. V. Kanaev. Four-wave mixing in fibers with random birefringence. *Optics Express*, 12(10):2033–2055, 2004.

[Mol90] L. F. Mollenauer. Experimental study of soliton transmission over more than 10000 km in dispersion-shifted fiber. *Optics letters*, 15:1203–1205, 1990.

[MS01] Djafar K. Mynbaev and Lowell L. Scheiner. *Fiber-optic communications technology*. Prentice Hall, 1st edition, 2001. ISBN 0139620699.

[MS02a] Antonia Mecozzi and Mark Shtaif. The statistics of polarization loss in optical communication systems. *IEEE Photonics Technology Letters*, 14(3):313–1315, 2002.

[MS02b] Antonio Mecozzi and Mark Shtaif. The statistics of polarization-dependent loss in optical communication systems. *IEEE Journal of lightwave technology*, 14(3), 2002.

[MSGM89] L. F. Mollenauer, K. Smith, J. P. Gordon, and C. R. Menyuk. Resistance of solitons to the effects of polarization dispersion in optical fibers. *Optics letters*, 14:1219–1221, 1989.

[Muk97] B. Mukherjee. *Optical communication networks*. McGraw-Hill, 1st edition, 1997. ISBN 0070444358.

[New93] D. E. Newland. *Random vibrations, spectral and wavelet analysis*. Elsevier, 3th edition, 1993. ISBN 0582215846.

[NGJK00] L. E. Nelson, J. P. Gordon, R. M. Jopson, and H. Kogelnik. Meausrement of polarization mode dispersion vectors using the polarization-dependent signal delay method. *Optics express*, 6: 158–167, 2000.

[Ors00] M. Orszag. *Quantum Optics*. Springer, 1st edition, 2000. ISBN 3540650083.

[PB98] D. Penninckx and F. Bruyere. Impact of the statistics of second-order polarization-mode dispersion on system performance. *Proc. OFC'98, Dallas, Mar.98, ThR2*, pages 340–342, 1998.

[Poi92] H. Poincare. Theorie mathematique de la lumiere. *Gautier-Villars*, 2, 1892.

[PPB00] D. L. Philen, D. W. Peckham, and I. Brener. Measurement of nonlinear index of refraction for various fiber types. *Prof.of OFC'2000, Baltimore*, 2000.

[RW03] Etienne Rochat and Stuart D. Walker. C-band polarisation orthogonality preservation in 5 Gb/s, 50um multimode fibre links up to 3km. *Optics Express*, 11(6), 2003.

[RWP04] E. Rochat, S. Walker, and M. Parker. Polarization and wavelength division multiplexing at 1.55 micrometer for bandwidth enhancement of multimode fibre based access networks. *Optics Express*, 12(10):2280–2292, 2004.

[Sha48] C. E. Shannon. A mathematical theory of communication. *Bell System technical journal*, 27:379–423,623–656, 1948.

[She84] Y. R. Shen. *Principles of Nonlinear Optics*. Wiley-Interscience, reprint edition, 1984. ISBN 0471430803.

[Shu62] W. A. Shurcliff. *Polarized light*. Harvard University Press, Cambridge, 1st edition, 1962. ISBN 0317080512.

[SL78] R. H. Stolen and C. Lin. Ultrashort pulses in fibers. *Physics review*, A17:1448, 1978.

[SL83] A. W. Snyder and J. D. Love. *Optical waveguide theory*. Chapman and Hall, 4th edition, 1983. ISBN 0412099500.

[SM91] T. Saito and T. Mukai. *Coherence, Amplification and quantum effects in semiconductor lasers*. John Willey and sons, 1st edition, 1991. ISBN 0471512494.

[Son00] Shuxian Song. The impact of polarization-mode dispersion on four wave mixing in WDM systems. *Fiber Optics communications*, 6, 2000.

[Sto52] G. G. Stokes. Stokes parameters. *Phil. Soc.*, 21(9):399, 1852.

[SZ01] Marlan O. Scully and M. Suhail Zubairy. *Quantum Optics*. Oxford Science publications, 1st edition, 2001. ISBN 0521435951.

[VB02] A. Vannucci and A. Bononi. Statistical characterization of the jones matrix of long fibers affected by polarization mode dispersion (PMD). *IEEE Journal of lightwave technology*, 20(5): 811, 2002.

[WM99] D. Wang and C. R. Menyuk. Polarization evolution due to the kerr nonlinearity and chromatic dispersion. *IEEE Journal of lightwave technology*, 17:2520–2529, 1999.

[YLKD03a] X. Yang, D. Lenstra, G. D. Khoe, and H. J. S. Dorren. Nonlinear polarization rotation in semiconductor optical amplifiers: theory and application to all-optical flip-flop memories. *IEEE Journal of Quantum Electronics*, 39(1), 2003.

[YLKD03b] X. Yang, D. Lenstra, G. D. Khoe, and H. J. S. Dorren. Nonlinear polarization rotation induced by ultrashort optical pulses in a semiconductor optical amplifier. *Optics communications*, 223:169–179, 2003.

[ZZCY04] Yuan Zheng, Xiaoguang Zhang, Lin Chen, and Bojun Yang. Analysis of degree of polarization ellipsoid as feedback signal for polarization mode dispersion compensation in NRZ, RZ and CS-RZ systems. *Optics communications*, 234:107–117, 2004.